COMPUTATIONAL ANALYSIS OF THERMO-FLUIDIC CHARACTERISTICS OF A CARBON NANO-FIN

A Dissertation

by

NAVDEEP SINGH

Submitted to the Office of Graduate Studies of
Texas A&M University
in partial fulfillment of the requirements for the degree of

DOCTOR OF PHILOSOPHY

December 2010

Major Subject: Mechanical Engineering

COMPUTATIONAL ANALYSIS OF THERMO-FLUIDIC CHARACTERISTICS OF A CARBON NANO-FIN

A Dissertation

by

NAVDEEP SINGH

Submitted to the Office of Graduate Studies of
Texas A&M University
in partial fulfillment of the requirements for the degree of

DOCTOR OF PHILOSOPHY

Approved by:

Chair of Committee,	Debjyoti Banerjee
Committee Members,	Kalyan Annamalai
	Raymundo Arroyave
	Karen Vierow
Head of Department,	Dennis O'Neal

December 2010

Major Subject: Mechanical Engineering

ABSTRACT

Computational Analysis of Thermo-Fluidic Characteristics of a Carbon Nano-Fin.

(December 2010)

Navdeep Singh, B. Tech, Punjab Technical University;

M. Tech, Thapar University

Chair of Advisory Committee: Dr. Debjyoti Banerjee

Miniaturization of electronic devices for enhancing their performance is associated with higher heat fluxes and cooling requirements. Surface modification by texturing or coating is the most cost-effective approach to enhance the cooling of electronic devices. Experiments on carbon nanotube coated heater surfaces have shown heat transfer enhancement of 60%. In addition, silicon nanotubes etched on the silicon substrates have shown heat flux enhancement by as much as 120%. The heat flux augmentation is attributed to the combined effects of increase in the surface area due to the protruding nanotubes (nano-fin effect), disruption of vapor films and modification of the thermal/mass diffusion boundary layers. Since the effects of disruption of vapor films and modification of the thermal/mass diffusion boundary layers are similar in the above experiments, the difference in enhancement in heat transfer is the consequence of dissimilar nano-fin effect. The thermal conductivity of carbon nanotubes is of the order of 6000 W/mK while that of silicon is 150 W/mK. However, in the experiments, carbon nanotubes have shown poor performance compared to silicon. This is the consequence of interfacial thermal resistance between the carbon nanotubes and the surrounding fluid since earlier studies have shown that there is comparatively smaller interface resistance to the heat flow from the silicon surface to the surrounding liquids.

At the molecular level, atomic interactions of the coolant molecules with the solid

substrate as well as their thermal-physical-chemical properties can play a vital role in the heat transfer from the nanotubes. Characterization of the effect of the molecular scale chemistry and structure can help to simulate the performance of a nanofin in different kinds of coolants. So in this work to elucidate the effect of the molecular composition and structures on the interfacial thermal resistance, water, ethyl alcohol, 1-hexene, n-heptane and its isomers and chains are considered. Non equilibrium molecular dynamic simulations have been performed to compute the interfacial thermal resistance between the carbon nanotube and different coolants as well as to study the different modes of heat transfer. The approach used in these simulations is based on the lumped capacitance method. This method is applicable due to the very high thermal conductivity of the carbon nanotubes, leading to orders of magnitude smaller temperature gradients within the nanotube than between the nanotube and the coolants. To perform the simulations, a single wall carbon nanotube (nanofin) is placed at the center of the simulation domain surrounded by fluid molecules. The system is minimized and equilibrated to a certain reference temperature. Subsequently, the temperature of the nanotube is raised and the system is allowed to relax under constant energy. The heat transfer from the nano-fin to the surrounding fluid molecules is calculated as a function of time. The temperature decay rate of the nanotube is used to estimate the relaxation time constant and hence the effective thermal interfacial resistance between the nano-fin and the fluid molecules. From the results it can be concluded that the interfacial thermal resistance depends upon the chemical composition, molecular structure, size of the polymer chains and the composition of their mixtures. By calculating the vibration spectra of the molecules of the fluids, it was observed that the heat transfer from the nanotube to the surrounding fluid occurs mutually via the coupling of the low frequency vibration modes.

To My Parents

ACKNOWLEDGMENTS

I would like to express my sincere gratitude to my advisor, Dr Debjyoti Banerjee, for his vision, ideas, guidance and generous support.

I would like to thank Dr Kalyan Annamali, Dr Raymundo Arroyave and Dr Karen Vierow for spending their valuable time as committee members.

I would like to thank Dr Lisa M Perez for countless enlightening discussions.

I would like to thank the Laboratory of Molecular Simulations (LMS) for the software and the Texas A&M Supercomputing facility for the hardware support.

I am grateful to the past and present members of the *Multi-Phase Flow and Heat Transfer Lab.*, including Mr Vijaykumar Sathyamurthi, Mr Donghyun Shin, Mr Saeil John and Mr Seokwon Kang for their continuous support and encouragement.

Finally, I thank my parents, my sisters and my wife for their encouragement, unwavering support and for being there for me all the time.

NOMENCLATURE

$\ddot{r}_i$	acceleration of i^{th} particle
$\dot{r}_i$	velocity of i^{th} particle
θ	chiral angle
a	length of carbon-carbon bond in carbon nanotube
C_h	chiral vector
d	diameter of carbon nanotube
E	intermolecular interaction energy
f_i	force acting on the i^{th} particle
m_i	mass of i^{th} particle
n, m	integers defining chiral vector
r, r_{ij}	distance between atoms i and j
r_i	displacement of i^{th} particle
r_c	cut off radius
t	time
t_{AB}	transmission coefficient
U	intermolecular potential energy of the system
C	correlation function

V velocity of an atom

TABLE OF CONTENTS

CHAPTER Page

LIST OF TABLES

LIST OF FIGURES

FIGURE Page

FIGURE Page

CHAPTER I

INTRODUCTION

Advances in microelectronics technology have led to miniaturization of electronic devices with the added advantage of enhanced performance of each chip. This advancement is also associated with enhanced heat flux from these chips leading to increase in demand for higher cooling requirements. So effective thermal management of these devices has become a major technological challenge for the microelectronics industry. Air based cooling systems are more common and reliable and are still favoured for cooling of low heat flux electronic devices. Attempts have been made to improve the thermal transport of these systems using fins and high performance fans, but due to the poor thermal characteristics of air, the effectiveness of these systems is compromised. Therefore, in many high heat flux applications liquid cooling is preferred. Liquid cooling is beneficial due to the superior thermal properties of liquids. Liquid cooling can be either single phase flow or multiphase flow with phase change. Phase change enables superior cooling performance compared to the single phase cooling due to the high latent heat.

In cooling applications, pool boiling is simple to achieve, reliable, quiet and inexpensive. According to Mudawar and Anderson [1], there are three ways to enhance heat transfer in pool boiling (a) modifying the boiling surface (b) sub-cooling the liquid (c) increasing the operating pressure. Sub-cooling of liquid requires extra equipment and increasing operating pressure in electronic devices is not a viable option. Hence, modifying the boiling surface is the most cost-effective approach to enhancing cooling of electronic devices.

The journal model is *IEEE Transactions on Automatic Control.*

Surfaces can be modified by texturing (e.g. chemical etching) or coating. Boiling experiments on nano textured surfaces have shown significant increase in the heat transfer. Pool boiling experiments are performed on silicon substrates coated with carbon nanotubes and etched silicon nanofins. Experiments performed on silicon heaters coated with carbon nanotubes have shown 60% increase in the critical heat flux as compared to the bare silicon surfaces in pool boiling [2, 3, 4]. Also nanotube coating with thickness of 25μm were found to increase in the film boiling flux by 66-148% as compared to the bare silicon surface. However, nanotube coatings with thickness of 9μm failed to show any enhancement in film boiling [3].

Pool nucleate boiling experiments performed by Sriraman et al [5] on silicon substrates with etched silicon nanofins showed heat flux enhancement of as much as 120% as compared to the bare silicon surface in nucleate boiling. Also in nucleate boiling the enhancement in heat flux was found to be independent of the length of the nanotube. To explain this phenomenon, consider a nucleation site and a vapor bubble attached on the nanofins and the silicon surface as shown in Figure 1. According to Derjaguin and Zorin [6] there is a very small layer of liquid film adhering on the silicon surface which is termed as the "micro-layer". This micro-layer acts as a barrier to the heat flow from the heater surface to the vapor surface. The height of this micro-layer is of the order of 100nm [5]. Nanofins of length greater than 100nm disrupt the micro-layer and protude inside the vapor bubble as shown in Figure 1. This leads to the disruption of the micro-layer and increases area of liquid micro-layer in contact silicon surface. Hence the heat transfer from the silicon surface increases. The length of nano-fin inside the vapor bubble is not in contact with the liquid and experiences insulation. So nanofins of height greater than 100nm are equally effective as nanofins of length of 100nm and do not enhance heat transfer.

In case of film boiling, a layer of vapor is formed on the silicon heater. This layer

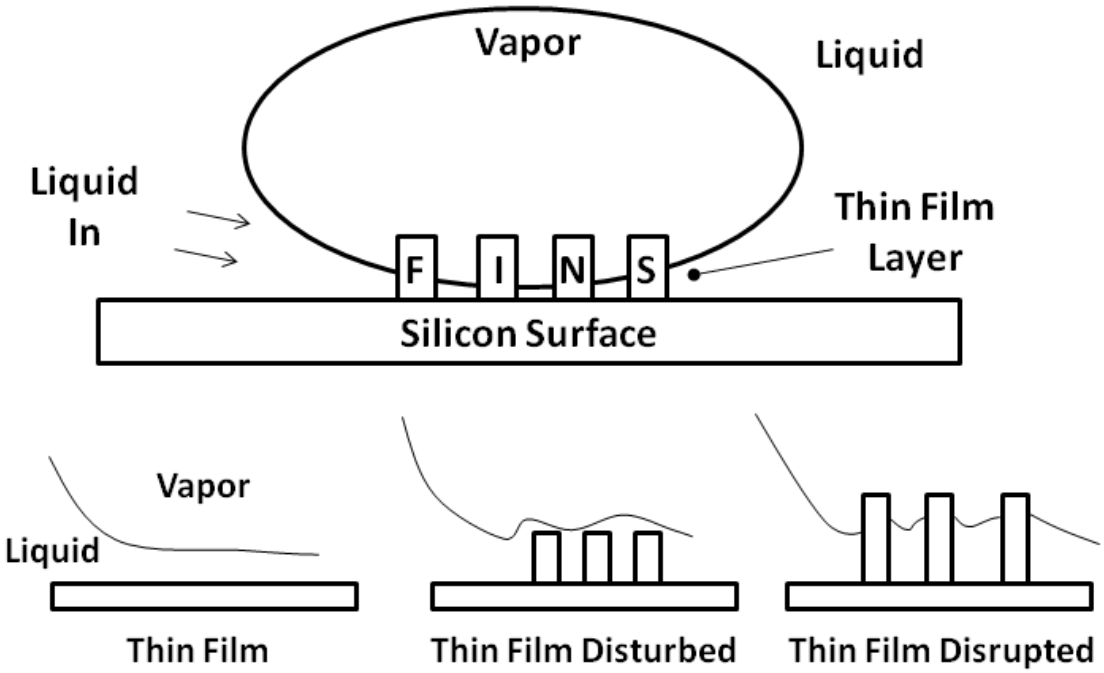

Fig. 1. Sketch of the (top) bubble on a solid surface with nanofins during pool boiling showing the presence of thin film liquid layer (micro layer) under the bubble (bottom) perturbation and disruption of the micro layer due to the presence of the nanofins during

is of the order of 15-20μm [7, 8]. Nanotubes with height greater than 20μm disrupt the vapour layer and protrude inside the liquid leading to greater efficacy in enhancing the heat transfer. This mechanism of disruption of vapor film by long nanotubes is depicted in Figure 2. Experiments have shown that nanotubes of length of 25μm enhance heat transfer while nanotubes of length of 9μm don't show any enhancement as compared to bare silicon wafer [3].

From the above discussion both silicon nanofins and carbon nanotubes are able to enhance the heat flux. The heat flux augmentation was attributed to combined effect of increase in the surface area due to the protruding nanotubes (nano-fin effect), disruption of vapor films and modification of the thermal/mass diffusion boundary

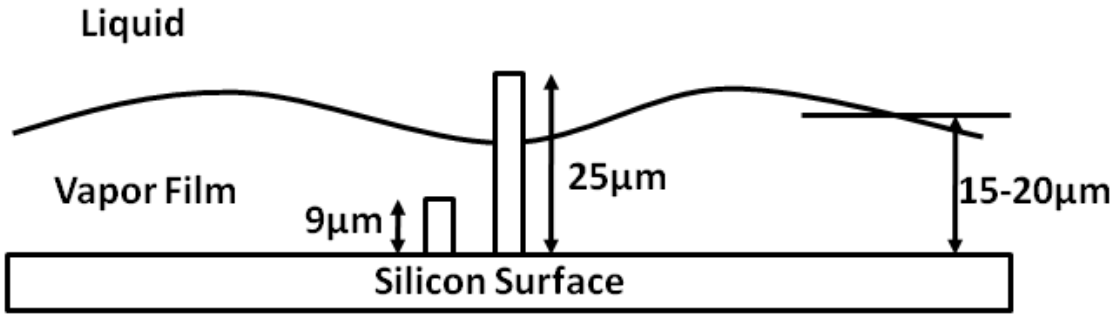

Fig. 2. Vapor blanket on the heater surface in film boiling for nanotubes of different lengths

layers.

Heat flux augmentation is also reported for experiments using *nanofluids*. Coolants doped with a small concentration of nano particles (around 1% or less) are called "Nanofluids". The nano particles used for synthesis of nanofluids can be metal, metal-oxide or carbon nanotubes, which form colloidal mixtures, since their size range is typically 100nm $\sim$ 1nm . Heat flux was enhanced by 10-30% for a coolant doped with 0.6% of nano-particles [9, 10, 11, 12, 13]. Nelson et al [12] found that these nano particles precipitate on the heater surface to form *nano-fins*.

A. Objective

Nano-fin coatings on the heater surface leads to enhancement in heat transfer. The factors responsible for the enhancement in heat transfer are either the high thermal conductivity of the nano-fin coatings or due to the enhancement in the surface area. The thermal conductivity of silicon is of the order of 150W/mK [14] whereas for carbon nanotubes is of the order of 3000W/mK for multi-walled nanotubes [15] and 6000W/mK for single wall carbon nanotubes [16]. Since enhancement in heat transfer is observed experimentally in case of both silicon and carbon nano-fins, therefore

rather than thermal conductivity, surface area effect is the dominant factor. The primary factor limiting the enhancement in heat transfer performance of carbon nano-fins, due to enhancement in surface area, is the presence of interfacial resistance to the heat flow from the surface of the carbon nano-fins to the surrounding fluid.

Hence, the objective of this work is to study the various factors affecting the interfacial thermal resistance between the carbon nano-fin and the surrounding fluids. In essence, the objective is to study the effect of molecular composition and molecular structure of the surrounding fluids on the inetrfacial thermal resistance.

B. Problem Statement

Chemical composition of a coolant can play a vital role in the heat transfer from the carbon nanotubes. The differences in the atomic structure of the molecules with the same type and number of atoms can lead to very different properties of the system. In order to study the performance of the nanotubes as nanofins in different types of coolants, characterization of the effect of the atomic (chemical) and structural properties of the molecules on the interfacial thermal resistance needs to be studied systematically. Interfacial resistance in nano-structures dominate the overall thermal resistance and significantly affects the thermal transport properties. The main focus of this study will be on using non-equilibrium molecular dynamics simulations to explain the effect of chemical and structural properties on the interfacial resistance between coolant molecules and a carbon nanotube acting as *nano-fin*.

Common coolants used for heat removal like water, ethyl alcohol, 1-hexene and single long chain hydrocarbons, n-heptane and its isomers, chains and their mixtures, manufactured by the catalytic oligomerisation of Poly Alpha-Olefins (PAOs) are considered in this study. PAOs are commonly used for cooling electronics platforms,

especially for avionics cooling applications owing to their superior physical and chemical properties, such as greater fluidity at low temperature, lower volatility, a higher viscosity index, lower pour point, better oxidative and thermal stability and low toxicity [17]. PAOs are manufactured via catalytic oligomerisation of alphaolefins. For avionics applications, a second catalytic process breaks the double bonds in PAOs, producing a mixture of chemically saturated polymers. These polymers possess much lower pour point suitable for cooling electronics platforms and are the subject of this study.

C. Significance of the Study

Recent literature reports explored the use of carbon nanotube arrays as nanofins for cooling applications [4, 5, 18]. The major hurdle to the heat dissipation by these nanofins is due to the dominance of the interfacial thermal resistance between the nanofins and the surrounding fluid. To better understand the performance of these nanofins, information about of all the factors affecting interfacial thermal resistance is of paramount importance. At the molecular scale, chemical and structural properties of the molecules play a vital role in determining the system behaviour. This is the first study to systematically elucidate the effect of atomic and structural variations on the interfacial thermal resistance between the carbon nanotubes and coolants. The few studies done so far only focused on calculating the magnitude of the interfacial thermal resistance between a carbon nanotube and surrounding polymer matrix. This study is expected to make the following contributions.

- The effect of chemical composition of fluids on the interfacial thermal resistance.
- The effect of molecular structure of the fluids on the interfacial thermal resistance.

- The effect of polymer chains of a molecule on the interfacial resistance.
- The effect of isomers of a polymer chain on the interfacial thermal resistance.
- The effect of mixture of polymer chains and their isomers on the thermal resistance.
- Dominant mechanism of energy transfer from carbon nanotubes to surrounding molecules

D. Hypothesis

Experiments have shown enhancement in heat transfer using both carbon and silicon nanofins. The factors responsible for enhancement in the heat transfer are increase in the surface area due to the presence of the nanofins leading to disruption of vapor films and modification of the thermal/mass diffusion boundary layers and high thermal conductivity of the nanofins. Carbon nanotubes have much higher thermal conductivity than silicon nano-fins but experiments have shown enhancement in heat transfer using both types of nano-fins. So enhancement in surface area is the dominant factor in enhancing the heat transfer. Figure 3 shows the thermal resistance model for a single nanofin. From the figure the following thermal resistances are identified, the resistance due to the finite thermal conductivity of the silicon substrate (R_1), resistance at the nano-fin-silicon substrate interface (R_2), resistance due to the finite thermal conductivity along the length of the nano-fin (R_3) and the resistance to the heat transfer from the nano-fin to the surrounding liquid molecules (R_4) also known as "interfacial thermal resistance" or "Kaptiza resistance". The resistance R_1 is not as important since it is the heater surface that is common to all the configurations. The resistance R_2 is only present in case of carbon nanotfins and is of

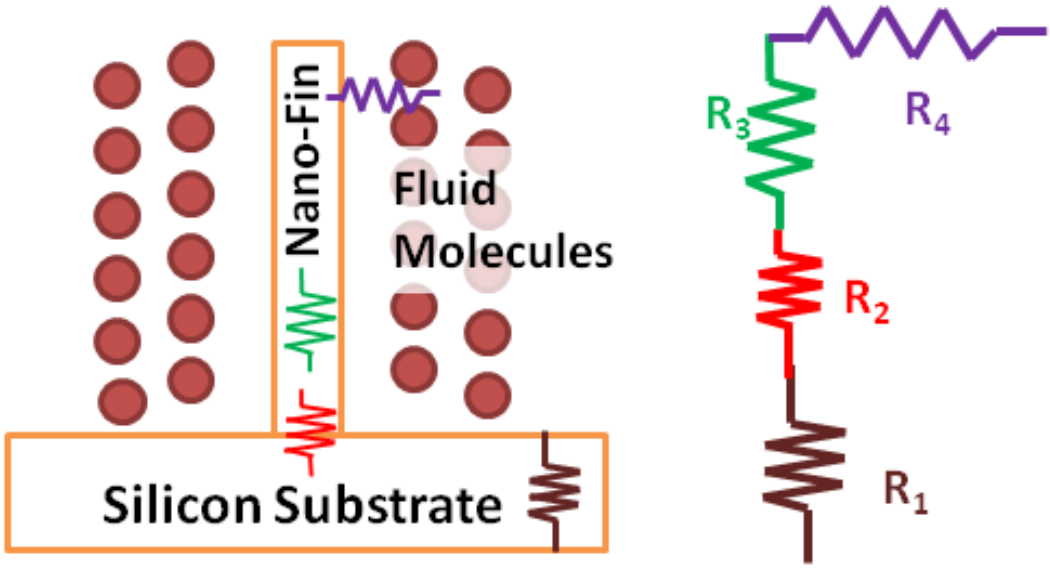

Fig. 3. Resistance model of a nano-fin on a silicon substrate

the order of $\sim 10^{-10} m^2 K/W$ [19], where as the silicon nano-fins are etched on the heater surface. The resistance R_3 is very small owing to the small length of nano-fins. Interfacial thermal resistance, R_4, is of the order of $\sim 10^{-11} m^2 K/W$ [20] in case of silicon nano-fins while is the order of $\sim 10^{-8} m^2 K/W$ [21] in case of carbon nano-fins. So in case of carbon nano-fins the interfacial resistance is three order's of magnitude higher than that of silicon nano-fins. This shows that rather than conductive resistance, the interfacial resistance is more dominant factor in modulating heat flux from nano-structures. Hence, this resistance severely limits the effectiveness of the carbon nano-fins.

Nanotubes have also been used as a filler material in composites to increase thermal conductivity. Nanotubes are expected to enhance the thermal conductivity of the composites many fold owing to their high aspect ratio and very high thermal conductivity. But experiments show small increase in the thermal conductivity [22, 23, 24] compared to the theoretical calculations. This anomaly has been attributed

to the interfacial thermal thermal resistance between the carbon nanotubes and the polymer composite molecules.

E. Scope and Limitations

The present study is limited to the investigation of a (5,5) carbon nanotube as a nano-fin. Also for the matrix system water, alcohol, 1-Hexene, n-heptane and its dimers and trimers and isomers are studied. The isomers of these polymers considered in this study are limited to a single methyl group being placed at different locations on the polymer chain.

F. Organization of the Dissertation

Experimental studies have shown that the nano-fin effect is responsible for the enhancement in the heat flux in pool boiling. These experiments also show that nanotube coated heaters provide lower heat transfer enhancement than silicon nano-fins. This can be attributed to the modulation of thermal resistance to the heat flow from nano-structures to the coolant. So the interfacial thermal resistance needs to be explored in order to determine the overall effectiveness of nano-fins.

Chapter II provides a background on the carbon nanotubes, its novel properties and present as well as future applications. Next, Molecular Dynamics simulations are discussed. This section also describes the velocity verlet method used to numerically integrate the equations of motion and the polymer consistent force field (PCFF) used in the present study. At the end of the chapter the literature on interfacial thermal resistance is reviewed. Chapter III describes the methodology of Molecular Dynamics Simulations to calculate the interfacial thermal resistance. Simulation results are presented and discussed in Chapter IV. Chapter V summarizes the results and identifies

the future scope of work.

CHAPTER II

BACKGROUND

This chapter provides background information on carbon nanotubes, molecular dynamics simulations and interfacial thermal resistance. The first section discusses carbon nanotubes, their structure, properties and potential applications. The second section introduces the molecular dynamics simulations. This section discusses the basic equations describing the motion of the atoms, the force field to calculate potential energy of the system, boundary conditions , the ensembles employed in this work and space time correlation to calculate the properties of the system. The last two sections details the interfacial thermal resistance, theories developed to calculate interfacial resistance, importance of interfacial resistance at nano scales and the simulation techniques developed and used in calculating the interfacial thermal resistance.

A. Carbon Nanotubes

There are three known allotropes of carbon viz diamond, graphite and fullerenes (or carbon nanotubes). The bonding hybridization of diamond is sp^3 while of graphite, fullerenes and carbon nanotubes is sp^2. Carbon nanotubes are formed by wrapping the two dimensional planar graphite sheets. Graphite sheets can be single or multi-layer forming single and multi-wall carbon nanotubes respectively. Also depending upon how a graphite sheet is rolled, a variety of nanotube structures can be formed. The physical structure of a carbon nanotube is uniquely defined by a vector (also known as "chirality") connecting two crystallographically equivalent sites on the 2D graphene sheet[25] known as chiral vector. Graphene is an atom thick sheet of sp^2 carbon atoms packed in a honeycomb crystal lattice. The chiral vector is expressed

as

$$\overrightarrow{C}_h = n\hat{a}_1 + m\hat{a}_2 \tag{2.1}$$

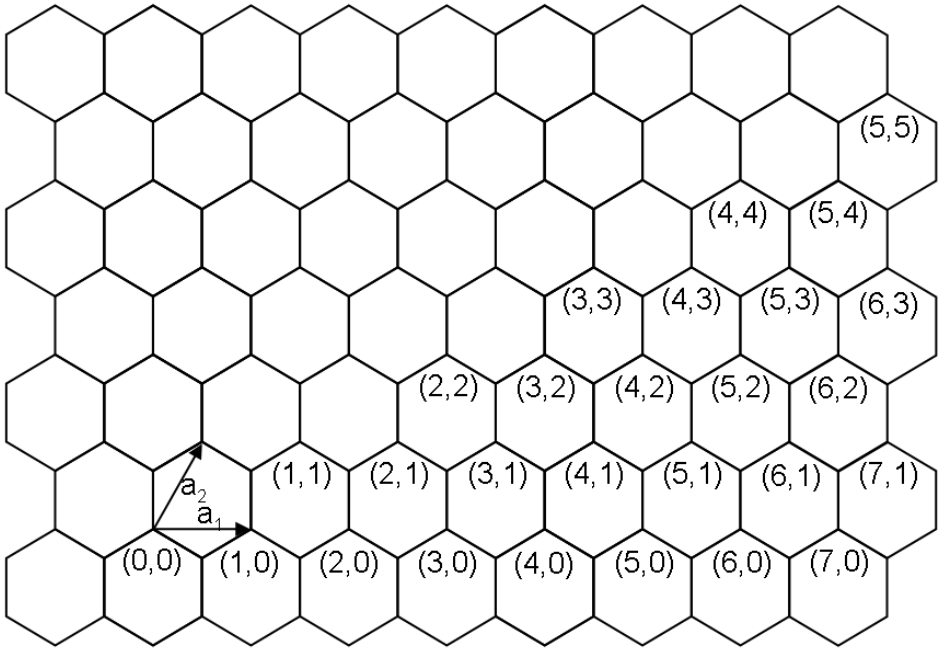

Fig. 4. 2D graphene sheet

Fig.4 shows the unit vector $\hat{a}_1$ and $\hat{a}_2$ and the (n, m) integer pair on a graphene sheet for defining different crystal structures of carbon nanotubes. Since the graphene lattice is rotationally symmetrical, n and m are considered such that $0 \leqslant m \leqslant n$. Each pair of (n, m) represents a unique structure of the nanotube, divided into three categories armchair, zigzag and chiral. $m = 0$ corresponds to zigzag tubes and $m = n$ corresponds to armchair tubes. All other tubes are known as chiral. The angle between the zigzag tube and the chiral vector is known as chiral angle θ. For zigzag tubes the chiral angle is 0°while for armchair the chiral angle is 30°. For chiral

nanotubes $0 < \theta < 30$°and is defined as

$$\theta = sin^{-1}\frac{\sqrt{3m}}{2\sqrt{n^2+nm+m^2}} \tag{2.2}$$

If the length of the carbon-carbon bond is known, the diameter of the nanotube is given by

$$d = \sqrt{3}a\sqrt{n^2+nm+m^2}/\pi = C_h/\pi \tag{2.3}$$

where a is the carbon-carbon bond length and C_h is the length of the chiral vector $\overrightarrow{C}_h$. Fig. 5 shows the formation of carbon nanotubes with different crystal structures from the graphene sheet.

1. Properties and Applications of Carbon Nanotubes

The ability to manipulate the molecular structure by changing the chiral angle makes carbon nanotubes remarkable material with tunable properties. The extended network of C-C bonds result in enhanced material properties. The C-C bond of graphite is the strongest bond in nature [26]. This makes carbon nanotubes very strong and stiff material with a tensile strength of 0.15TPa and a Young's modulus of 0.9TPa [27]. So nanotubes find application in composites as filler materials to enhance properties like tensile strength and stiffness[28]. Nanotubes have a very large aspect ratio. A nanotube of 1nm diameter can be synthesized upto a length of few cm [29].

Nanotubes are considered in various studies for electronic applications. The carbon nanotubes possess very high electrical conductivity due to the free movement of the de-localized pi-electron (donated by each atom) about the entire structure in a CNT. Graphite is a semiconductor with a zero band gap , but nanotubes can be either metallic or semiconductor depending upon the chiral vector. For $n = m$, armchair nanotubes are metallic in nature whereas if $n - m$ is a multiple of 3, the

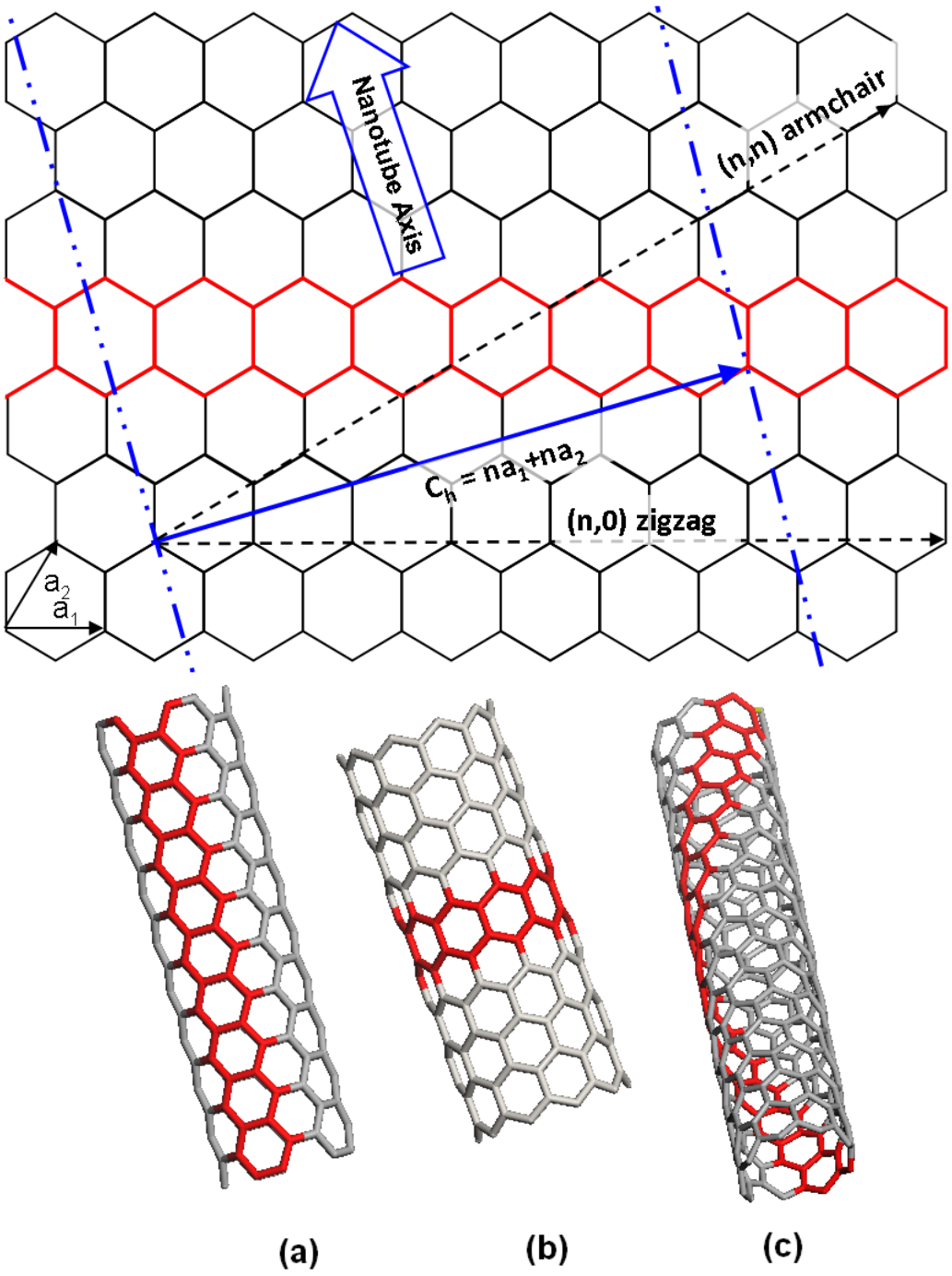

Fig. 5. Formation of carbon nanotubes from a 2D graphene sheet (top) chiral vectors on the graphene sheet (bottom) carbon nanotube structures showing alignment of hexagons in (a) (5,5) nanotube (b) (10,0) nanotube and (c) (8,1) nanotube

nanotube is semiconducting with a very small band gap. All other nanotubes are semiconductors with moderate band gap that inversely depends upon the diameter of the nanotube[30, 31]. Due to the one-dimensional structure, metallic nanotubes are able to carry high currents without excessive heating over long lengths, with a current density approaching 4×10^9 Acm^{-2}, which is many times the order of metals such as copper and aluminium[32, 33]. So nanotubes and graphenes are considered to be ideal materials for interconnects in Very Large Scale Integration (VLSI) circuits owing to high thermal conductivity, thermal stability and large current carrying capacity. The high thermal conductivity of carbon nanotubes arises from the high-frequency carbon-carbon bond vibrations. Highly conducting nanotubes are therefore considered ideal filler material in composite to increase their overall thermal conductivity[28]. Nanotubes are also used to synthesize nano-fluids which find applications in cooling and thermal storage technologies. Nanotubes have, therefore, been proposed for applications as nano-fins to cool high heat flux electronic devices and as highly conducting thermal interface materials between microprocessor chips and heat sinks. [18, 34, 35].

B. Molecular Simulations

"Molecular Simulation" is a generic term for theoretical methods and computational techniques based on advanced statistical tools to model or mimic the behaviour of molecules. Molecular Simulations provide exact solutions for the problems involving models based on statistical mechanics. The results of the molecular simulations depends solely on the nature of the theoretical method. In molecular simulations the atomic system evolves in spatial and/or temporal domain in accordance with the extensive calculations of intermolecular energies. This is also the fundamental difference between the molecular simulations and the other computational methods.

There are two main families of molecular simulation methods, Monte Carlo (MC) and Molecular Dynamics (MD). Hybrid molecular methods are also developed which combines features of these two techniques. Monte Carlo method is a stochastic technique that relies on the probabilities and random numbers. In a Monte Carlo simulation a starting configuration domain is defined, then a new trail configuration is generated randomly by displacing, exchanging, removing or adding a molecule and is evaluated against an acceptance criterion, which is based on the calculated change in energy or other property of the system and at last the trial configuration is either accepted or rejected based on the criterion. Since not all states contribute to configurational properties, states making most significant contributions are sampled by generating Markov chains. In Markov chain, the new accepted state is always more favourable than the existing state. In contrast Molecular Dynamics is a deterministic method in which time evolution of the system is determined by solving the equations of motion for each atom and/or molecule.

Both methods have their advantages and disadvantages depending upon the system being solved and the properties being simulated. MC simulations are time independent, they only define the state of the system at some point in time whereas MD simulations defines the time evolution of the system. Since the MD simulations solve equations of motion for each atom at each time step, these are computationally very costly whereas in MC simulations the atom movement is stochastically sampled which is computationally cheap. But increase in the sample rejection rate can dramatically increase the computation cost in MC. So MC method is better suited for studying systems of liquids with moderate densities, gases, systems with large number of coupled degree of freedom such as fluids, disordered materials, strongly coupled solids and cellular structures. MD simulations are better suited for higher density fluids, gases under high pressure and temperatures and systems with dynamic properties

such as transport coefficients, time-dependent responses to perturbations, rheological properties and spectra [36].

1. Molecular Dynamics Simulations

Molecular Dynamics is a powerful computational technique to study the dynamical evolution of classical many body systems such as solids, liquids and gases. Classical laws of mechanics are obeyed by the motion of the atoms/molecules.This is a reasonably excellent approximation for wide range of systems and properties. MD simulations numerically integrate the Newton's equations of motion for all the atoms/molecules in the model system, and output their temporal evolution of coordinates and momenta. Newton's equation of motion is a simple consequence of the Lagrange's equations of motion of classical mechanics. The temporal evolution is discrete and at each time step it is equivalent to a microstate in the same ensemble. So classical statistical mechanics equations can be used to derive the desired properties from these states. So MD simulations can be used to test hypothesis, characterize theories and experiments, simulate conditions impossible to achieve in experiments and estimate missing or unreliable data. The power of MD lies in its ability to investigate atomic/molecular movements not accessible to experiments. Recent advances in algorithms and computers have made MD simulations feasible for large systems for longer time scales.

In general, Newton's equation of motion for an atom i can be expressed as

$$m\ddot{r}_i(t) = f_i(t) \tag{2.4}$$

Consider a system of N atoms, whose intermolecular potential energy is defined by $U(r^N)$, r^N representing center of mass of atoms $r^N = r_1, r_2, r_3, ..., r_N$. The intermolecular potential energy of the system is defined by a set of parameters and their functional form, known as the force field. This is discussed in the next section. If

no dissipative forces are acting among the atoms, for conserved intermolecular forces, the force acting on a atom i relates to the potential as,

$$f_i(t) = -\frac{\partial U(r^N)}{\partial r_i} \tag{2.5}$$

Combining above two equations, we get,

$$m\ddot{r}_i(t) = f_i(t) = -\frac{\partial U(r^N)}{\partial r_i} \tag{2.6}$$

Integrating above equation once gives the atomic momentum at the next time step and integrating twice yields the atomic positions. If the integration continues for a long time, we get the atomic momentum and position trajectories, which can then be used to obtain the macroscopic properties using the classical mechanics equations. The equations of motion are too complex to integrate for atomic systems, so numerical integration techniques are employed. There are number of schemes available but the two most commonly used are Verlet Algorithm and Gear Predictor-Corrector. In this work Verlet algorithm is used and will be discussed. The Gear Predictor-Corrector scheme is discussed in details in the literature[37, 38, 39].

The Verlet algorithm is the most widely used method to integrate equations of motion initially adopted by Verlet [40, 41] and attributed to Carl Stormer by Gear [39]. This methods gives direct solution of the equation 2.6. The basic idea is to calculate the positions at the next time step $(r + \delta t)$ from the previous $(r - \delta t)$ and the current time step (t). Writing the position $r(t)$ as Taylor series expansion from the previous and next time step,

$$r(t - \delta t) = r(t) + \dot{r}(t)\delta t - \frac{1}{2!}\ddot{r}(t)\delta t^2 + \frac{1}{3!}\dddot{r}(t)\delta t^3 + \mathcal{O}(\delta t^4) \tag{2.7}$$

$$r(t + \delta t) = r(t) + \dot{r}(t)\delta t + \frac{1}{2!}\ddot{r}(t)\delta t^2 + \frac{1}{3!}\dddot{r}(t)\delta t^3 + \mathcal{O}(\delta t^4) \tag{2.8}$$

Adding the above two equations lead to

$$r(t+\delta t) = 2r(t) - r(t-\delta t) + \ddot{r}(t)\delta t^2 + \mathcal{O}(\delta t^4) \tag{2.9}$$

In the above equation, $\ddot{r}(t)$ is calculated from equation 2.6. The truncation error is of the order of δt^4. However, there is no way to directly compute the velocities ($\dot{r}(t)$), which are used to calculate kinetic energy of the system and hence other quantities like total energy, temperature and pressure. The velocities are computed from the positions as

$$\dot{r}(t) = \frac{r(t+\delta t) - r(t-\delta t)}{2\delta t} + \mathcal{O}(\delta t^2) \tag{2.10}$$

However, the velocities are one step behind the positions and also the error associated with this scheme is of the order of δt^2. The velocities at time $(t+\delta t)$ can be calculated as

$$\dot{r}(t) = \frac{r(t+\delta t) - r(t)}{\delta t} + \mathcal{O}(\delta t) \tag{2.11}$$

But now the accuracy is of the order of δt. To increase the accuracy of the velocities, this verlet algorithm has been modified. One of the modified scheme is called leaf-frog [42]. The leaf-frog method was not able to handle the velocities satisfactorily. So a Velocity Verlet algorithm was proposed by Swope et al[43]. This algorithm stores positions, velocities, and accelerations at the same time step and minimizes the round off errors. The standard velocity verlet algorithm is implemented as

$$r(t+\delta t) = r(t) + \dot{r}(t)\delta t + \frac{1}{2}\ddot{r}(t)\delta t^2 \tag{2.12}$$

$$\dot{r}(t+\frac{\delta t}{2}) = \dot{r}(t) + \frac{1}{2}\ddot{r}(t)\delta t \tag{2.13}$$

$$\ddot{r}(t+\delta t) = -\frac{1}{m}\frac{\partial U(r)}{\partial r} \tag{2.14}$$

$$\dot{r}(t+\delta t) = \dot{r}(t+\frac{\delta t}{2}) + \frac{1}{2}\ddot{r}(t+\delta t)\delta t \tag{2.15}$$

Using this algorithm the positions, velocities and accelerations are all computed at the same time step, but still order of the global error is δt^2. So choice of the time step is very crucial to the successful implementation of algorithm. A large time step will accrue errors as the simulation proceeds and a too small time step will increase the simulation time and round off errors.

a. Force Field

Force field or potential energy functions are simplified mathematical equations to model interaction between the particles in a system. According to Brenner [44], an effective force field should possess following four critical properties,

- Flexibility: A potential function must be flexible enough to accommodate a wide range of fitting data derived from experiments and ab-initio calculations.
- Accuracy: A potential function should be able to accurately reproduce an appropriate fitting data base.
- Transferability: A potential function should be able to describe at least qualitatively, if not with quantitative accuracy, structures not included in a fitting data base.
- Computational efficiency: The function evaluation should be computationally efficient depending upon the system size and time scales of interest as well as the available computer resources.

There are a large number of force fields available in the literature, which can be broadly grouped into generic force fields, biological force field and class II force fields [45]. For this work class II force field, polymer consistent force field (PCFF), is used. Class II force fields make extensive use of anharmonic and cross-coupling terms to

accurately represent the potential energy surface obtained from ab-inito calculations. PCFF is derived from the CFF [46] developed by Biosym. Biosym merged with Molecular Simulations into the current company Accelrys [47].

The total potential energy of a system is the sum of the bonded and non-bonded interactions. The bonded interaction can be further represented as sum of valence and cross-terms.

$$E_{total} = E_{bond} + E_{non-bond} = E_{valence} + E_{crossterm} + E_{non-bond} \tag{2.16}$$

Fig. 6 illustrates the various bonded interactions. The bonded valence energy consists of bond stretching, two bond angle bending, twisting (dihedral) and molecules going out of plane (oop).

$$E_{valence} = E_{bond} + E_{angle} + E_{torsion} + E_{oop} \tag{2.17}$$

The cross terms interactions account for changes caused by the surrounding atoms, include bond-bond, interaction between adjacent bonds; angle-angle, interaction between angles having common vertex atom; bond-angle, interaction between an angle and one of its bond; end-bond-torsion, interaction between a dihedral and one of its end bond; middle-bond-torsion, interaction between a dihedral and its middle bond; angle-torsion, interaction between a dihedral and one of its angles; angle-angle-torsion, interaction between a dihedral and its two valence angles.

$$\begin{aligned} E_{crossterm} = {} & E_{stretch-stretch} + E_{angle-angle} + E_{bond-angle} + E_{end\_bond-torsion} \\ & + E_{middle\_bond-torsion} + E_{angle-torsion} + E_{angle-angle-torsion} \end{aligned} \tag{2.18}$$

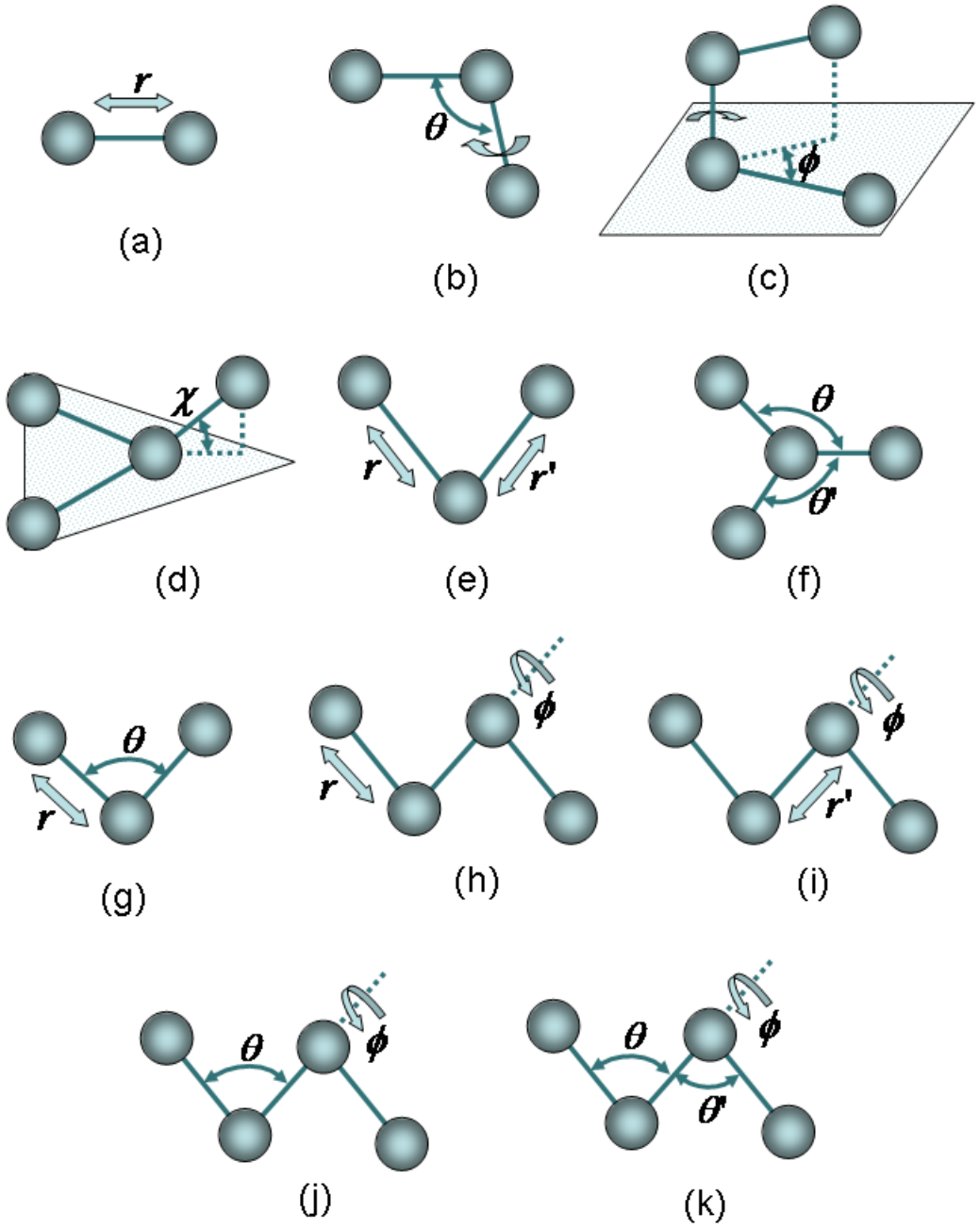

Fig. 6. Various types of bonded interactions between the atoms, considered in the PCFF force field

The equations representing these interactions in PCFF to calculate potential energy are defined as [48]

$$E_{bond} = \sum_{r}[K_2(r-r_0)^2 + K_3(r-r_0)^3 + K_4(r-r_0)^4] \tag{2.19}$$

$$E_{angle} = \sum_{\theta}[H_2(\theta-\theta_0)^2 + H_3(\theta-\theta_0)^3 + H_4(\theta-\theta_0)^4] \tag{2.20}$$

$$E_{torsion} = \sum_{\phi}\sum_{n=1}^{3}[V_n(1-cos(n\phi-\phi_n^0)] \tag{2.21}$$

$$E_{oop} = \sum_{\chi} K_\chi \chi^2 \tag{2.22}$$

$$E_{bond\_bond} = \sum_{r}\sum_{r'} F_{rr'}(r-r_0)(r'-r_0') \tag{2.23}$$

$$E_{angle\_angle} = \sum_{\theta}\sum_{\theta'} F_{\theta\theta'}(\theta-\theta_0)(\theta'-\theta_0') \tag{2.24}$$

$$E_{bond\_angle} = \sum_{r}\sum_{\theta} F_{r\theta}(r-r_0)(\theta-\theta_0) \tag{2.25}$$

$$E_{end\_bond-torsion} = \sum_{r}\sum_{\phi}(r-r_0)[V_1 cos\phi + V_2 cos2\phi + V_3 cos3\phi] \tag{2.26}$$

$$E_{middle\_bond-torsion} = \sum_{r'}\sum_{\phi}(r'-r_0')[V_1 cos\phi + V_2 cos2\phi + V_3 cos3\phi] \tag{2.27}$$

$$E_{angle-torsion} = \sum_{\theta}\sum_{\phi}(\theta-\theta_0)[V_1 cos\phi + V_2 cos2\phi + V_3 cos3\phi] \tag{2.28}$$

$$E_{angle-angle-torsion} = \sum_{\phi}\sum_{\theta}\sum_{\theta'} K_{\phi\theta\theta'} cos\phi(\theta-\theta_0)(\theta'-\theta_0') \tag{2.29}$$

The non-bonded interactions are composed of two types, van der Waal's interactions and Coulomb's interactions.

$$E_{nonbonded} = E_{LJ} + E_{coulomb} \tag{2.30}$$

$$E_{LJ} = \sum_{i>j} E_{ij}\left[2\left(\frac{r_{ij}^0}{r_{ij}}\right)^9 - 3\left(\frac{r_{ij}^0}{r_{ij}}\right)^6\right] \tag{2.31}$$

$$E_{coulomb} = \sum_{i>j} \frac{q_i q_j}{r_{ij}} \tag{2.32}$$

where q_i and q_j are partial charges, where r_{ij}^0 is collision diameter (units of length), the distance at which the interparticle potential is zero and E_{ij} is the dissociation energy and r_{ij} is the distance between the atoms. In PCFF, r_{ij}^0 and E_{ij} are calculated using the sixth power rule, as follows,

$$r_{ij}^0 = \left(\frac{(r_i^0)^6 + (r_j^0)^6}{2} \right)^{\frac{1}{6}} \tag{2.33}$$

$$E_{ij} = 2\sqrt{E_i E_j} \left(\frac{(r_i^0)^3 . (r_j^0)^3}{(r_i^0)^6 + (r_j^0)^6} \right) \tag{2.34}$$

In a system with N particles, the number of pairwise interactions are N^2, which are computationally very costly. To minimize the computation cost, a cut off radius , r_c is defined. The atoms or molecules within the cut off distance are only considered for the pairwise interactions as shown in Figure 7.

Mathematically, this can be defined as

$$E_{LJ,short-range} = \begin{cases} V_{LJ}(r) - V_{LJ}(r_c) & r_{ij} \leq r_c \\ 0 & r_{ij} > r_c \end{cases} \tag{2.35}$$

This technique is very efficient but it completely ignores the interactions beyond the cut-off range. The LJ potential decays as $1/r^6$, where r is the distance between the atoms. So it is acceptable to use cut-off distance to calculate potential energy and then add correction factor to account for the long range interactions. The long range interactions are given by [49]

$$E_{LR} = 2\pi N \rho \int_{r_c}^{\infty} r^2 E_{LJ} dr \tag{2.36}$$

However, in case of Coulomb interactions the potential decays very slowly as $1/r^1$ leading to divergence of correction integrals. So for long range coulombic interactions,

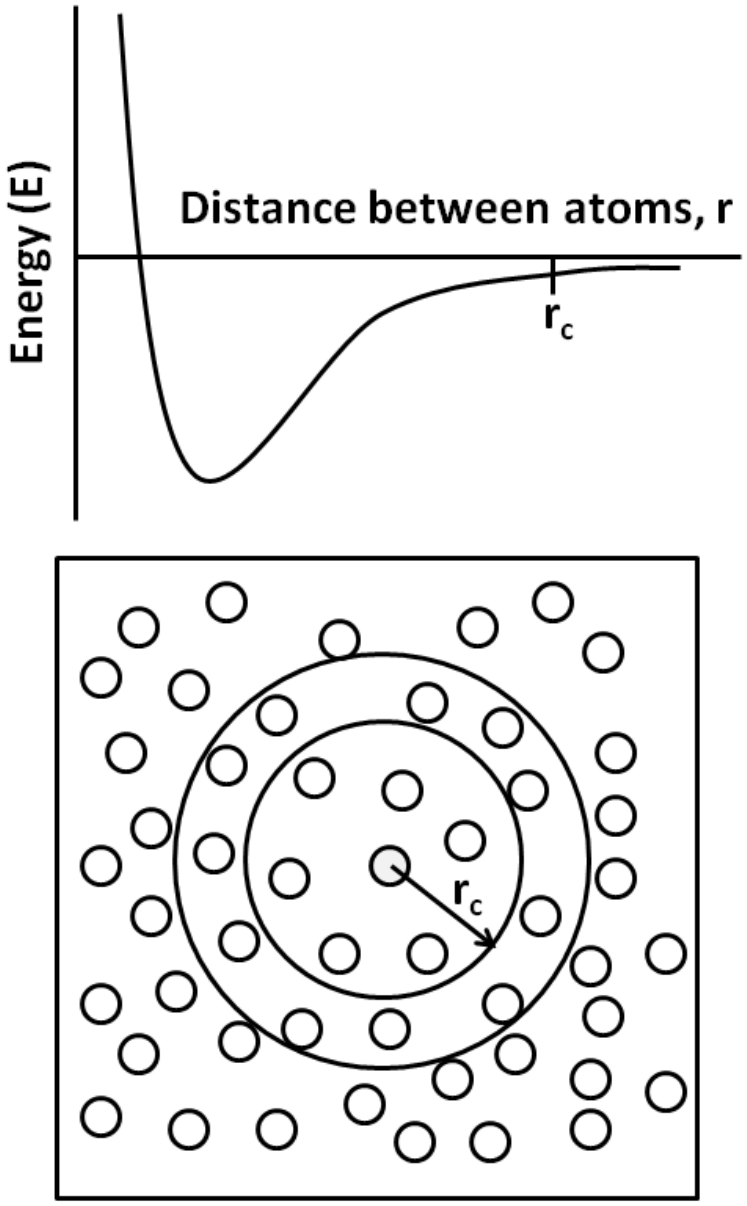

Fig. 7. Non-bonded Leonard-Jones potential between two atoms and the use of cut off radius to reduce the computational cost by eliminating calculations between atoms separated by large distance.

other techniques are employed. One of the most popular method is Ewald sum technique [50]. For a neutral system of N particles with charges q_i and at position r_i, the total coulombic energy is given as

$$E_{coulomb} = \frac{1}{2} \sum_{m}^{\infty} \sum_{i,j=1}^{N}{}' \frac{q_i q_j}{|r_{ij} + nL|} \tag{2.37}$$

where r_{ij} is the distance between i and j atoms, n is the count of periodic images and L is the length of the unit cell assuming it is cubic in shape. Prime ($'$) denotes that sum for $i = j$ will be ignored for the original box, $n = 0$. The energy given by above equation strongly varies at small distances but slowly decays at large distances. A computational trick is to split the energy equation into two exponentially converging sums. This trick is computationally expensive as one part of the sum is solved in reciprocal space thus needing several Fourier transformations. This method is accelerated by using fast Fourier transformation (FFT) method by replacing the charges with a regular mesh. The most common mesh based technique used is Particle-Particle and Particle-Mesh (PPPM) method [51]. A very comprehensive treatment of these methods can be found in the literature [49, 52, 53].

b. Boundary Conditions

The computation cost for performing the molecular dynamics simulations is very high. So small systems with a small number of atoms are typically considered for the MD simulations. For small systems, the atoms near the edges of the simulation box have few atoms to interact with. These edge atoms introduce the surface effects, which in turn affect the bulk properties of the system owing to its small size. To eliminate these surface effects, one way is to use a very large system. But solving a large system is not computationally feasible. The other way to overcome this problem is to use

periodic boundary conditions.

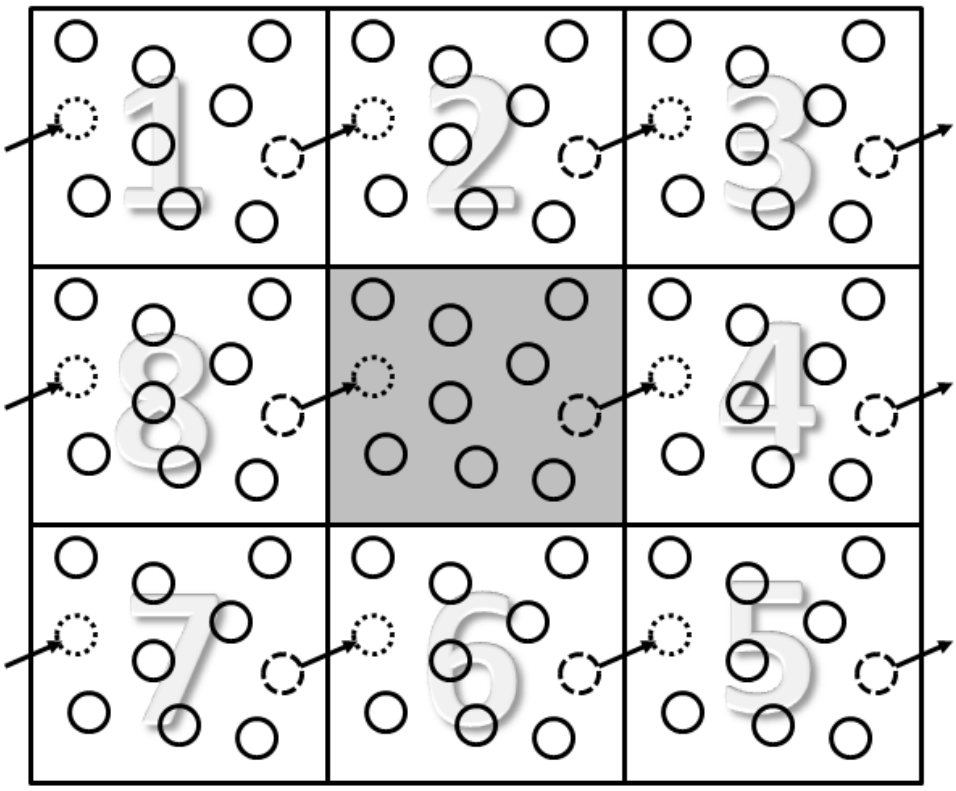

Fig. 8. Periodic boundary conditions

With periodic boundary conditions, the simulation box is replicated infinitely in the space lattice. During the simulation if one particle leaves the simulation box, another particle will enter the original box from the opposite face from the periodic image. This mechanism is demonstrated in Figure 8 in a two dimensional version. In 2D, the original box is surrounded by eight images of the box. As a particle crosses the right edge of the box, its image from the left edge enter the original box. So the original simulation box is devoid of any boundaries and thus eliminates the surface effects due to the presence of the boundaries. Apart from eliminating surface defects, periodic boundary conditions are useful in building the neighboring lists. As discussed

above neighboring lists contains the list of particles within the cut off distance for each particle to calculate the non-bonded interactions. For the particles near the center of the simulation box, neighbors will be in the same box. But for a particle near the boundary, there are no particles to interact with beyond the boundary if periodic conditions are not used. With periodic boundary conditions, an image of the box is utilized, so the particle can interact with its neighbors similar to a particle at the center of the cell.

c. Ensembles

Ensemble is an idealization consisting of very large number of states of a system, considered all at once, one of which represent the state of the real system at any given instant. All possible states appear with an equal probability. So an ensemble is a system with different microscopic states representing an identical macroscopic or thermodynamics state.

Newton's equations of motion explore only constant energy surfaces, characteristic of isolated systems. However, real systems interact with the surrounding, are exposed to pressure and external forces and exchange thermal energy. These macroscopic constraints leads to different types of ensembles. The following ensembles are employed in this work:

- Microcanonical Ensemble (NVE): Collection of all the systems having constant total energy. This corresponds to a thermally isolated system. The thermodynamic state of the system is characterized by constant number of atoms, N, constant volume, V and constant energy E.

- Canonical Ensemble (NVT): Ensemble of systems, which exchange energy with a large heat reservoir. Heat capacity of the heat reservoir is large enough to

maintain constant temperature for the coupled system. The thermodynamic state of the system is characterized by constant number of atoms, N, constant volume,V and constant temperature, T.

- Isobaric-Isothermal Ensemble (NPT): Ensemble of systems, which exchange energy with a large heat reservoir of constant temperature and the volume of systems changes in response to the applied external pressure. The thermodynamic state of the system is characterized by constant number of atoms, N, constant pressure, P and constant temperature,T.

d. Space Time Correlation Functions

Molecular Dynamics simulations provide information about the position, velocity and acceleration of the atoms of a given system over time. So in essence, MD simulations give the apace and time evolution of the system. This time evolution of the system can then be used to determine a number of dynamic properties using the space time correlation functions. If A and B are two variables dependent upon the momentum and position (p, q) of atoms, the time correlation function of variables A and B is defined as

$$C(t) = \langle A(0)B(t)\rangle = \int\int f(p,q)A(p,q:0)B(p,q:t)dpdq \tag{2.38}$$

$f(p, q)$ represents the equilibrium distribution of p and q. When A and B are equal the correlation is called autocorrelation function.

The most famous autocorrelation function is the velocity autocorrelation function. For a velocity autocorrelation function both A and B are equal to the velocity of the atoms of the system and is defined as

$$C(t) = \langle V(0).V(t)\rangle \tag{2.39}$$

Taking Fourier transformation of the velocity correlation function reveals important information regarding the frequency dependent properties such as diffusion of particles in the system, density of states of phonons and vibration spectrum of the atoms. Since in molecular dynamics velocities are known at each time step, the complications related to the dependence of velocities on the position and momentum are avoided. So for the sake of calculations, the velocity autocorrelation function can be written as

$$C(t_k) = \langle V(0).V(t_k) \rangle \tag{2.40}$$

k subscript is added as the time is quantized into discrete steps. Also usually in calculating the correlation function, a group of atoms is considered and since the equilibration is done after minimization, the autocorrelation function does not need to start from time zero. Also to better visualize the results, usually the autocorrelation function is normalized with respect to the initial value. Taking all these convections and approximations into account, for a group of N atoms the normalized velocity autocorrelation function is defined as

$$\widehat{C}(t_k) = \frac{C(t_k)}{C(0)} = \frac{\sum_{i=1}^{N} V_i(\tau) V_i(\tau + t)}{\sum_{i=1}^{N} V_i(\tau) V_i(\tau)} \tag{2.41}$$

Fourier transform of this velocity autocorrelation function represents the spectral density of the atomic motions, which can then be used to determine the dominant modes of vibrations.

C. Interfacial Thermal Resistance

The interfacial thermal resistance represents a barrier to the heat flow at the boundary between two phases or two dissimilar materials. The existence of thermal resistance at the interface was first reported by Kapitza, with his measurements of the temperature drop at the interface between Helium and a solid [54]. So the interface thermal resistance is also known as Kapitza Resistance. For a temperature drop of ΔT at the interface, the heat flux J_Q, is related to the Kapitza resistance, R_k, as

$$R_k = \frac{\Delta T}{J_Q} \tag{2.42}$$

The inverse of interface resistance R_k is called interfacial conductance and is usually denoted by Λ. So interfacial conductance is analogous to bulk conductivity in a macroscopic system. For a matrix system with constant thermal conductivity (λ), the Kapitza length (L_k) is defined as

$$L_k = R_k \lambda \tag{2.43}$$

Kapitza length is the equivalent thickness of matrix, with the same thermal conductivity λ, over which the drop in temperature is same as the drop at the interface. Kapitza length gives an idea of the relative importance of the interfacial resistance.

Khalatnikov [55] presented a model known as Acoustic Mismatch (AM) Model, to explain and estimate the thermal resistance at the boundaries to Helium. According to this model, interfacial thermal resistance is due to the mismatch in the acoustic impedances of two dissimilar materials at the interface. Mazo [56] proposed the modern form of AMM. They applied acoustic theory and approximated liquid helium and the solid as a continuous elastic medium. Classical wave propagations equations were used to determined the transmission and reflection coefficients for phonons. Plane

wave solution founded in the two mediums were matched at the boundary. By imposing displacement and stress boundary conditions and assuming no scattering takes place at the interface, transmission coefficient, t_{AB}, for phonon energy in material A incident normal to the interface of material B is given by

$$t_{AB} = \frac{4Z_A Z_B}{(Z_A + Z_B)^2} \tag{2.44}$$

where $Z = \rho c$ is acoustic impedance, ρ is the mass density and c is the speed of sound in the material [56]. The transmission coefficient is ratio of the total flux in the transmitted wave to the incident wave. Using this model the authors predicted the boundary resistance of the order of $1000 cm^2 K/W$ at 1K and varies as T^{-3}. Little [57] extended the acoustic mismatch model for to solid-solid interface. They showed that for a perfectly joined interface the heat flow is proportional to the difference of the fourth powers of the temperature on each side of the interface but results deviate for rough surfaces and for surfaces pressed into contact with one another. Experimentalists observed that the Kapitza resistance is 2 orders small than predicted by AMM theory at 1K, but thermal resistance between solids was higher than calculated for the AMM theory perposed by Little. Lee and Fairbank [58] and Anderson et al [59] measured boundary resistance between cooper and He^3 and found similar magnitude and temperature dependence to that found for a copper-superfluid He^4 boundary. Anderson et al also found lower magnitudes of boundary resistance between between solid He^3 or liquid He^4 and copper. According to AMM boundary resistance is a strong function of pressure however the authors found that boundary resistance is affected by pressure only near 0.1K; around 1K it is independent of pressure. Challis et al [60] proposed transmission increase due to the existence of compressed layer of liquid on the surface of the solid formed due to the van der Waal's attraction of liquid atoms to the solid. Matsumoto et al [61] measured thermal

resistance across cooper-epoxy-cooper sandwiches over a temperature range of 0.05-10K. Their data also supported the suggestion that low-frequency phonons contribute to thermal transport across the sandwich. They showed that thermal resistance between solid-solid interface can match AMM theory results depending upon the surface preparation. Shiren [62] found that resistance of a defective interface is much higher than a clean one. Swartz et al [63] measured boundary resistance from 0.6 to 200K between metal films and dielectric substrates onto which the films were deposited. The authors demonstrated that at low temperatures, below 40K, the results were in good agreement with the AM model but at higher temperature the results vary significantly. They also found that other than carefully prepared surfaces, phonons in the frequency range above a few gigahertz strongly scattered at all the surfaces. So in order to estimate the effect of diffuse scattering, they proposed the diffuse mismatch model (DMM). In contrast to AM, diffuse mismatch (DM) model all phonons striking an interface scatter to one side or other side of interface with the probability that is proportional to the phonon density of states. Thus both models assume the interface without any intrinsic properties and so the structure of the interface does not effect the energy transmitted. In essence these theories assume phonon transmission to be completely specular without scattering or diffuse scattering without any dependence on angle of incidence. So none of the two models is able to predict the precise value of the interfacial resistance, but they provide a good reference against which to compare the experimental results.

D. Simulations of Interfacial Thermal Resistance

Interfacial thermal resistance between dissimilar materials has been experimentally studied quite extensively since its first introduction by Kapitza. Based on the exper-

imental results AMM and DMM theories were developed to explain the phenomenon of interface thermal resistance. Experimental results have shown that the interfacial resistance is affected by the surface conditions but these theories do not take surface conditions into account. Numerical simulations have been used to fill in the gap between the experimental results and the theoretical analysis. Maris and others [64, 65] used traditional lattice dynamic simulations to study the thermal boundary resistance between two dissimilar solids. Numerical calculations were performed to obtain the phonon transmission coefficient and group velocity, which were then used to obtain the phonon flux density across the interface. From the phonon flux density, Kapitza resistance is obtained. But these calculations are limited only to simple interfaces and are not a viable approach for grain boundary problems. To handle complex problems like grain structures, molecular dynamics simulations were devised. Molecular dynamics methods were well established for the calculations of thermal conductivity. Using equilibrium models, Green-Kubo method [66, 67, 68], and non-equilibrium direct methods [69, 70], molecular dynamics methods can be used to calculate the thermal conductivity of the materials at the atomistic level. However, only non-equilibrium methods can be employed to calculate the interfacial thermal resistance.

To calculate the interfacial thermal resistance using non-equilibrium molecular dynamics (NEMD) simulations a thermal current is created in the system. There are two approaches to create a thermal current in the system. The first approach is the constant heat flux method in which equal amount of energy is added and removed from two plates of the system as shown in Figure 9.

The most popular methods used to add or remove energy from the system was developed by Jund and Jullien [69]. In this method, the energy is added or removed from the system by scaling the instantaneous velocities of the atoms at discrete time

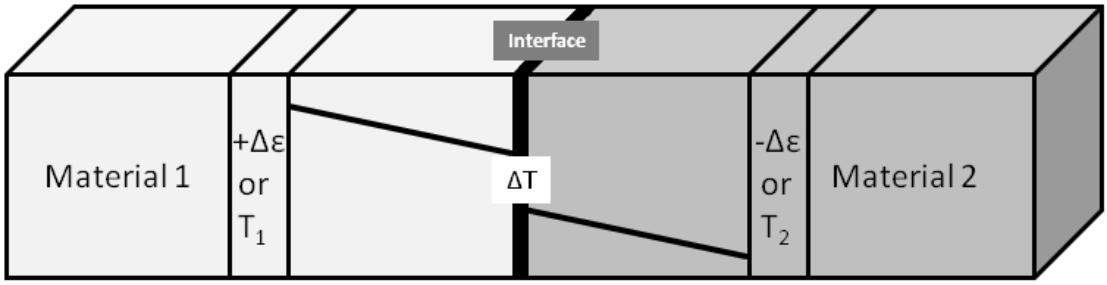

Fig. 9. Basic schematic used for performing the non-equilibrium molecular dynamic simulation. $\triangle\varepsilon$ denotes the heat added or removed from the system in constant heat flux simulations and T_1 and T_2 denotes the fixed high and low temperatures for constant temperature simulations.

steps as

$$\overrightarrow{v}_i = \overrightarrow{v}_g + \alpha(\overrightarrow{v}_i - \overrightarrow{v}_g) \tag{2.45}$$

where $\overrightarrow{v}_g$ is the velocity of the center of mass of the particles in the plate and

$$\alpha = \sqrt{1 \pm \frac{\triangle\varepsilon}{KE}} \tag{2.46}$$

$+$ sign is used for atoms in the hot plate and $-$ sign for atoms in the cold plate, $\triangle\varepsilon$ is the amount of energy added or subtracted from the plates and usually taken as 1% of k_BT to introduce only small temperature gradients within the system . The relative kinetic energy is given by

$$KE = \frac{1}{2}\sum_{i=1}^{n} m_i \overrightarrow{v}_i^2 - \frac{1}{2}\sum_{i=1}^{n} m_i \overrightarrow{v}_G^2 \tag{2.47}$$

A second method to add and remove energy from the system was proposed by Muller-Plathe [70]. In this method the velocity of the fastest atom in the cold plate is exchanged with the velocity of the slowest atom in the hot plate. In this way, energy is added to the hot plate and same amount of energy is removed from the cold plate. Additional calculations to sort the velocities have to be performed to get the slowest and the fastest atoms.

The second approach to create thermal current in the system is by keeping the two plates at different temperatures. One plate is kept at higher constant temperature and the other at lower constant temperature. The difference in the temperatures leads to a thermal current in the system as heat flows from hot plate to cold plate. As the heat flows from hot plate to cold plate, the temperature of hot plate decreases and that of cold plate increases. The temperature of the plates is kept constant by either scaling the velocities of the atoms in the plate or by using a temperature thermostat. Murad and Puri [20] used Gaussian thermostat to keep the temperatures of the plates constant while simulating the effect of pressure and surface wetting on the interfacial thermal resistance between the Si crystal and water molecules. Cummings et al [71] used the velocity scaling method to keep the temperatures of the plates constant while studying the thermal conductivity in Y-junction nanotubes and the effect of defects in straight nanotubes.

In velocity scaling procedure, the desired temperature is reached by scaling instantaneous velocities of the atoms in a plate at discrete time steps as

$$v_{i,new} = v_{i,old}\sqrt{\frac{T_{desired}}{T_{current}}} \tag{2.48}$$

where $v_{i,new}$ is the new velocity of the i^{th} atom, $v_{i,old}$ is the old velocity of the i_{th} atom, $T_{current}$ and $T_{desired}$ are current and desired temperature of the plate carrying the i^{th} atom. The amount of energy added to the hot plate and subtracted from the cold plate is equivalent to the net change in the kinetic energy of the atoms in that plate and is given as

$$\triangle E_{plate} = \frac{1}{2}\sum_{i=1}^{n} m_i(v_{i,new}^2 - v_{i,old}^2) \tag{2.49}$$

where m_i is the mass of i^{th} atom in the plate, n is the number of atoms in the plate, assuming all the atoms in a given plate have same mass, i.e. for mono-atomic

systems. Then the heat flux in the system is calculated from the average energy added or removed from the hot and cold plates over the period of the data collection as

$$J = \frac{1}{2A} \frac{\sum_{i=1}^{N} | \triangle E_{hot,plate} + \triangle E_{cold,plate}|}{t} \tag{2.50}$$

where N is the number of velocity rescaling operations performed during the simulations, A is the cross-section area of the system, perpendicular to the flow of heat flux and t is the total time of the simulation. Since the hot and cold plates are situated in the middle of the material 1 and material 2, as shown in Figure 9, the heat flows in both the directions. So factor of $1/2$ is added to the above equation, assuming heat equally divides in both the directions.

In both these approaches, once the equilibrium is reached, the thermal conductivity of a material can be obtained using the Fourier law. Also from the temperature drop at the interface and the heat flux in the system, interfacial thermal resistance can be obtained using equation 2.42.

Originally these methods were developed to calculate the bulk thermal conductivity of the materials, but have been modified to calculate the interfacial thermal resistance. Maiti et al [72] performed the first non-equilibrium MD simulations to study the interfacial thermal resistance. This method was based on the approach used by Tenenbaum et al [73] to calculate the thermal conductivity of the materials. They studied Kapitza resistance on the Si grain boundaries by creating thermal current within the system using constant temperature plates. They also demonstrated that local equilibrium can be achieved in a small system by running simulations for a very long time. Schelling et al [74] used an approach similar to that used by Maiti et al to calculate the Kapitza resistance between three twisted Si grain boundaries. They found that increase in the structural disorder at the grain boundary leads to a

significant increase in the Kapitza resistance. Xue et al [75] studied the liquid-solid interaction using the constant temperature model. They found out that magnitude of the inter-molecular forces between the liquid and the solid atoms plays a key role in determining the interfacial thermal resistance.

Xiang et al [76] studied the role of the interface on interfacial thermal resistance in microscale and nanoscale heat transfer processes using MD simulations. They found that the thermal contact resistance increases exponentially with decreasing area of the micro contact and also increases with increasing micro contact layer thickness. They also found that the material defects increase the thermal resistance. Wang and Liang [77] studied cross-plane thermal conductivity and interfacial thermal resistance between bilayered films using non-equilibrium MD simulations. The bilayer films consists of argon atoms and another material identical to argon but with different atomic mass. The results showed large temperature jump at the interface suggesting important role of interfacial resistance to heat transfer. They found interfacial resistance to be dependent on the mass ratio of the atoms but independent of the film thickness. Murad and Puri [20] studied the effect of pressure and liquid properties on the interfacial thermal resistance. They found that high fluid pressure and hydrophilic surfaces facilitates better acoustic matching and thus decrease the interface resistance.

Maruyama et al [78] performed the first molecular dynamic simulations to study the interfacial thermal resistance between carbon nanotubes in a bundle. They calculated the resistance as $6.46 \times 10^{-8} m^2 K/W$. Zhong and Lukes [79] studied the dependence of the interfacial thermal resistance between two carbon nanotubes as a function of nanotube spacing, overlap and length. From the simulations they found that there was a fourth order of magnitude reduction in the interfacial thermal resistance if the nanotubes are brought into intimate contact. The resistance was also

reduced for longer nanotubes and nanotubes with more overlap area. They attributed the increase to the increase in area available for heat transfer between the nanotubes. Greaney et al [80] employed MD simulations to elucidate the factors responsible for heat transfer between carbon nanotubes. Their calculations showed that sharp resonance between nanotubes allows efficient energy transfer.

Huxtable et al [21] made transient absorption measurements on individual single-walled carbon nanotubes encased in cylindrical micelles of sodium dodecyl sulphate (SDS) surfactant, dispersed in D_2O to study nanotube-matrix interface resistance. Ti:sapphire mode-locked laser was used to produce a series of subpicosecond pulses with wavelength in the range of 740 - 840 nm. The decay constant of 45ps was calculated for the heat flow from the carbon nanotube to SDS corresponding to interfacial resistance of $8.04 \times 10^{-8} m^2 K/W$. Shenogin et al [81] studied the interfacial thermal resistance between the carbon nanotubes and octane molecules surrounding it. They found a large value of interfacial thermal resistance and the resistance was found to decrease as the length of the carbon nanotubes increased and then stabilized to a constant value. They attributed this large resistance to the weak coupling between the rigid tube structure and the soft organic liquid. Clancy and Gates [82] studied the effect of chemical functionalization of carbon nanotubes on the interfacial thermal resistance and thermal conductivity of nano-composites. They grafted linear hydrocarbon chains on the nanotube surface using covalent bonds. They found that the interfacial thermal resistance between functionalized nanotubes and the surrounding polymer matrix was reduced by the presence of the grafted functional groups. Unikrishnan et al [83] studied the effect of chemical additives like CuO on the carbon nanotubes suspended in water. There was a marginal increase in the resistance with the addition of impurities in the water. Recently Carlborg et al [84] studied thermal boundary resistance between single-walled carbon nanotube and matrices of solid

and liquid argon by performing classical molecular-dynamics simulations. They found that the resistance does not depend on the length of the nanotube of length greater than $20\mathring{A}$. Also they suggested that resonant coupling between the low-frequency modes of the carbon nanotube and the argon matrix are responsible for heat transfer from the carbon nanotube to the matrix molecules.

CHAPTER III

METHODOLOGY

These simulations are based upon the lumped capacitance analysis. This analysis is applicable to any system which has a very small Biot's number. Biot number is defined as

$$Bi = \frac{hL}{k} \tag{3.1}$$

where h is the heat transfer coefficient at the interface, L is the characteristic length of the system and k is the thermal conductivity of the solid. In essence, this analysis is applicable for systems in which the thermal gradients within solid body are negligibly small as it cools with time i.e. for a body that has a very high thermal conductivity. Also the characteristic length is small and the coefficient of heat transfer from the solid body to the surrounding fluid is also small.

Carbon nanotubes have very high thermal conductivity. So the temperature gradients within the carbon nanotube are negligibly small. Consider a system with carbon nanotube at temperature T_{hot} surrounded by fluid with temperature T_{cold}. The pool of liquid is large enough such that it remins at T_{cold}. Let m be the mass of the nanotube, c is its specific heat, A_s the surface area and G the interfacial conductance (inverse of interfacial resistance), then mathematically

$$mc\frac{dT}{dt} = -GA_s(T - T_{cold}) \tag{3.2}$$

At time $t = 0$ the temperature of the object is T_{hot} and cold fluid is T_{cold} and after time t the temperature of the hot object is T (assuming bulk temperature of the fluid remains unchanged). Integrating above equation from time $t = 0$ to t, we get

$$T - T_{cold} = (T_{hot} - T_{cold})\ exp\left[-\frac{GA_s}{mc}t\right] \tag{3.3}$$

or this equation can be written as

$$\triangle T(t) = \triangle T_{initial}\ exp\left[-\frac{t}{\tau}\right] \tag{3.4}$$

where τ is the thermal time constant. The solution indicates that the difference in the temperature of solid and fluid, $\triangle T(t)$, approaches zero as the time approaches infinity. The quantity $C = \frac{mc}{A_s}$, heat capacity per unit area, is constant for carbon nanotube [21]. So, once we know the time constant we can find the interfacial thermal resistance using the following equation.

$$R_k = \frac{\tau}{C} \tag{3.5}$$

The flow chart, Figure 10, shows the simulation procedure to calculate the interfacial thermal resistance using molecular dynamics simulations. Each step is described below. All the simulations are performed using the LAMMPS software [85, 86]. LAMMPS stands for Large-scale Atomic/Molecular Massively Parallel Simulator. LAMMPS is a classical open source molecular dynamics simulation code to be used as particle simulator at the atomic, meso, or continuum scale. It was originally developed in FORTRAN and later ported to C++. It uses message passing interface (MPI) protocol and is designed to run efficiently on parallel computers.

A. Problem Setup

The first step in the simulation is to prepare the starting structure. The starting structure is prepared by placing the carbon nanotube at the centre of the simulation box. The axis of the nanotube are aligned along the z-axis. The matrix molecules surround the carbon nanotube. The density of the unit cell is same as the density of the bulk matrix at room temperature. Figure 11 shows a typical starting structure. The

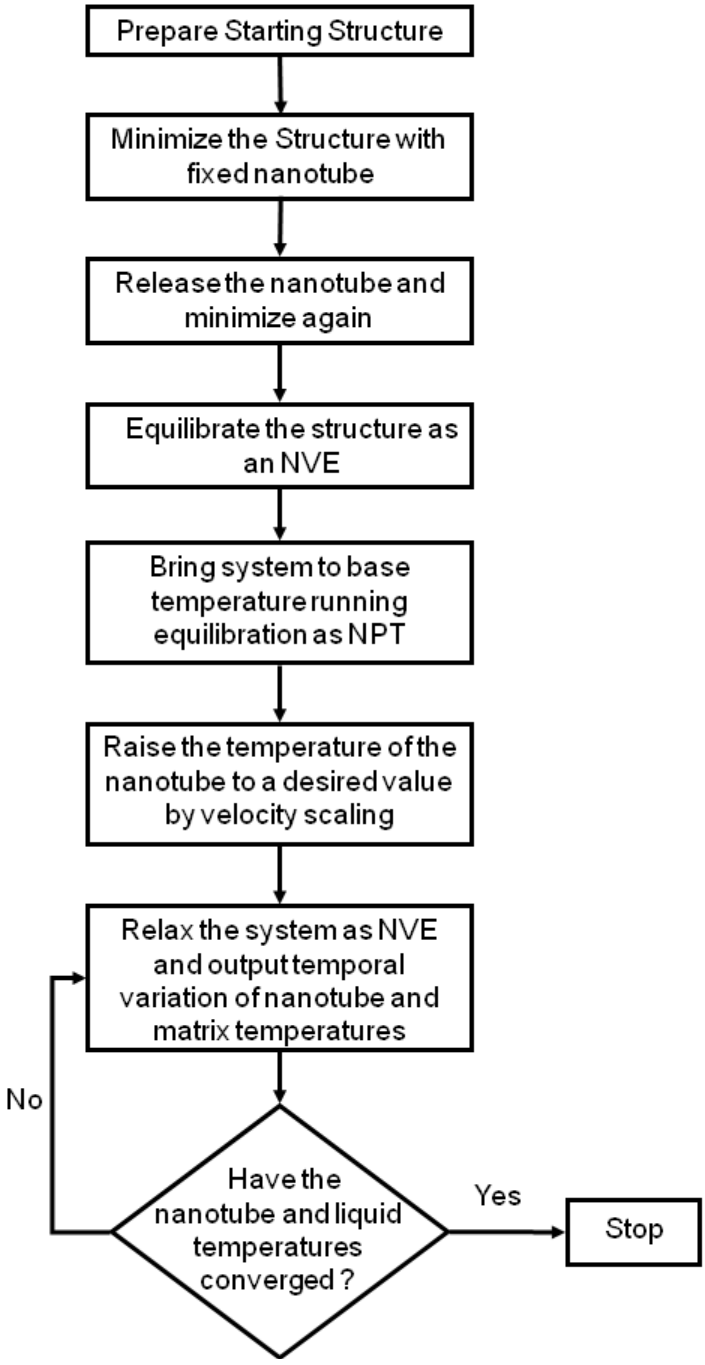

Fig. 10. Procedure to calculate the interfacial thermal resistance

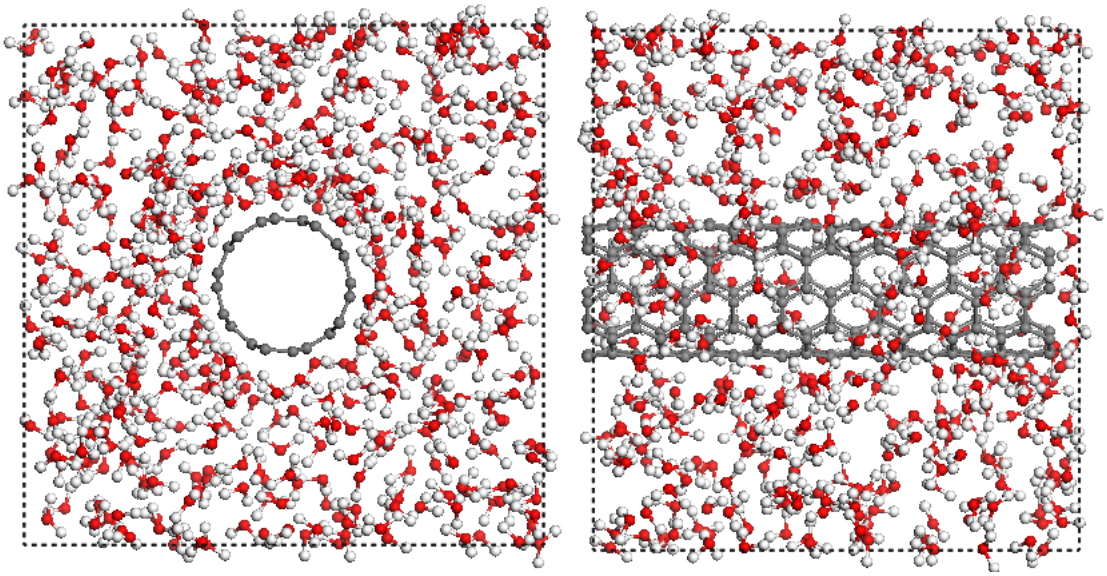

(a) Nanotube surrounded by water molecules

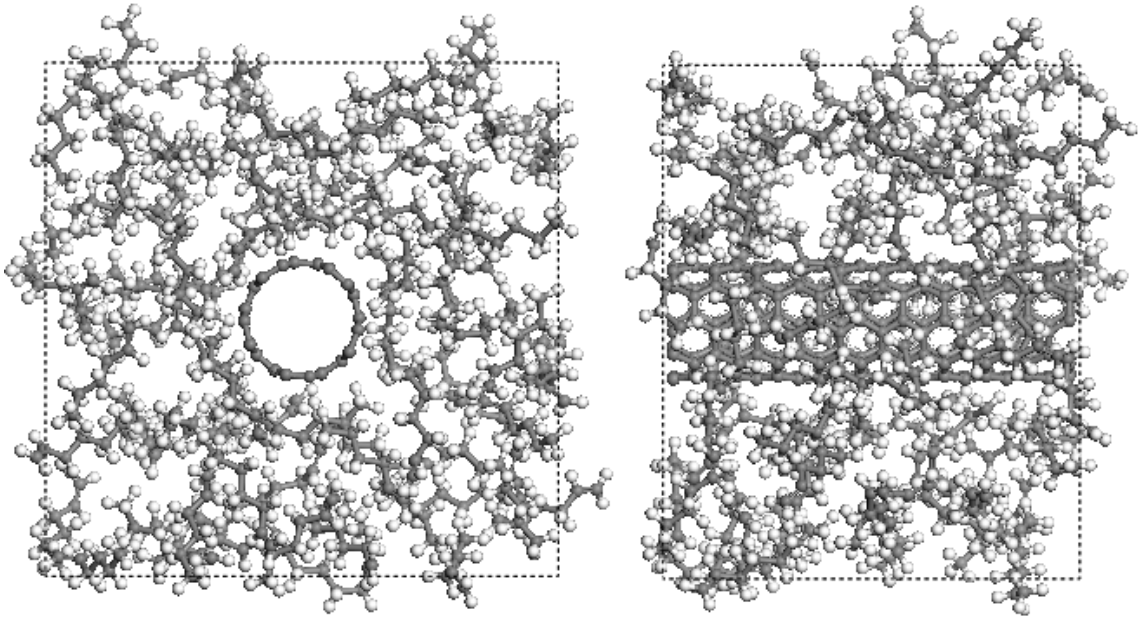

(b) Nanotube surrounded by 1-hexene molecules

Fig. 11. Typical starting structures with carbon nanotube surrounded by matrix molecules

starting structure is created using Materials Studio (MS), a commercially available software. The initial structure created by amorphous builder module of MS is not suitable for these simulations, as the nanotube axis is not aligned in the z-direction. So the structure is manually edited to align the nanotube along the z-axis and to move any matrix molecules inside the nanotube. This structure is exported and a script file converts the MS files to LAMMPS input file. This file acts as the starting input structure for LAMMPS.

B. Minimization

The starting structure is formed by randomly placing the molecules inside the simulation box. The atoms of the matrix molecules may be very close to or overlapping with atoms of carbon nanotube or other matrix molecules. If simulations are performed with this starting structure, very large forces will be exerted on the atoms, as a result imparting very high velocities to the atoms. This will cause computational instabilities. To avoid this, potential energy of the system, bonded and non-bonded energy, is minimized before running the dynamics. The kinetic energy of the system is not considered during minimization. LAMMPS uses Polak-Ribiere version of the conjugate gradient (CG) algorithm to minimize the energy [87]. In this study the minimizations is done in two steps. First the nanotube is fixed at its place and energy of the surrounding matrix molecules is minimized. Then the nanotube is relaxed and the whole system is allowed to minimize. First step is necessary, as during the structure preparation, some matrix molecules are too close to the nanotube. The proximity of these matrix molecules will dent the nanotube and distort it beyond the point of recovery. So in the first step, only the matrix molecules will move. Once the matrix molecules are at a distance from the nanotube, the nanotube is relaxed. In

this way in the final structure the nanotube is not significantly distorted.

C. Equilibration

Minimization is followed by equilibration. After minimization the system is theoretically at 0K. To start dynamics the system has to be brought to base temperature of interest, 300K. For this work, this is done in two steps. In the first step, velocities are assigned to the atoms randomly at 300K, and the system is allowed to relax as a NVE ensemble for 50ps. As the initial configuration (coordinates) is not an equilibrium one, during relaxation some of the kinetic energy is converted to potential energy. So the final temperature of the system is lower than 300K. In all the simulations, the final temperature converges to a value close to 160K. In the second step, the temperature of the system is raised from 160K to 300K by equilibrating the system as a NPT ensemble for 25ps followed by equilibrating at 300K for 250ps at a pressure of 1 atmosphere. The pressure and the temperature of the system is controlled using the Nose-Hover thermostat [88] and barostat [89]. During equilibration, pressure of 1 atmosphere is applied on the sides of the simulation box, that responds independently of the pressure component along the axis of the tube. Thus the box length can change in x and y direction, but not in the z direction.

D. Production Run

After the system is equilibrated to a uniform temperature of 300K, the temperature of the nanotube is instantaneously increased to 700K in case of n-heptane and its variants and 750K in case of other matrix systems by simple velocity scaling procedure. If T_{base} is the base temperature and $T_{desired}$ is the desired temperature, the new velocities of

the atoms, v_{new}, from the old velocities v_{old} are given by

$$v_{new} = v_{old}\sqrt{\frac{T_{desired}}{T_{base}}} \tag{3.6}$$

Subsequently the system is allowed to relax under constant energy as a NVE ensemble. As the simulation proceeds the energy from the nanotube is slowly transferred to the matrix molecules. Snapshots of the temperature distribution within the box are obtained at fixed intervals of 100 steps. Also after every 100 steps the average temperature of the nanotube and matrix molecules is calculated and stored. The simulation is terminated as the temperature of the carbon nanotube approaches the liquid temperature.

CHAPTER IV

RESULTS AND DISCUSSION

Non-equilibrium molecular dynamic simulations have been performed to study the effect of chemistry and molecular structure on the interfacial thermal resistance between a carbon nanotube and coolant molecules. The coolants considered in this study are water, ethyl alcohol, 1-Hexene, n-Heptane and its dimers, trimers and their isomers. To study the effect of the chemical composition of the coolants on the thermal interfacial resistance, the molecules considered are water, ethyl alcohol, 1-hexene and n-heptane. Also, n-heptane, n-tridecane and n-nonadecane are studied to study the effect of polymer chains (structural variations) on the interfacial resistance. Also isomers of n-heptane, n-tridecane and n-nonadecane are considered to study the effect of branching and mixtures of chains on the interfacial resistance. Figure 12, 13 and 14 shows the molecular structure of coolants considered in this study.

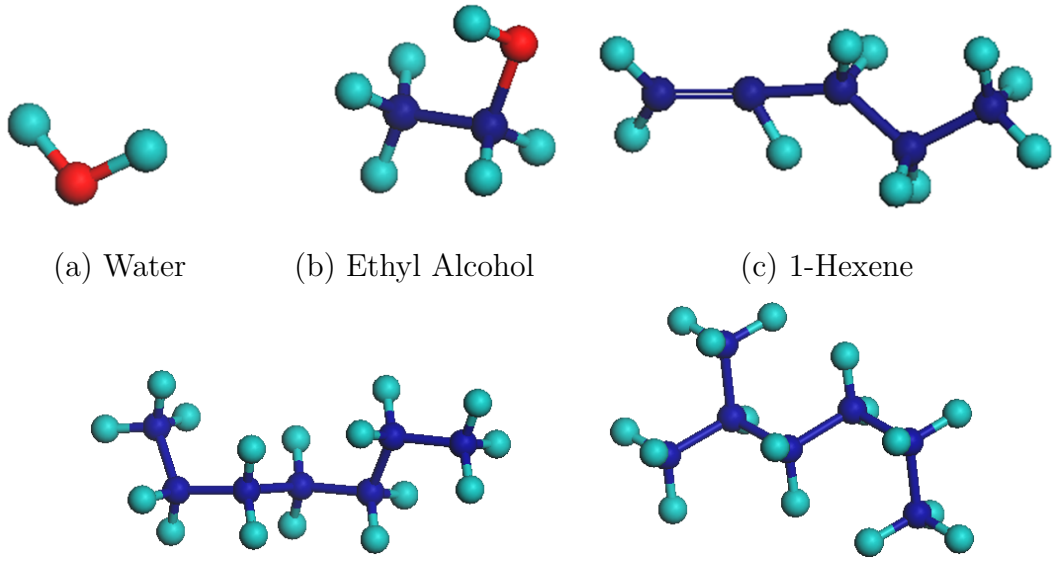

(a) Water (b) Ethyl Alcohol (c) 1-Hexene

(d) n-Heptane (e) 2-Methyl Hexane

Fig. 12. Equilibrium structure of common coolant molecules considered in this work.

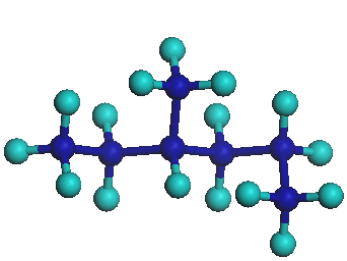

(a) 3-Methyl Hexane

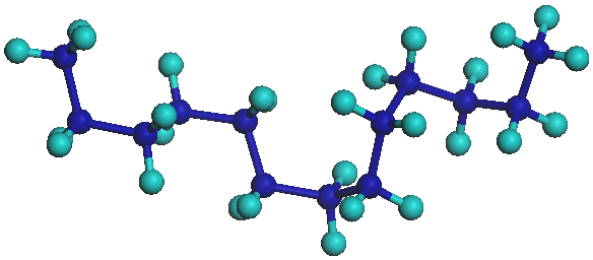

(b) n-Tridecane

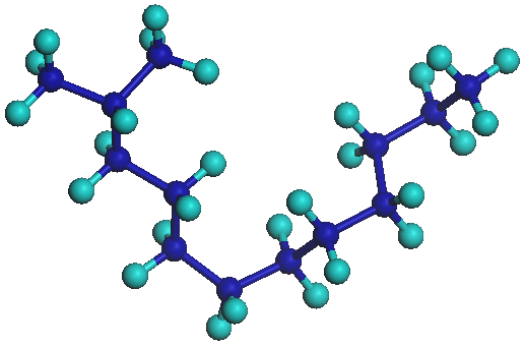

(c) 2-Methyl Dodecane

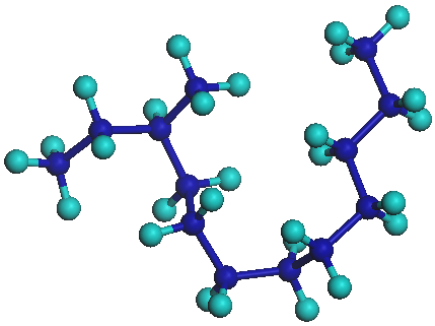

(d) 3-Methyl Dodecane

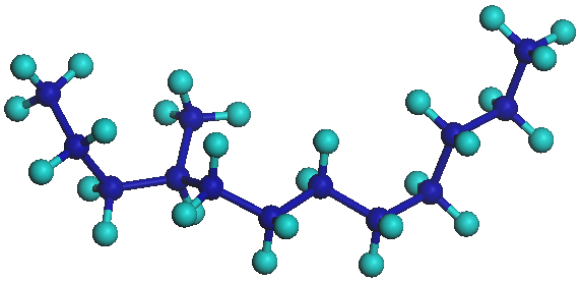

(e) 4-Methyl Dodecane

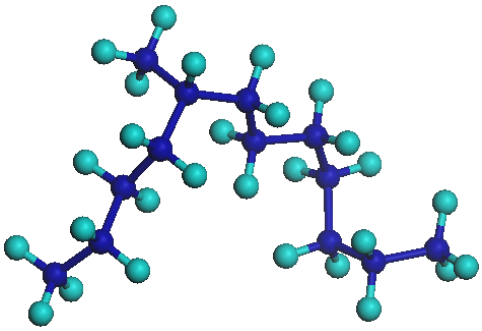

(f) 5-Methyl Dodecane

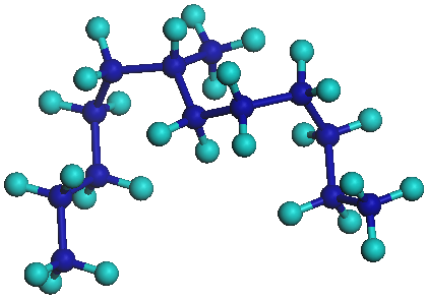

(g) 6-Methyl Dodecane

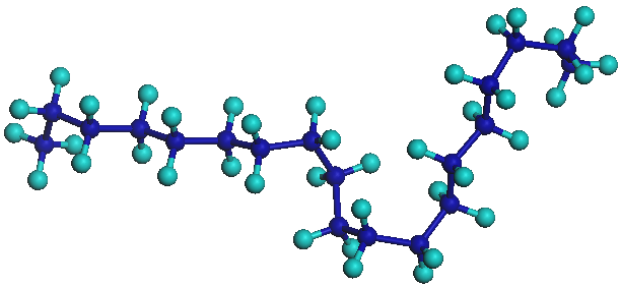

(h) n-Nonadecane

Fig. 13. Equilibrium molecular structure of isomers of n-tridecane.

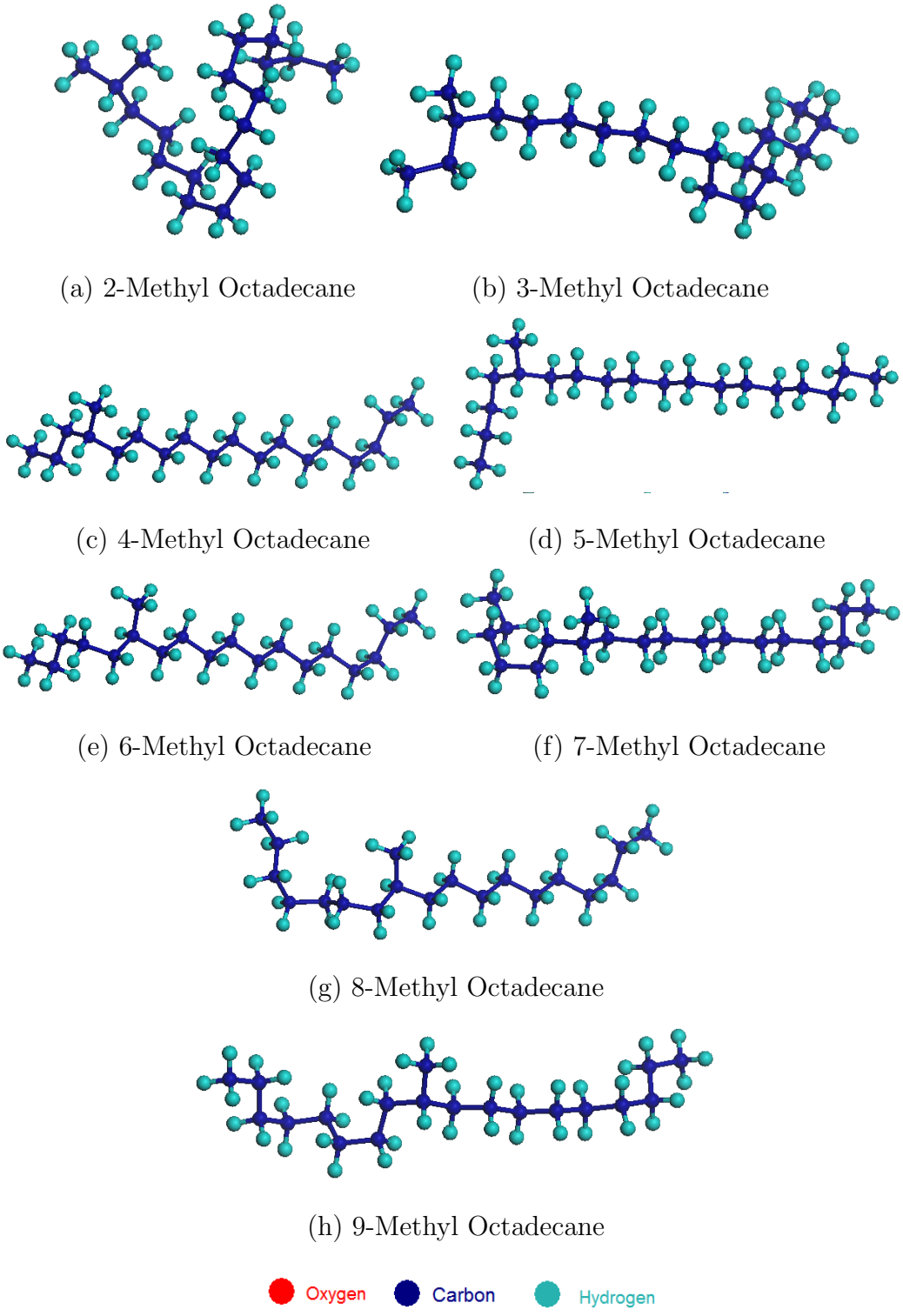

(a) 2-Methyl Octadecane

(b) 3-Methyl Octadecane

(c) 4-Methyl Octadecane

(d) 5-Methyl Octadecane

(e) 6-Methyl Octadecane

(f) 7-Methyl Octadecane

(g) 8-Methyl Octadecane

(h) 9-Methyl Octadecane

Fig. 14. Equilibrium molecular structure of n-nonadecane isomers.

A. Molecular Structure

Liquid near the solid surface is much more ordered and more dense than the bulk liquid and therefore the properties are akin to that of solid than a liquid. The liquid density exhibits molecular level oscillation in the direction normal to the liquid-solid interface [90]. With distance from the interface the density peaks to a large value followed by small oscillations and then approaches to the bulk density. The magnitude of the layering extends to a few atomic distances and strongly depends upon the solid-liquid atomic molecular mutul interaction parameters. This trend of ordering and fluctuations is observed in these simulations. All the coolants considered in this study exhibit the molecular ordering and density fluctuations near the nanotube wall. Figure 15 shows the molecular structure and the density fluctuations for n-tridecane molecule. In the molecular structure, we see clearly a gap of about 3Åbetween the carbon nanotube and the surrounding coolant molecules due to presence of the weak van der Waal's forces. Also from the figure it is clear that the atoms are densely packed at a distance of about 7 Å. This distance corresponds to the first peak density. From the spatial variation in the density, the figure shows that the oscillations occur in the density profile and later the density settles down to bulk density of the liquid at the room temperature to about $0.75 g/cc^3$.

B. Temporal Temperature Distribution

As discussed above, these simulations are based on the lumped capacitance method. The main prerequisites of the lumped capacitance with reference to these simulations are that the there should not be any temperature gradients within the carbon nanotube. The very large thermal conductivity of the carbon nanotube addresses this requirement. The other prerequisites are that the temperature of the fluid surround-

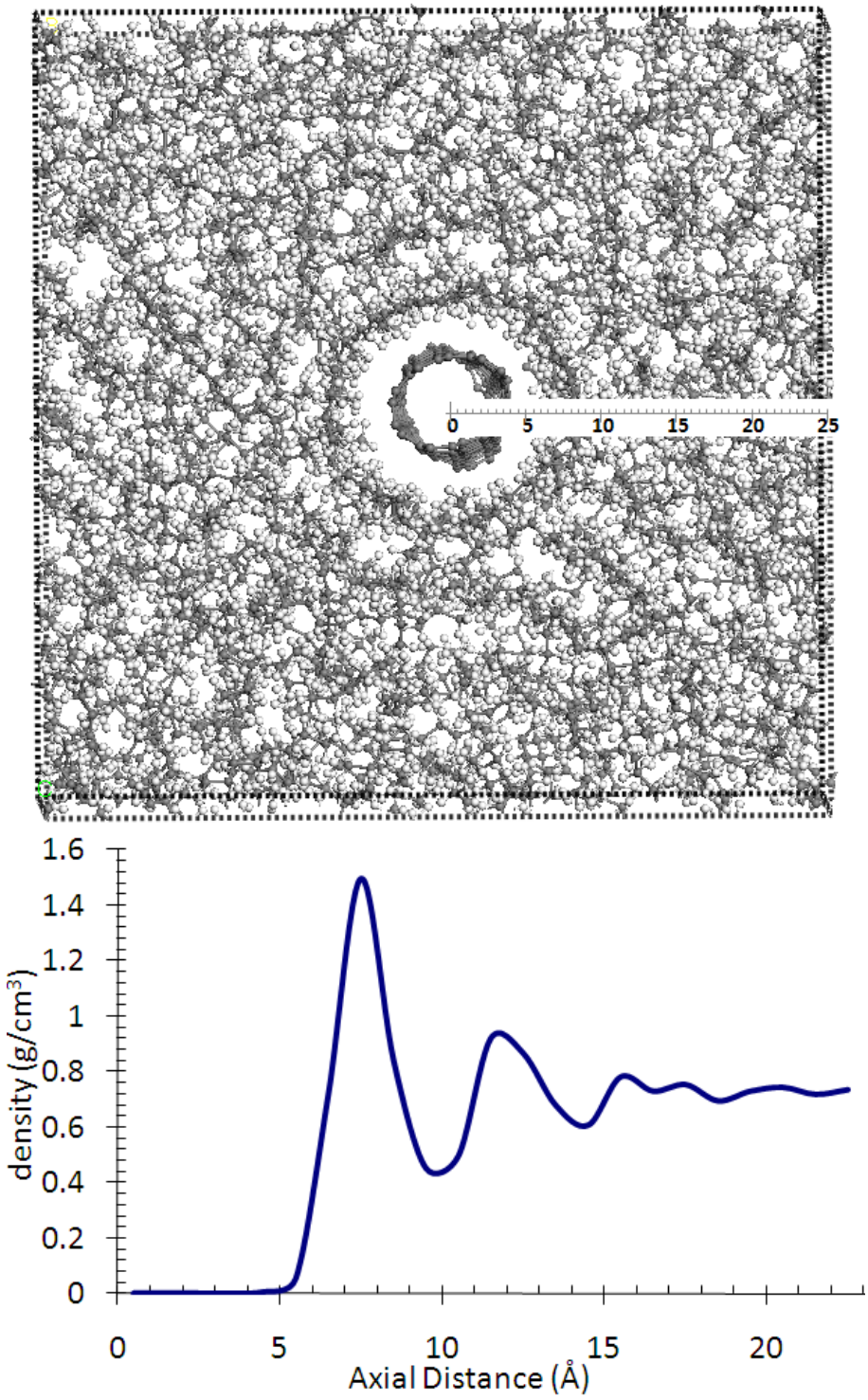

Fig. 15. (top) Molecular structure of carbon nanotube surrounded by n-tridecane at equilibrium. The scale shown is in Å(bottom) radial variation of coolant density within the simulation box

ing the nanotube should remain constant and should not vary significantly with time. Also the temporal decay of the temperature difference between the carbon nanotube and surrounding fluid is expected to be exponential. To ascertain these assumptions, temporal distribution of the temperature between the carbon nanotube and coolants is studied. Figure 16 shows the typical variation of the temperature in the carbon nanotube and surrounding fluid molecules. From the figure it is clear that the temperature of the fluid molecules remains constant. Also the temperature difference between the nanotube and the fluid is observed to decay exponentially.

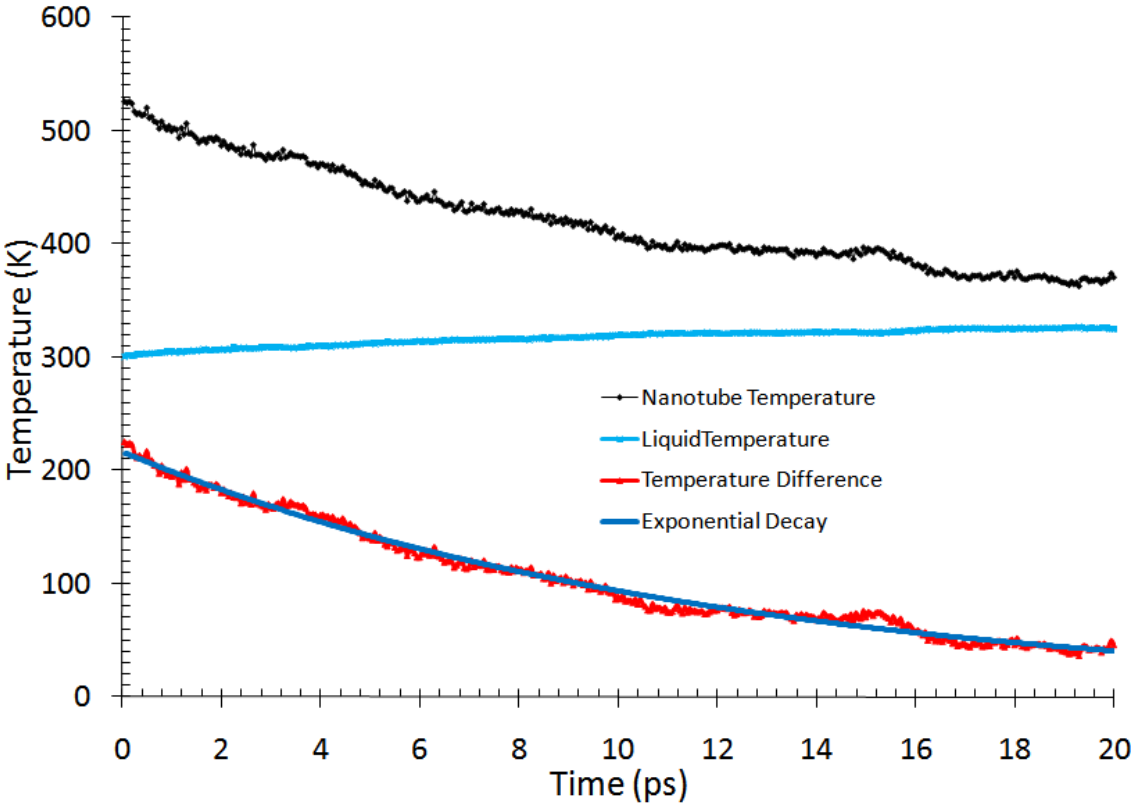

Fig. 16. Typical temporal variation of temperature of carbon nanotube and surrounding water molecules during a production run

C. Effect of Chemistry

To study the effect of chemistry on the interfacial thermal resistance water, ethyl alcohol and 1-hexene molecules are considered. Table I shows the parameters of the simulations that were used in this study. The cross-section area of the simulation box in all these simulation is $26.3 \times 26.3\mathring{A}^2$. The length of the nanotube is varied to study if the length of the nanotube has any affect. It was observed that with small nanotubes, the value of the interfacial resistance fluctuates but becomes steady for large length. Figure 17 shows the temporal variation of temperature difference

Table I. Parameters of molecules considered to study the effect of chemistry on the interfacial thermal resistance

Matrix System	No. of Matrix Molecules	No. of Atoms in CNT	CNT Length	Cross section Area (Å^2)
Water	435	200	24.6	26.3×26.3
	870	400	49.19	26.3×26.3
	1087	500	61.49	26.3×26.3
	1523	700	86.04	26.3×26.3
Ethyl Alcohol	123	200	24.6	26.3×26.3
	308	400	49.19	26.3×26.3
1-Hexene	64	200	24.6	26.3×26.3
	133	400	49.19	26.3×26.3

of carbon nanotube and fluids in this study on a semi logarithmic scale. Since the temporal decay of temperature difference is exponential, on the semi logarithmic scale the results are straight lines. Inverse of the slope of the lines give the time constant for

the temperature decay. The interfacial thermal resistance at nanotube-liquid interface is calculated as

$$R_k = \frac{\tau A_{cnt}}{C_T} \tag{4.1}$$

where τ is the relaxation time constant, A_{cnt} is the area of the nanotube, and C_T is the heat capacity of the nanotube. The heat capacity of the nanotube per unit area is usually taken as constant, $5.6 \times 10^{-4} J/m^2K$ [21].

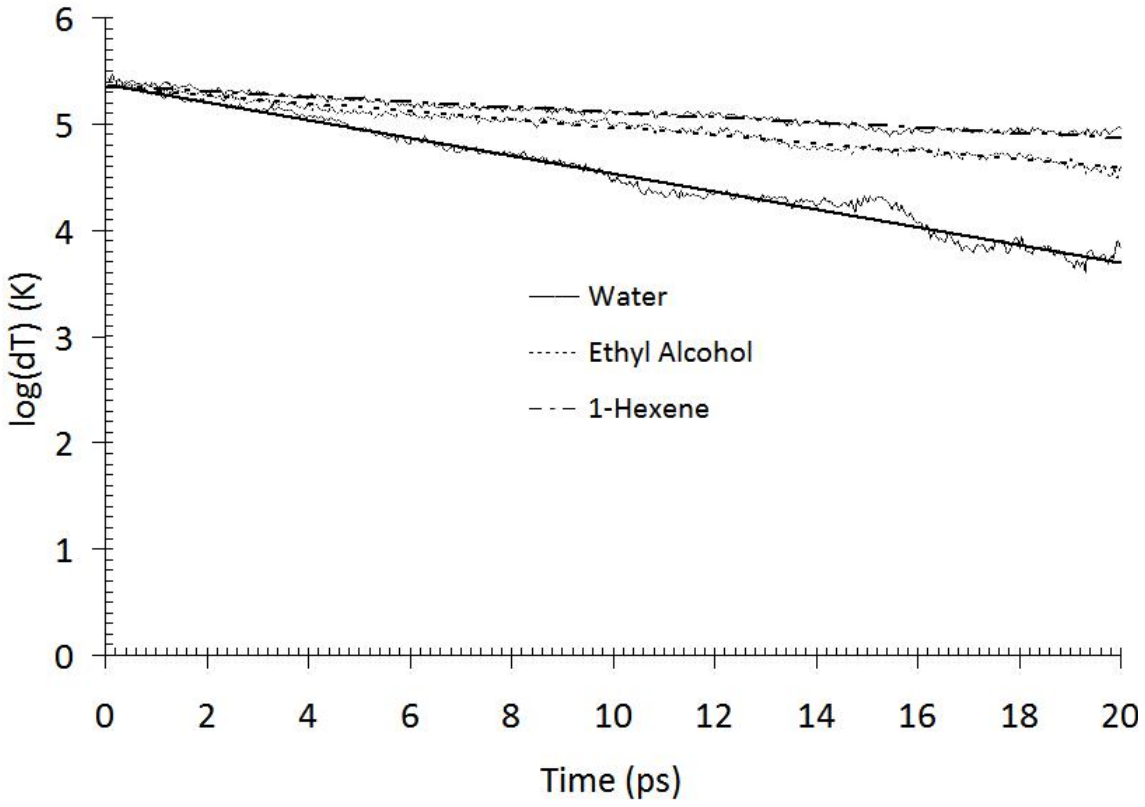

Fig. 17. Decay in temperature difference with time for water, ethyl alcohol and 1-hexene for carbon nanotube of length 49.19Å

Table II shows the time constant and interfacial thermal resistance for the molecules under consideration. The intervals of the interfacial thermal resistance have a confidence level of 99% calculated using the regression analysis. From the table it is clear that the chemical composition (chemistry) of the fluid affects the interfacial resis-

Table II. Table showing the effect of chemistry on relaxation time constant and interfacial thermal resistance

Matrix System	Relaxation Time Constant τ (ps)	Interfacial Resistance $R_k \times 10^8$ (m^2K/W)
Water	11.9	$2.13^{+0.04}_{-0.04}$
Ethyl Alcohol	26.5	$4.74^{+0.10}_{-0.11}$
1-Hexene	40.8	$7.29^{+0.20}_{-0.20}$

tance. The heat transfer from the nanotube to the surrounding fluids occurs through the weak van der Waal's interactions. These interactions depend on the chemical composition. The interaction between non-bonded carbon-oxygen atoms will be different from the non-bonded carbon-carbon interactions. The difference in these interactions leads to the difference in the interfacial thermal resistance.

D. Effect of Polymer Chains

Hydrocarbons formed by the catalytic oligomerisation of poly alphaolefins usually consists of long chain hydrocarbons like n-heptane and their dimers, trimers, tetramers etc. In this work, n-heptane and its dimer, n-tridecane and trimer, n-nonadecane are studied to elucidate the effect of polymer chains on the interfacial thermal resistance. Table III shows the parameters considered in this work.

Figure 18 shows the temporal variation of temperature difference between the carbon nanotube and fluids on a semi-logarithmic scale. Table IV shows the interfacial thermal resistance between the carbon nanotube and the fluids considered in this work. From the results it is clear that polymer chains affect the interfacial thermal resistance. Since the polymers chains are formed from the same type of atoms, the

Table III. Molecule systems and parameters considered to study the effect of polymer chains on the interfacial thermal resistance

Matrix System	No. of Matrix Molecules	No. of Atoms in CNT	CNT Length	Cross section Area (Å^2)
n-Heptane	229	200	24.6	50.0×50.0
	700	300	36.89	69.86×69.86
n-Tridecane	208	300	36.89	50.0×50.0
	749	360	44.27	88.74×88.74
n-Nonadecane	181	300	36.89	55.0 × 50.0
	700	300	36.89	99.97×99.97

Table IV. Table showing results for the effect of polymer chains on the relaxation time constant and interfacial thermal resistance

Matrix System	Relaxation Time Constant τ (ps)	Interfacial Resistance $R_k \times 10^8$ (m^2K/W)
n-Heptane	35.6	$6.35^{+0.11}_{-0.12}$
n-Tridecane	57.1	$10.20^{+0.19}_{-0.14}$
n-Nonadecane	45.9	$8.19^{+0.26}_{-0.22}$

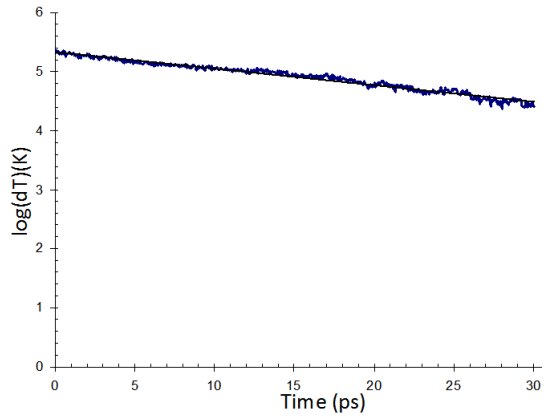

(a) n-Heptane

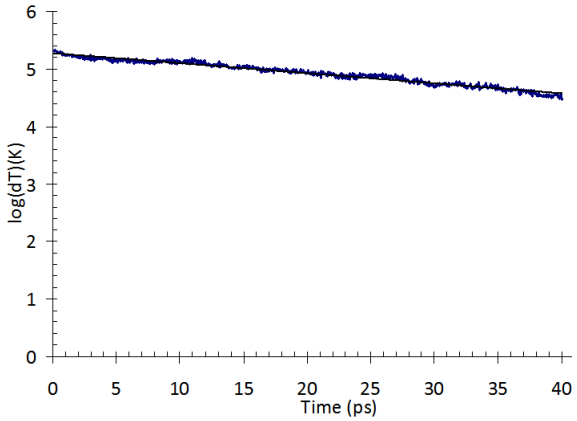

(b) n-Tridecane

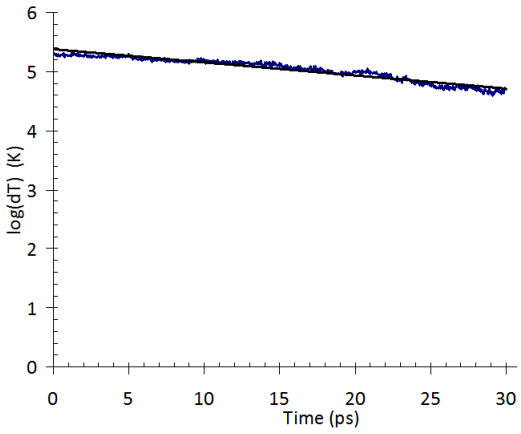

(c) n-Nonadecane

Fig. 18. Temporal decay of temperature on a semi logrithmic scale for n-heptane, n-tridecane and n-nonadecane

mechanism of heat transfer, the weak van der Waal's forces between the atom types in all the fluids will be same, it can be expected that chemical composition cannot be the cause for the difference in the interfacial resistance. From the results for n-heptane the base molecule has the lowest resistance. This is due to the fact that n-heptane is able to efficiently wrap around the carbon nanotube due to small carbon chain. In case of n-tridecane and n-nonadecane the chains are large and are not able to wrap around the nanotube as efficiently as n-heptane (stearic hindrance). Also n-nonadecane has a very long chain, which at equilibrium bends to form a chain with two legs at 90° . This type of configuration more efficiently wraps around the nanotube than a single straight chain like in the case of n-tridecane.

E. Effect of Isomers and Mixtures

To study the effect of isomers on the interfacial thermal resistance, isomers of n-heptane, n-tridecane and n-nonadecane are considered in this work. Since in the isomers the atoms of the compound are organised in different ways, the change in the structure can affect the interfacial resistance. Also the hydrocarbons produced by the catalytic oligomerisation of poly alpha olefins leaves a mixture of hydrocarbons, their isomers, dimers, trimers etc. The presence of mixtures may reduce the interfacial thermal resistance as the chains of different lengths and orientations may fit together much better than the single compounds. Table V shows the parameters of the systems of isomers and their mixtures considered in this study.

Figure 19, 20, 21 and 22 shows the temporal variation of temperatures differences between the nanotube and the fluids on a semi logarithmic scale. The calculated time constant and hence the interfacial thermal resistances using equations 4.1 are shown in Table VI. In case of n-heptane and its isomers, n-heptane has lower interfacial thermal

Table V. Parameters of molecules and their isomers and mixtures considered in this work to study the effect of isomers on interfacial thermal resistance

Matrix System	Fluid Molecules	Atoms in CNT	CNT Length	Cross section Area (Å^2)
n-Heptane	700	300	36.89	69.86×69.86
2-Methyl Hexane	336	300	36.89	50.0×50.0
3-Methyl Hexane	348	300	36.89	50.0×50.0
Mix. n-heptane isomers	342	300	36.89	50.0×50.0
n-Tridecane	208	300	36.89	50.0×50.0
2-Methyl Dodecane	700	300	36.89	88.74×88.74
3-Methyl Dodecane	209	300	36.89	50.0×50.0
4-Methyl Dodecane	209	300	36.89	50.0×50.0
5-Methyl Dodecane	209	300	36.89	50.0×50.0
6-Methyl Dodecane	209	300	36.89	50.0×50.0
Mix. of n-tidecane isomers	300	300	36.89	60.0×60.0
n-Nonadecane	700	300	36.89	99.97×99.97
2-Methyl Octadecane	700	300	36.89	101.0×101.0
3-Methyl Octadecane	700	300	36.89	101.0×101.0
4-Methyl Octadecane	700	300	36.89	101.0×101.0
5-Methyl Octadecane	700	300	36.89	101.0×101.0.
6-Methyl Octadecane	700	300	36.89	101.0×101.0
7-Methyl Octadecane	700	300	36.89	101.0×101.0
8-Methyl Octadecane	700	300	36.89	101.0×101.0
9-Methyl Octadecane	700	300	36.89	101.0×101.0.
Mixture of n-Nonadecane	639	300	36.89	100.53×100.53
and isomers	846	360	49.19	100.18×100.18

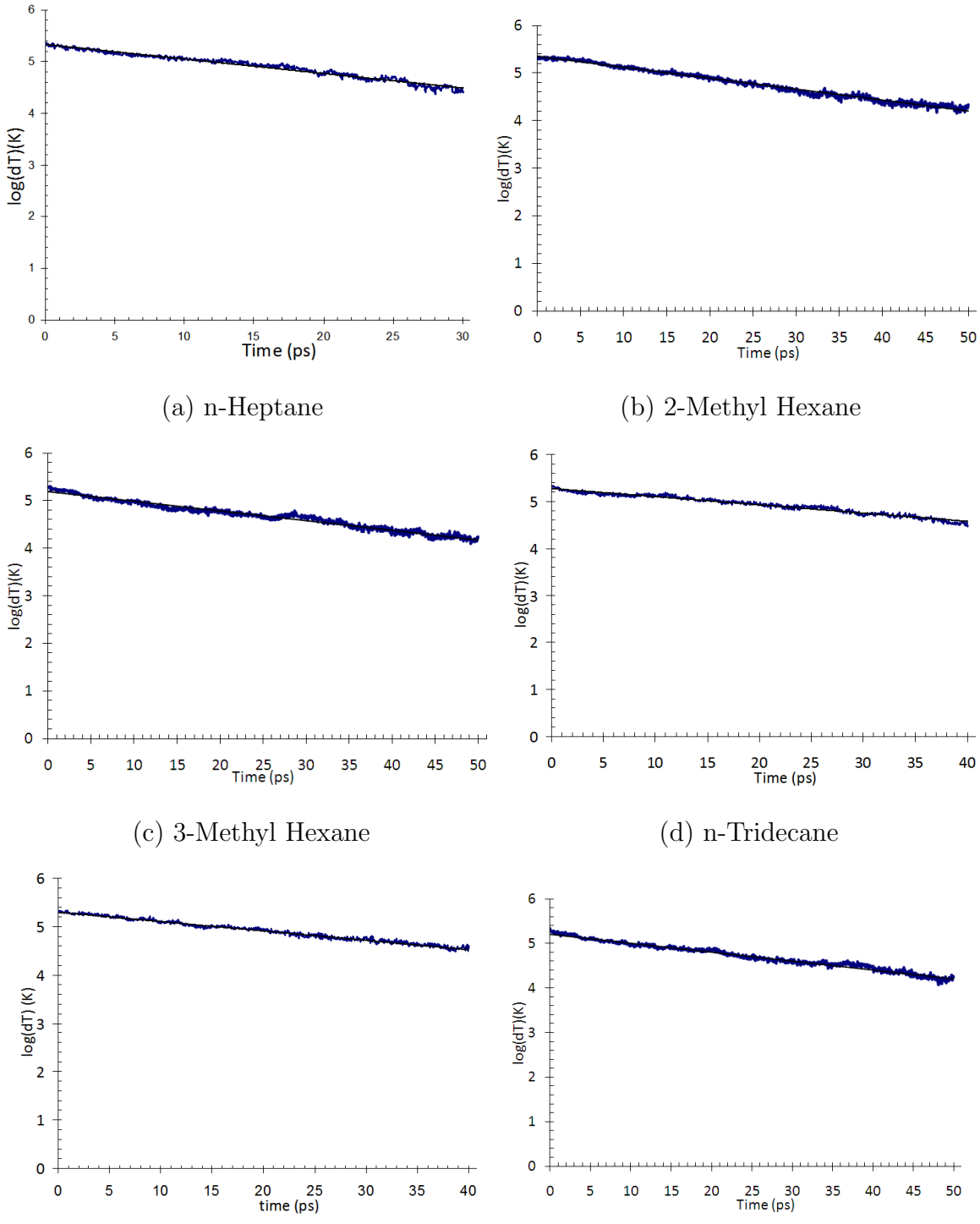

(a) n-Heptane

(b) 2-Methyl Hexane

(c) 3-Methyl Hexane

(d) n-Tridecane

(e) 2-Methyl Dodecane

(f) 3-Methyl Dodecane

Fig. 19. Temporal decay of temperature difference for n-heptane, n-tridecane and their isomers on a semi-logarithmic scale

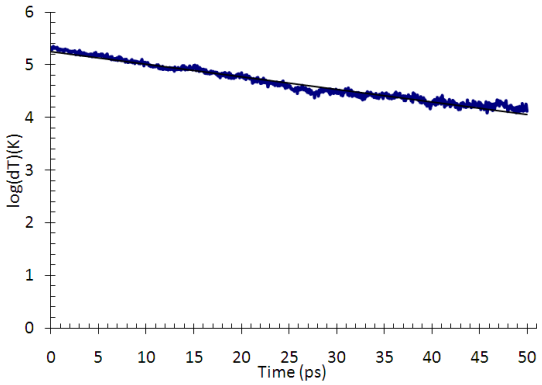

(a) 4-Methyl Dodecane

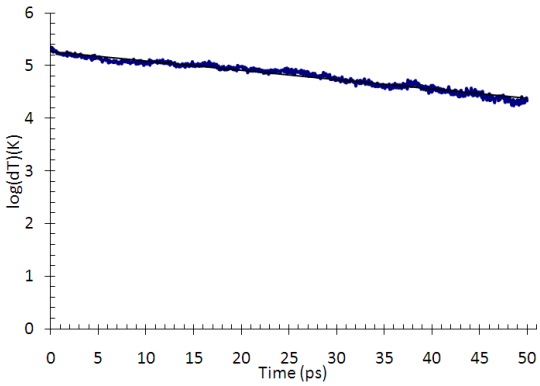

(b) 5-Methyl Dodecane

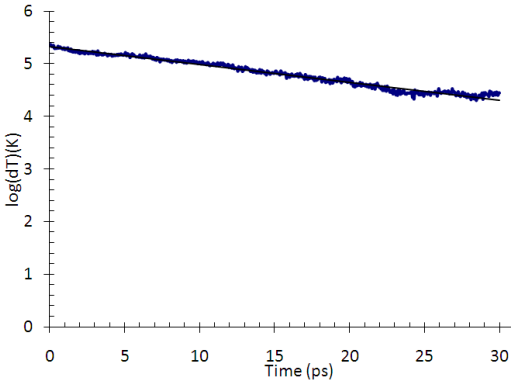

(c) 6-Methyl Dodecane

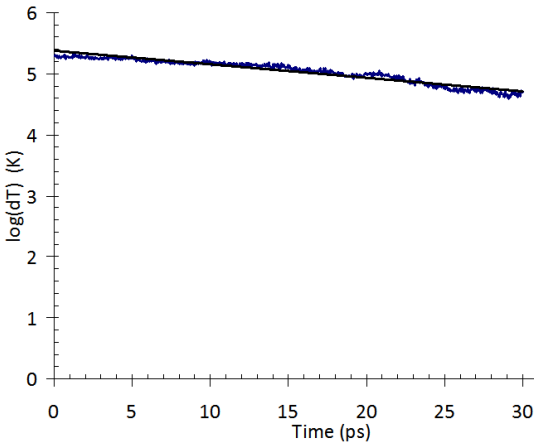

(d) n-Nonadecane

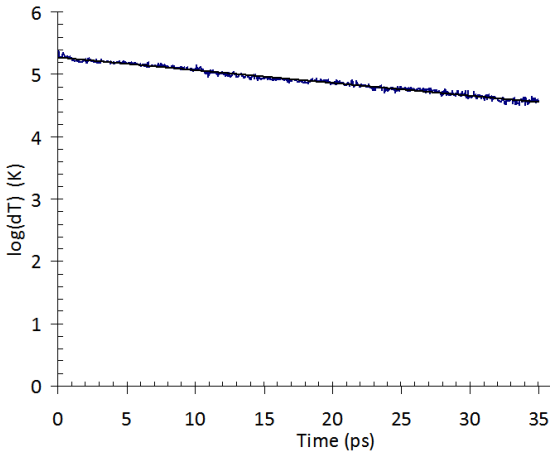

(e) 2-Methyl Octadecane

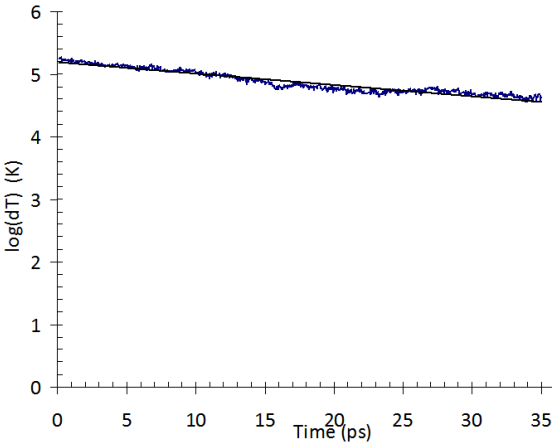

(f) 3-Methyl Octadecane

Fig. 20. Temporal decay of temperature difference of isomers of n-tridecane and n-nonadecane on a semi-logarithmic scale

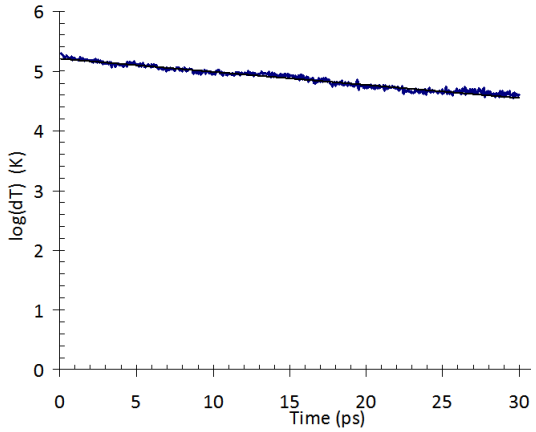

(a) 4-Methyl Octadecane

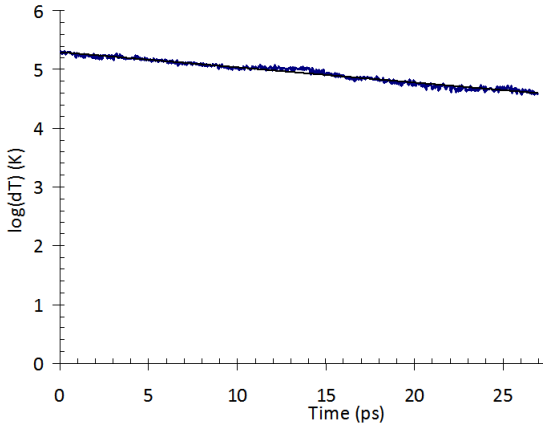

(b) 5-Methyl Octadecane

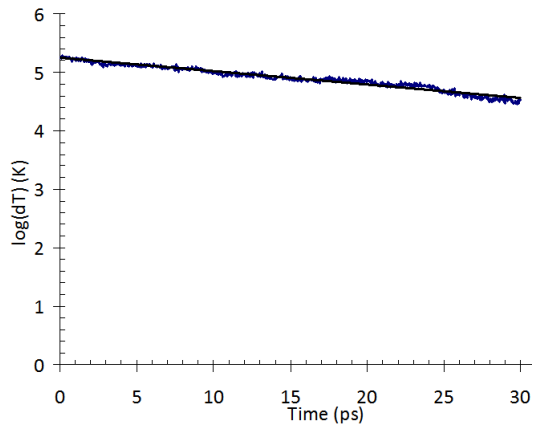

(c) 6-Methyl Octadecane

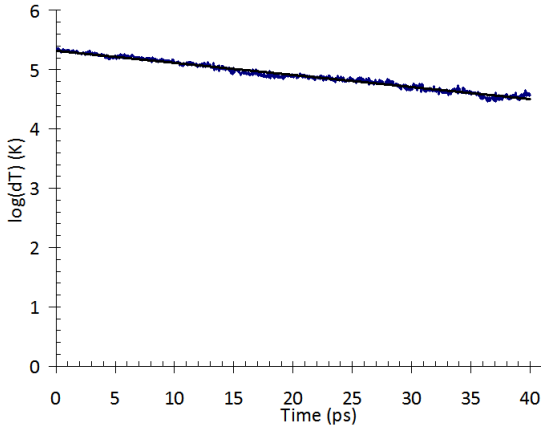

(d) 7-Methyl Octadecane

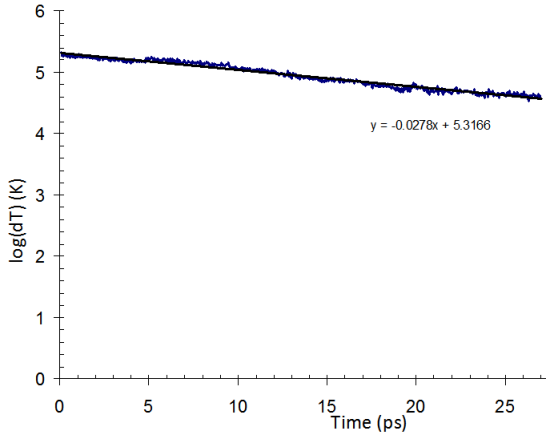

(e) 8-Methyl Octadecane

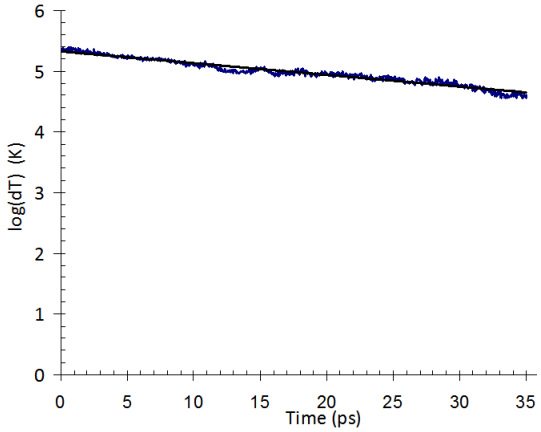

(f) 9-Methyl Octadecane

Fig. 21. Temporal decay of temperature difference for n-nonadecane isomers on a semi-logarithmic scale

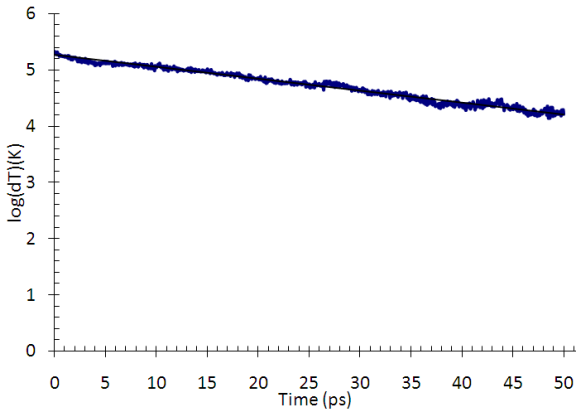

(a) Mixture of n-Heptane and its isomers

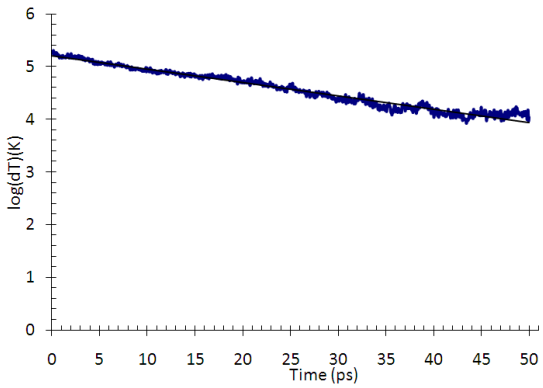

(b) Mixture of n-Tridecane and its isomers

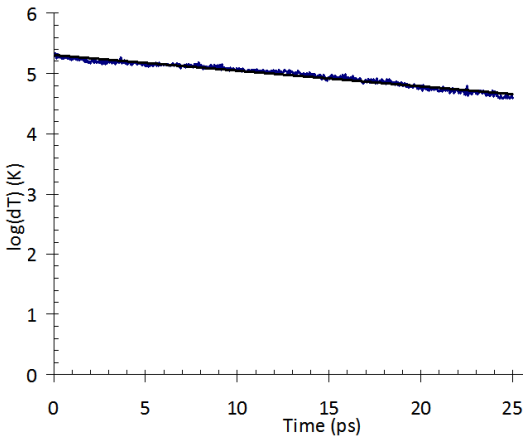

(c) Mixture of trimers

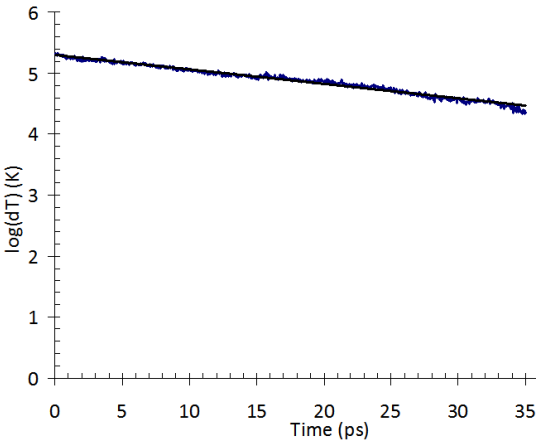

(d) Mixture of trimers

Fig. 22. Temporal decay of temperature difference of mixtures of isomers of n-heptane, n-tridecane and n-nonadecane on a semi-logarithmic scale

Table VI. Results showing the effect of isomers of molecules on the relaxation time constant and interfacial thermal resistance

Matrix System	Relaxation Time Constant τ (ps)	Interfacial Resistance $R_k \times 10^8 (m^2K/W)$
n-Heptane	35.6	$6.35^{+0.11}_{-0.12}$
2Methyl Hexane	43.2	$7.72^{+0.08}_{-0.08}$
3Methyl Hexane	49.5	$8.85^{+0.12}_{-0.13}$
Mix. of n-Heptane isomers	47.4	$8.46^{+0.09}_{-0.10}$
Tridecane	57.1	$10.20^{+0.19}_{-0.14}$
2Methyl Dodecane	51.8	$9.25^{+0.13}_{-0.09}$
3Methyl Dodecane	49.9	$8.91^{+o.11}_{-0.11}$
4Methyl Dodecane	42.1	$7.52^{+0.12}_{-0.11}$
5Methyl Dodecane	56.3	$10.06^{+0.15}_{-0.16}$
6Methyl Dodecane	37.5	$6.70^{+0.11}_{-0.12}$
Mix. of n-Tridecane isomers	39.5	$7.06^{+0.10}_{-0.10}$
Nonadecane	45.9	$8.19^{+0.26}_{-0.22}$
2Methyl Octadecane	48.5	$8.67^{+0.10}_{-0.13}$
3Methyl Octadecane	55.9	$9.98^{+0.30}_{-0.28}$
4Methyl Octadecane	46.1	$8.23^{+0.16}_{-0.17}$
5Methyl Octadecane	38.5	$6.87^{+0.15}_{-0.12}$
6Methyl Octadecane	44.2	$7.90^{+0.18}_{-0.18}$
7Methyl Octadecane	48.8	$8.71^{+0.12}_{-0.12}$
8Methyl Octadecane	36.0	$6.42^{+0.12}_{-0.14}$
9Methyl Octadecane	50.8	$9.06^{+0.07}_{-0.16}$
Mix. of n-Nonadecane isomers(22(c))	38.6	$6.89^{+0.16}_{-0.16}$
Mix. of n-Nonadecane isomers(22(d))	41.7	$7.44^{+0.10}_{-0.10}$

resistance than its isomers 2-methyl hexane and 3-methyl hexane. For n-tridecane molecule the interfacial thermal resistance is higher than its isomers. Fig. 12 shows the equilibrium molecular structure of n-heptane, n-tridecane and their isomers. From the equilibrium structure, for n-heptane and its isomers the branching of the methane group leads to steric hindrance and thus leading to ineffective wrapping of molecules around the carbon nanotube. In case of n-tridecane and its isomers the resistance decreases as the methyl group advances from first carbon atoms to adjacent atoms. As seen from the equilibrium molecular structures, n-tridecane has a long straight chain, whereas its isomers form a branched structure. Due to the branching the isomers effectively wrap around the carbon nanotubes. As a result the resistance to energy transfer form carbon nanotubes to the molecules decreases significantly. Result of the interfacial thermal resistance for 5-Methyl Dodecane is anomalous, as the resistance is much higher than the expected results.

In case of n-nonadecane and its isomers, it is difficult to deduce a trend in the interfacial resistance. We can see oscillations, as resistance increases, then decreases, and again increases and decreases as the methyl group moves away from the first carbon atom. These oscillations are attributed to the relative effectiveness of these isomer chains in wrapping around the carbon nanotube. Consider the molecular structure, 5-Methyl Octadecane has a branched structure while 6-Methyl Octadecane is nearly a straight chain. So 5-Methyl Octadecane would wrap around the carbon nanotube effectively and should have lower interfacial resistance than 6-Methyl Octadecane. As expected this trend can be seen from the simulation results in Table VI.

The mixtures also show deviation in the interfacial thermal resistance from the single molecule systems. In all the cases, however, the resistance is more than the smallest value for a single molecule but very close to it. This shows the combined effect of the individual interfacial thermal resistances. The presence of different type

of chains, with different sizes and orientations, enables the individual molecules to pack more efficiently and wrap more effectively around the nanotube. But due to the presence of all types of chains, the effective behaviour of some chains to wrap around the nanotube is countered by the ineffective behaviour of other chains. So as a system, mixtures are not as efficient as the chain with the smallest value for the interfacial resistance but allows for a value that is similar in magnitude.

F. Energy Transfer Mechanism

As discussed in Chapter II, space time correlations can be used to study the dynamic properties of a system. To study the energy transfer mechanism in a system, vibration spectrum of the atoms are analyzed. Vibration spectrum allows a physical insight into frequency modes of the systems. The vibration spectrum is generated by taking the Fourier spectrum of the velocity autocorrelation function of atoms under consideration. Fig 23(a) shows the temporal variation of normalized velocity autocorrelation function (NVACF) of carbon atoms of n-heptane molecules. The normalized velocity correlation function starts with a value of one and fluctuates around a zero value. As the simulation is run for a very long time the NVACF becomes zero indicating that equilibrium has reached. Figure 23(c) shows the vibration spectrum for the carbon atoms of n-Heptane. The peak at around 90THz corresponds to the C-H vibration modes [91, 92]. The peaks around 45THz and less corresponds to the C-C stretching and other modes of vibration such as angle change, dihedrals, stretch-stretch etc [93, 94]. The peaks corresponding to small frequencies from 0.2THz to 5THz, enhanced in Figure 23(b), corresponds to the non-bonded van der Waals interactions. These frequencies correspond to non-bonded interaction within the n-heptane molecules and also with the carbon atoms in the nanotube.

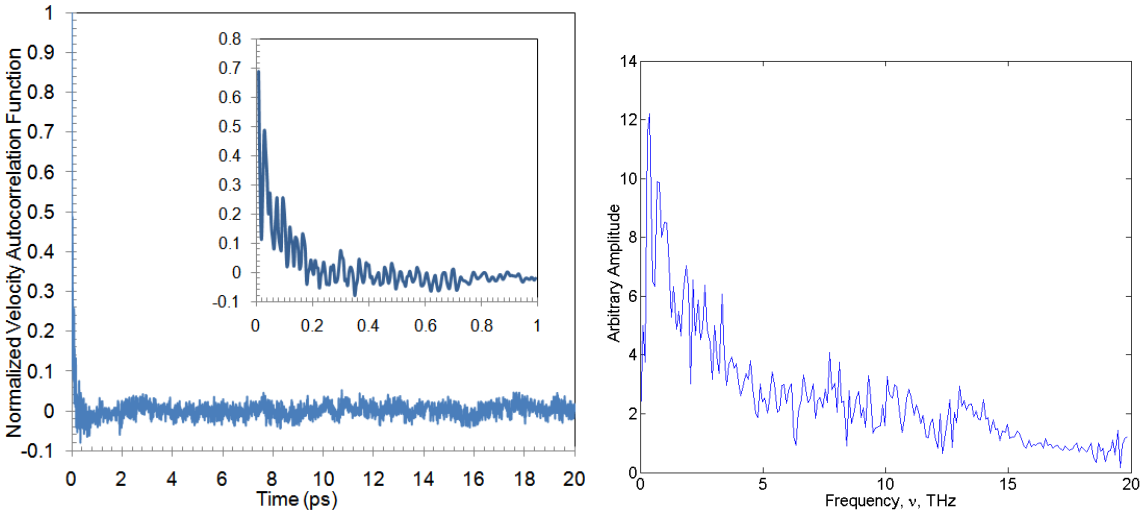

(a) Normalized auto-correlation function (b) Vibration spectrum for small frequencies

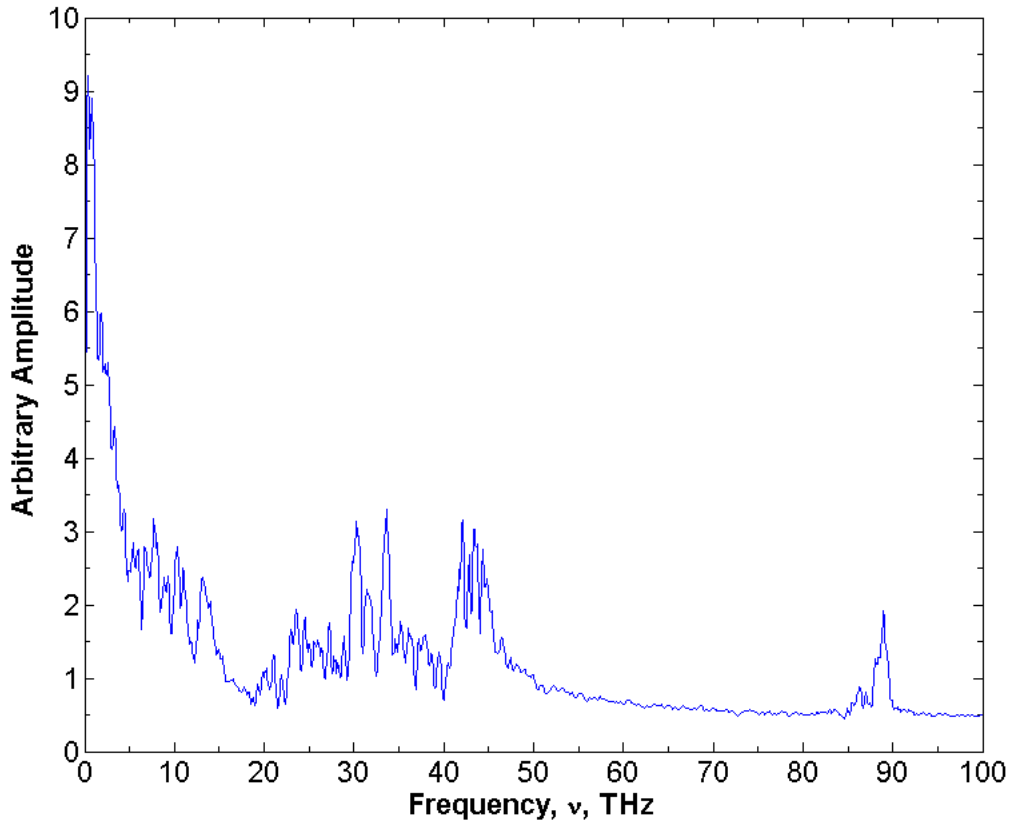

(c) Vibration spectrum for carbon atoms of n-heptane

Fig. 23. Velocity auto correlation function and vibration spectrum of carbon atoms in n-heptane molecules

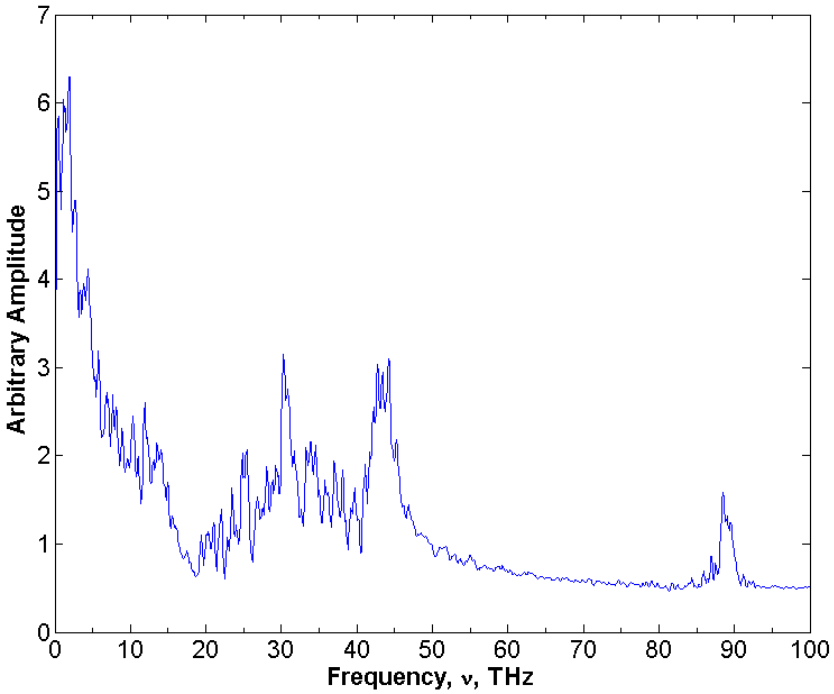

(a) n-Tridecane

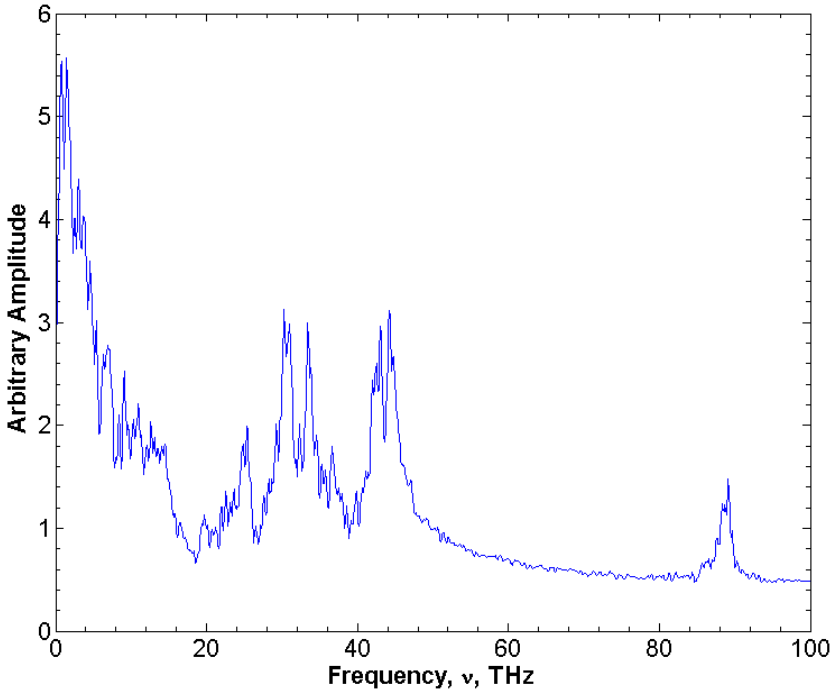

(b) n-Nonadecane

Fig. 24. Vibration spectrum of n-trdecane and n-nonadecane

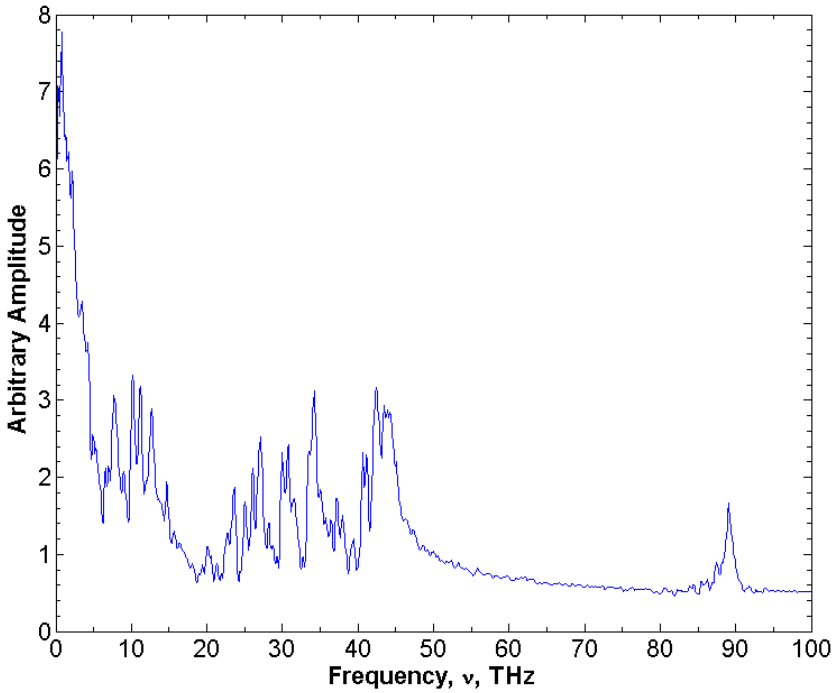

(a) 2-Methyl Hexane

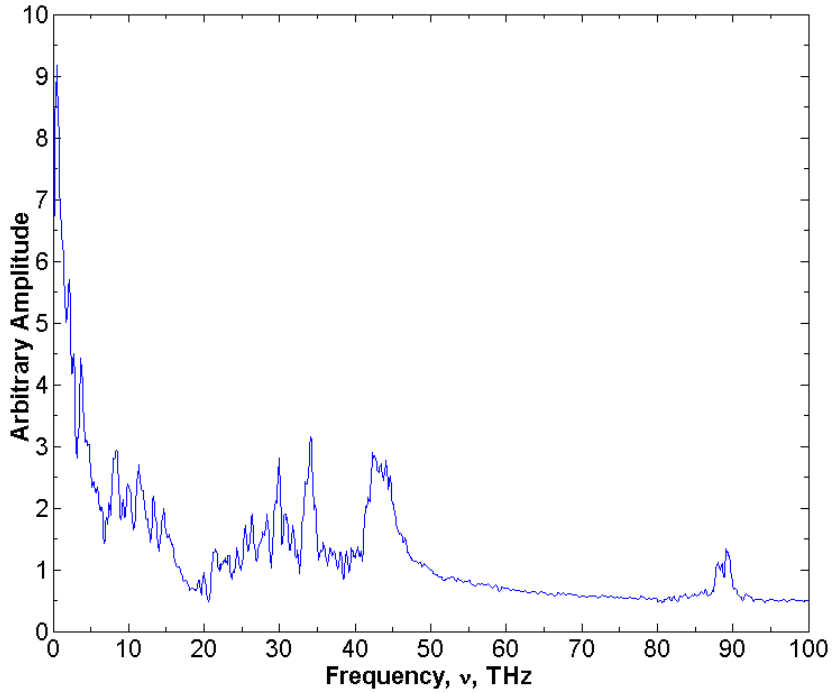

(b) 3-Methyl Hexane

Fig. 25. Vibration spectrum of 2-methyl hexane and 3-methyl hexane

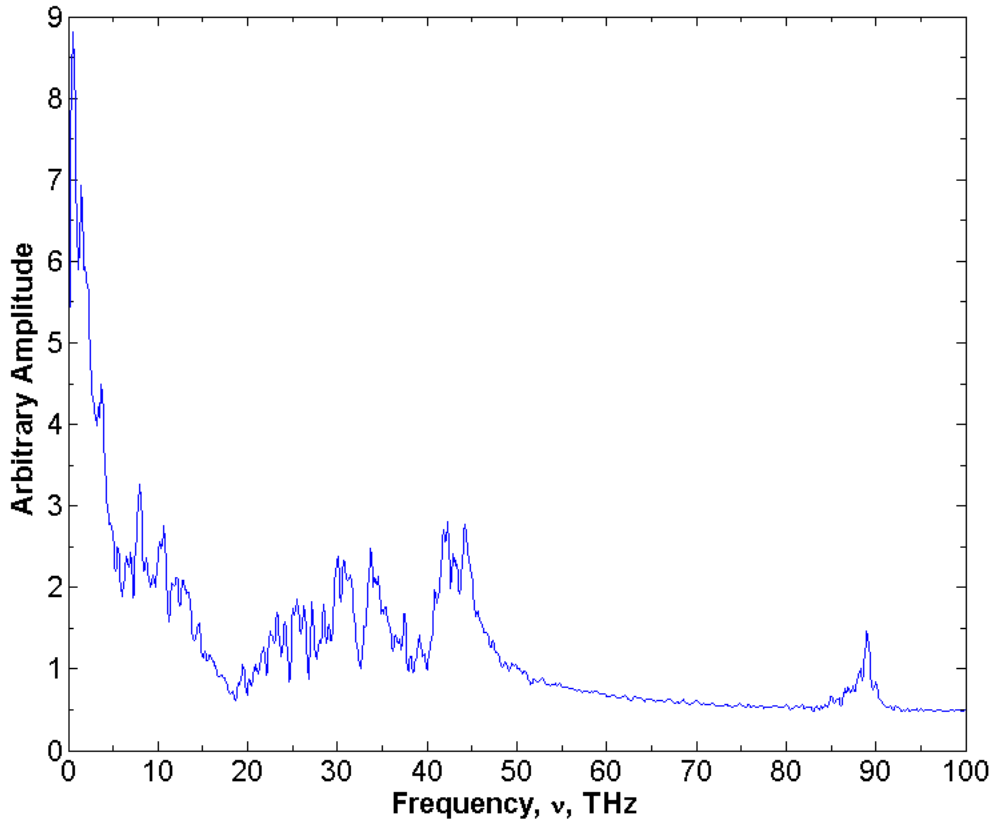

(a) Mixture of n-heptane and its isomers

Fig. 26. Vibration spectrum for the mixture of n-heptane and its isomers.

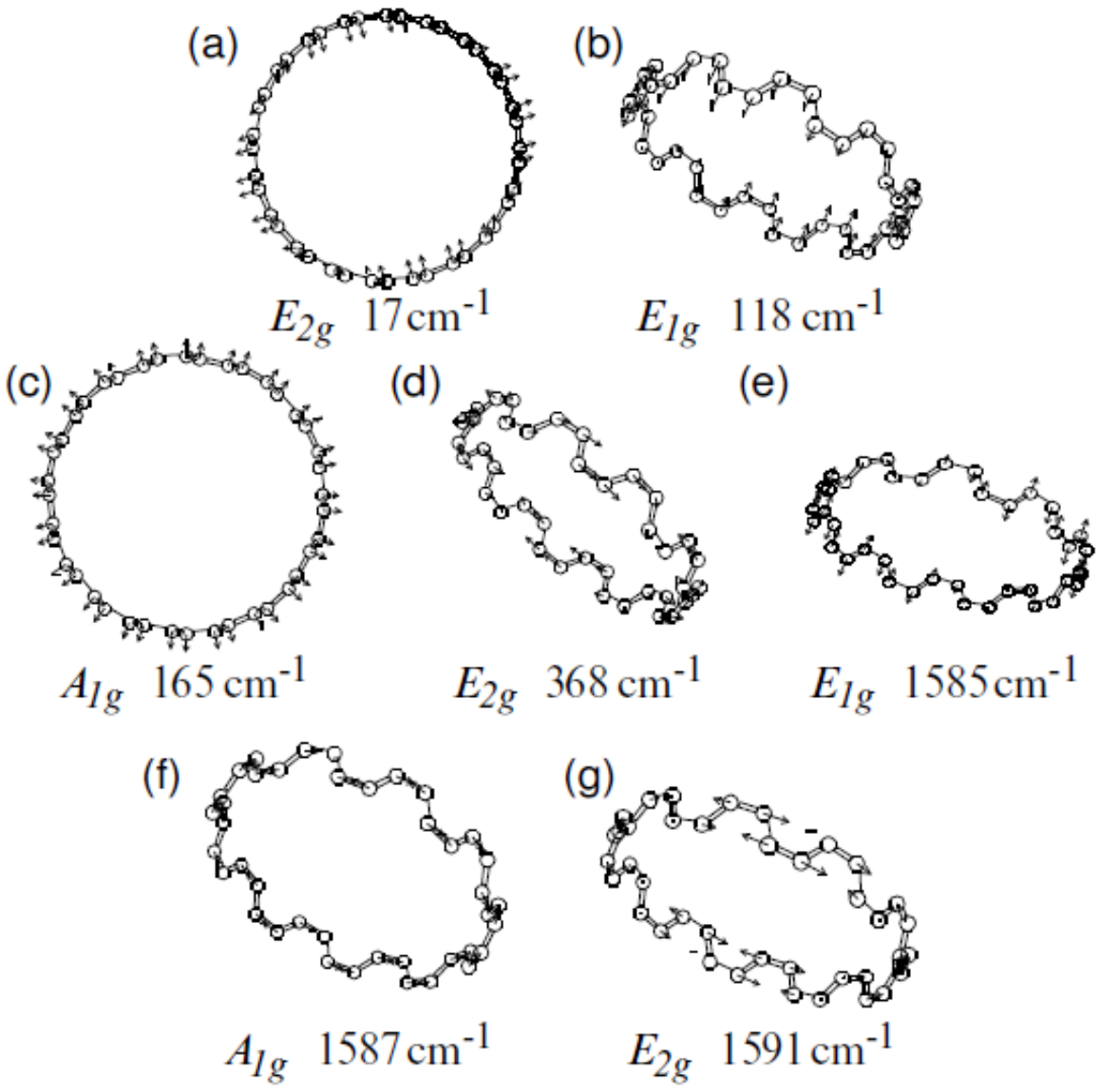

Fig. 27. Atomic displacements, frequencies and symmetries for selected normal modes for an armchar nanotube (the symmetry and frequencies for these modes are not strongly dependent on the chirality of the nanotube)

(Figure published with permission from [95], Original Source of Publication :

http://www.informaworld.com/)

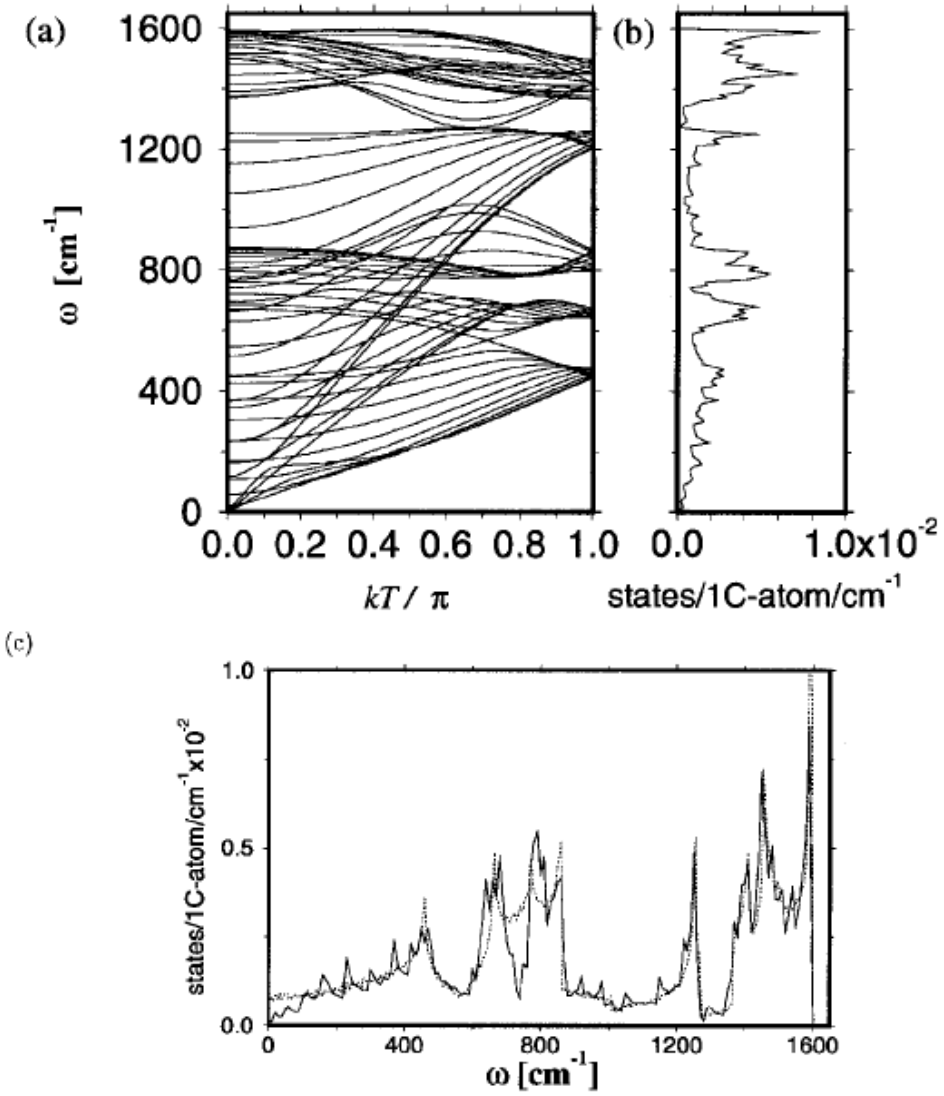

Fig. 28. (a) phonon dispersion relations of an armchair nanotube, (b) phonon density of states for the armchair nanotube (c) comparison of phonon density of states for nanotube in solid lines and graphite sheet in dotted lines.

(Figure published with permission from [95], Original Source of Publication :

http://www.informaworld.com/)

Similarly, vibration spectrum is generated for n-Tridecane and n-Nonadecane, 2Methyl Hexane, 3Methyl Hexane and for the mixture system which consists of n-heptane and its isomers. These vibration spectra are shown in Figure 23, 24, 25 and 26. Figure 28 shows the phonon spectrum and vibration modes for carbon nanotubes. Some of the selected normal vibration modes, their frequency and directions of displacement are shown in Figure 27. These modes correspond to stretching, twisting and radial breathing modes in the carbon nanotube. Figure 28 also shows the vibration spectrum modes for graphite sheet.

Figure 23 shows the temporal variation of normalized velocity autocorrelation function and vibration spectrum for n-heptane. The vibration spectrum for isomers, dimers and trimer of n-heptane is shown in Figure 26. These spectrum are identical for the peak frequencies as expected due to the fact that the vibrating atoms in all these hydrocarbons are C-C and C-H. The low frequencies vibrations exists due to weak van der Waals coupling between the atoms. Figure 28 shows the normal modes of vibration and phonon spectra for arm chair carbon nanotube. These modes are not strongly dependent upon the chirality of the nanotube [95]. The energy transfer occurs when the atoms vibrate in resonance with each other. Since in the hydrocarbons, the van der Waals vibration frequency range is 0.4THz to 5THz, the energy will be transferred to these atoms from the atoms of the nanotube vibrating in the same frequency range. So modes in nanotube responsible for heat transfer from the nanotube to the surrounding atoms are modes (a), (b) and (c) in Figure 27 which corresponds to squeezing, in-plane twisting due to bond bending and in-plane longitudinal due to bond stretching.

G. Nano-Scale Thermo-Diffusion Effects

Figure 22 (Appendix A) shows the variation of different types carbon atoms (C_1, C_2 and C_3) in the radial direction. C_1 denotes the carbon atoms attached to three carbon and one hydrogen atom, C_2 denotes carbon atoms attached to two carbon and two hydrogen atom and C_3 denotes carbon atoms attached to one carbon and three hydrogen atom. There is a clear accumulation of carbon atoms near the carbon nanotube. Also from the different peaks locations of different carbon types, preferential accumulation of C_2 carbon types can be deduced. This causes local concentration gradient near the carbon nanotube leading to mass diffusion away from the carbon nanotube surface to the bulk phase. This diffusion causes transport of energy from the carbon nanotube to bulk liquid leading to Soret effect at the nano-scale.

H. Summary

From the results it is clear that the interfacial thermal resistance strongly depends upon the chemical composition of the fluids. The dependence is due to the variations in the vibration frequencies of the atoms in the fluid molecules. Interfacial thermal resistance also depends on the molecular structure and varies for polymer chains, their isomers and mixtures. The variation is due to the difference in the effectiveness of different structures to wrap around the nanotube. So fluids with small and branched chains have low interfacial thermal resistance compared to long chains. In mixtures the presence of structures of different sizes and orientation enables the individual molecules to wrap around the nanotube more effectively and thus have resistance closer to chain with the smallest resistance. Regarding the energy transfer mechanism it is deduced that the energy form the carbon nanotubes to the fluid is transferred due to the presence of weak van der Waal's interactions. The low frequency modes

in the nanotube and the fluid match (vibrate in resonance) leading to the transfer of the thermal energy. These modes corresponds to non-bonded interactions in fluids and squeezing, in-plane twisting due to bond bending and in-plane longitudinal due to bond stretching in carbon nanotubes.

CHAPTER V

SUMMARY AND FUTURE DIRECTION

With the latest development in the high performance, miniaturized electronic devices comes the need to remove large amounts of heat from small areas. Pool boiling is a very efficient mode for heat transfer. Experiments have been performed to enhance the heat transfer in pool boiling by modifying the boiling surface. Recently, carbon nanotubes have attracted a great deal of attention owing to their excellent thermal, mechanical and electrical properties. Experiments performed using carbon nanotubes as nanofins on the boiling surfaces have shown enhancement in the heat transfer. But the enhancement level is not as high as expected from the nanotubes, especially because silicon nano-fins are found to result in higher pool boiling heat flux values. This degradation in the performance of the carbon nanotubes is attributed to the presence of a larger interfacial thermal resistance between the carbon nanotubes and the surrounding fluids.

A. Summary

In this work, non-equilibrium molecular dynamic simulations have been performed to study interfacial thermal resistance between carbon nanotubes and surrounding fluids, the main parameter affecting the performance of carbon nanotubes as nano-fins. The simulation strategy used in this work is based on the lumped capacitance method where the temperature difference between the object and the surrounding fluid decays exponentially. The simulation domain consists of a carbon nanotube placed at the center of the simulation box surrounded by fluid molecules. The system is brought to a base temperature and then the temperature of the carbon nanotube is instantaneously raised to a higher value. As the system relaxes under constant energy,

the energy is transferred from the carbon nanotube to the fluid. From the temporal variation of the temperature in both nanotube and matrix molecules, the interfacial thermal resistance has been obtained. Different fluid molecules are considered in this work to elucidate the effect of various chemical and structural properties on the interfacial thermal resistance. From the results it can be concluded that,

- The liquid molecules near a crystalline surface are more ordered with a higher density than the bulk liquid and exhibit properties that are akin to that of a solid. The density of the liquid near the carbon nanotube peaks to a high value followed by multiple oscillations and subsequently reaching the bulk liquid density value at a few atomic distance away. This trend is observed in all the simulations performed in this study.

- The interfacial resistance is found to be dependent on the chemical composition of the fluid surrounding the nanotube. To study the effect of chemical composition, interfacial resistances between the nanotube and common coolants, water, ethyl alcohol and 1-hexene were studied. From these simulations it has been found that atomic properties affect the interfacial resistance due to the difference in the interaction potential between the atoms of the fluid and the nanotube. The potential depends upon the oxidation state of a particular fluid atom and attached atoms. So an oxygen in water will have a different interaction attributes than an oxygen in ethyl alcohol while interacting with carbon atoms of the carbon nanotube. This change in the interaction changes the interfacial resistance.

- The interaction between the carbon nanotube and surrounding fluid also depends upon the ability of the fluid to wrap around the nanotube. Coolants used in avionics systems consist of olefins (hydrocarbon) as mixtures of monomers,

dimers, trimers etc. Molecules with short chains can effectively wrap around the nanotube but those with long chains cannot due to stearic hindrance. N-heptane and its dimer and trimer (n-tridecane and n-nonadecane respectively), are considered in this study, for investigating the effect of polymer chains on interfacial thermal resistance. It has been found that the small chains have lower interfacial resistance than longer chains owing to thier ability to effectively wrap around the nanotube. Also the equilibrium structure of the molecule chain effect the resistance.

- The isomers of a hydrocarbon chain have different molecular structure. Since the structure changes the effectiveness of the molecule to wrap around the nanotube, interfacial resistance for isomers will be different when compared to the straight chain isomer. Also the manufacturing processes for these hydrocarbons produces a mixture of polymer and isomers (i.e. dimers, trimers etc). To study the effect of isomers and their mixtures on interfacial resistance, polymer chains and isomers of n-heptane are considered. Simulations indicate that the isomers have variable interfacial resistance. The resistance values depends upon the effectiveness of their structure to wrap around the nanotube. Also the mixtures possess lower interfacial resistance due to the presence of different types of structures that can wrap effectively around the nanotube.

- To ascertain the transport mechanism for heat transfer from the carbon nanotubes to the surrounding molecules, vibration spectrum analysis of carbon atoms of n-heptane, n-tridecane, n-nonadecane and isomers and mixtures of n-heptane was performed. From the vibration analysis, it is observed that the weak van der Waal's interactions are responsible for the transfer of energy from the carbon nanotubes. This is also apparent from the snapshot of the system

at equilibrium, (Figure 15 on page 52), as there is a gap of about 3Åbetween the carbon nanotube and the fluid molecules due to weak van der Waal's interactions. Through these interactions only the low vibrating modes of the carbon nanotubes can interact with the surrounding carbon atoms. From the vibration spectrum analysis of carbon nanotube, squeezing, in-plane twisting due to bond bending and in-plane longitudinal due to bond stretching are responsible for the low frequency vibrating modes. So these modes are responsible for transferring energy from the carbon nanotube to the fluid molecules.

B. Future Direction

This work focused on the use of a (5,5) armchair carbon nanotube as a nanofin. The effect of nanotubes of other chiralities, chiral and zig-zag, and diameters on the interfacial thermal resistance was not considered. It has been established that the vibration spectrum of the nanotubes does not strongly depends upon the chirality of the carbon nanotube. So the basic modes of energy transfer from carbon nanotube to the fluids remains the same. But due to the presence of large diameter, the effectiveness of polymers chains to wrap around the nanotubes will change. The polymer chains will be more effective in wrapping around the nanotube of larger diameters, so it is expected that the interfacial resistance may be less for large diameter nanotubes. Further studies are needed to enumerate the effect of large diameter of carbon nanotubes on the interfacial thermal resistance for hydrocarbon chains, their isomer and mixtures.

Also in this work it is assumed that the nanotube is free to vibrate without any bonding restrictions. But this will not be true for the certain length of the nanotube near the end bounded on the silicon substrate. Even though this length

is of the order of few Angstrom and will not affect the bulk interfacial resistance of the nanotube, a true nanofin analysis of the nanotube can be done with one end of the nanotube fixed on a silicon substrate. To do this analysis, a nanotube of length of few hundred nanometres to micron has to be considered. This size of the system is prohibitive for the doing molecular dynamics simulation with the current computing power available but may be feasible in the near future with rapid progress in computational capabilities of commercially available systems.

Studies have shown that the presence of large number of defects change properties of the nanotubes. The nanotubes deposited on the silicon substrates using the chemical vapor deposition (CVD) process are not defect free. So their ideal thermal transport mechanics will be disturbed by the presence of these defects. This will also affect the interfacial thermal resistance as the vibration modes of the nanotube will change. Therefore, the effect of defects on the interfacial thermal resistance needs to be studied to explore the more realistic simulations corresponding to the results obtained from the experimental data reported in the literature.

The preferential accumulations of species near the carbon nanotube leads to thermo-diffusion effect. This diffusion help in the enhancement of the energy transport from carbon nanotube surface to the bulk fluid. Further studies of this effect will help in identifying coolants which are more effective in enhancing heat transfer.

REFERENCES

[1] I. Mudawar and T.M. Anderson, "Parametric investigation into the effects of pressure, subcooling, surface augmentation and choice of coolant on pool boiling in the design of cooling systems for high-power-density electronic chips," *Journal of Electronic Packaging*, vol. 112, pp. 375–383, 1990.

[2] H.S. Ahn, N. Sinha, M. Zhang, D. Banerjee, S. Fang, and R.H. Baughman, "Pool boiling experiments on multiwalled carbon nanotube (MWCNT) forests," *Journal of Heat Transfer*, vol. 128, pp. 1335–1342, 2006.

[3] V. Sathyamurthi, H.S. Ahn, D. Banerjee, and S.C. Lau, "Subcooled pool boiling experiments on horizontal heaters coated with carbon nanotubes," *Journal of Heat Transfer*, vol. 131, pp. 071501, 2009.

[4] S. Ujereh, T. Fisher, and I. Mudawar, "Effects of carbon nanotube arrays on nucleate pool boiling," *International Journal of Heat and Mass Transfer*, vol. 50, no. 19-20, pp. 4023–4038, 2007.

[5] S.R. Sriraman, "Pool boiling on nano-finned surfaces," M.S. thesis, Texas A&M University, College Station, 2007.

[6] B. V. Derjaguin and Z. M. Zorin, "Optical study of the absorption and surface condensation of vapors in the vicinity of saturation on a smooth surface," in *Proc. 2nd International Cogress on Surface Activity (London)*, 1957, vol. 2, pp. 145–152.

[7] D. Banerjee and V.K. Dhir, "Study of subcooled film boiling on a horizontal disc: Part 2 – experiments," *Journal of Heat Transfer*, vol. 123, pp. 285–293, 2001.

[8] D. Banerjee, G. Son, and V.K. Dhir, "Conjugate thermal and hydrodynamic analyses of saturated film boiling from a horizontal surface," *ASME Heat Transfer Div Publ HTD*, vol. 334, no. 3, pp. 57–64, 1996.

[9] Y. Ding, H. Alias, D. Wen, and R.A. Williams, "Heat transfer of aqueous suspensions of carbon nanotubes (CNT nanofluids)," *International Journal of Heat and Mass Transfer*, vol. 49, no. 1-2, pp. 240–250, 2006.

[10] S. Kakaç and A. Pramuanjaroenkij, "Review of convective heat transfer enhancement with nanofluids," *International Journal of Heat and Mass Transfer*, vol. 52, no. 13-14, pp. 3187–3196, 2009.

[11] D. Huitink, S. Ganguly, D. Banerjee, and K. Yerkes, "Convective heat transfer enhancements using nanofluids," in *Proceedings of the Nanofluids: Fundamentals and Applications (Engineering Conferences International)*, Copper Conference Center, Copper Mountain, CO, 2007.

[12] I.C. Nelson, D. Banerjee, and R. Ponnappan, "Flow loop experiments using polyalphaolefin nanofluids," *Journal of thermophysics and heat transfer*, vol. 23, no. 4, pp. 752–761, 2009.

[13] J.E. Jackson, B.V. Borgmeyer, C.A. Wilson, P. Cheng, and J.E. Bryan, "Characteristics of nucleate boiling with gold nanoparticles in water," in *Proceedings of the IMECE 2006, IMECE2006-16020*, 2006.

[14] H. R. Shanks, P. D. Maycock, P. H. Sidles, and G. C. Danielson, "Thermal conductivity of silicon from 300 to 1400°k," *Phys. Rev.*, vol. 130, no. 5, pp. 1743–1748, Jun 1963.

[15] P. Kim, L. Shi, A. Majumdar, and P.L. McEuen, "Thermal transport measurements of individual multiwalled nanotubes," *Physical Review Letters*, vol. 87, no. 21, pp. 215502, 2001.

[16] S. Berber, Y.K. Kwon, and D. Tomanek, "Unusually high thermal conductivity of carbon nanotubes," *Physical Review Letters*, vol. 84, no. 20, pp. 4613–4616, 2000.

[17] R. Benda, J. Bullen, and A. Plomer, "Synthetics basics: polyalphaolefins-base fluids for high-performance lubricants," *Journal of Synthetic Lubrication*, vol. 13, no. 1, pp. 41–57, 1996.

[18] K. Kordas, G. Toth, P. Moilanen, M. Kumpumaki, J. Vahakangas, A. Uusimaki, R. Vajtai, and PM Ajayan, "Chip cooling with integrated carbon nanotube microfin architectures," *Applied Physics Letters*, vol. 90, pp. 123105, 2007.

[19] H. Maune, H.Y. Chiu, and M. Bockrath, "Thermal resistance of the nanoscale constrictions between carbon nanotubes and solid substrates," *Applied Physics Letters*, vol. 89, pp. 013109, 2006.

[20] S. Murad and I.K. Puri, "Thermal transport across nanoscale solid-fluid interfaces," *Applied Physics Letters*, vol. 92, pp. 133105, 2008.

[21] S.T. Huxtable, D.G. Cahill, S. Shenogin, L. Xue, R. Ozisik, P. Barone, M. Usrey, M.S. Strano, G. Siddons, M. Shim, et al., "Interfacial heat flow in carbon nanotube suspensions," *Nature materials*, vol. 2, no. 11, pp. 731–734, 2003.

[22] S.U.S Choi, Z.G. Zhang, W. Yu, F.E. Lockwood, and E.A. Grulke, "Anomalous thermal conductivity enhancement in nanotube suspensions," *Applied Physics Letters*, vol. 79, pp. 2252–2254, 2001.

[23] M.J. Biercuk, M.C. Llaguno, M. Radosavljevic, J.K. Hyun, A.T. Johnson, and J.E. Fischer, "Carbon nanotube composites for thermal management," *Applied Physics Letters*, vol. 80, pp. 2767–2769, 2002.

[24] M.B. Bryning, D.E. Milkie, M.F. Islam, J.M. Kikkawa, and A.G. Yodh, "Thermal conductivity and interfacial resistance in single-wall carbon nanotube epoxy composites," *Applied Physics Letters*, vol. 87, pp. 161909, 2005.

[25] M. S. Dresselhaus, G. Dresselhaus, and Riichiro Saito, "Carbon fibers based on $c60$ and their symmetry," *Phys. Rev. B*, vol. 45, no. 11, pp. 6234–6242, 1992.

[26] R.S. Ruoff and D.C. Lorents, "Mechanical and thermal properties of carbon nanotubes," *Carbon*, vol. 33, no. 7, pp. 925–930, 1995.

[27] B.G. Demczyk, Y.M. Wang, J. Cumings, M. Hetman, W. Han, A. Zettl, and R.O. Ritchie, "Direct mechanical measurement of the tensile strength and elastic modulus of multiwalled carbon nanotubes," *Materials Science & Engineering A*, vol. 334, no. 1-2, pp. 173–178, 2002.

[28] E. T. Thostenson, C. Li, and T.W. Chou, "Nanocomposites in context," *Composites Science and Technology*, vol. 65, no. 3-4, pp. 491 – 516, 2005.

[29] L.X. Zheng, M.J. O'Connell, S.K. Doorn, X.Z. Liao, Y.H. Zhao, E.A. Akhadov, M.A. Hoffbauer, B.J. Roop, Q.X. Jia, R.C. Dye, et al., "Ultralong single-wall carbon nanotubes," *Nature materials*, vol. 3, no. 10, pp. 673–676, 2004.

[30] S.G. Louie, "Electronic properties, junctions, and defects of carbon nanotubes," *Topics in Applied Physics*, vol. 80, pp. 113–146, 2000.

[31] R.H. Baughman, A.A. Zakhidov, and W.A. de Heer, "Carbon nanotubes-the route toward applications," *Science*, vol. 297, no. 5582, pp. 787–792, 2002.

[32] W. Liang, M. Bockrath, D. Bozovic, J.H. Hafner, M. Tinkham, and H. Park, "Fabry-Perot interference in a nanotube electron waveguide," *Nature*, vol. 411, no. 6838, pp. 665–669, 2001.

[33] S. Hong and S. Myung, "Nanotube Electronics: A flexible approach to mobility," *Nature Nanotechnology*, vol. 2, no. 4, pp. 207–208, 2007.

[34] Y. Xu, Y. Zhang, E. Suhir, and X. Wang, "Thermal properties of carbon nanotube array used for integrated circuit cooling," *Journal of Applied Physics*, vol. 100, pp. 074302, 2006.

[35] Y. Xu, C.K. Leong, and D.D.L Chung, "Carbon nanotube thermal pastes for improving thermal contacts," *Journal of Electronic Materials*, vol. 36, no. 9, pp. 1181–1187, 2007.

[36] M.P. Allen, "Introduction to molecular dynamics simulation," *Computational Soft Matter: From Synthetic Polymers to Proteins*, vol. 23, pp. 1–28, 2004.

[37] CW Gear, *The numerical integration of ordinary differential equations of various orders*, ANL-7126, Argonne National Lab., Ill., 1966.

[38] C.W. Gear, *The simultaneous numerical solution of differential-algebraic equations*, Stanford Univ., Stanford, 1970.

[39] C.W. Gear, *Numerical initial value problems in ordinary differential equations*, Prentice Hall PTR Upper Saddle River, NJ, 1971.

[40] L. Verlet, "Computer experiments on classical fluids. i. thermodynamical properties of lennard-jones molecules," *Phys. Rev.*, vol. 159, no. 1, pp. 98103, Jul 1967.

[41] L. Verlet, "Computer experiments on classical fluids. II. Equilibrium correlation functions," *Phys. Rev*, vol. 165, no. 1, pp. 201–214, 1968.

[42] R.W. Hockney, "The potential calculation and some applications," *Methods Comput. Phys*, vol. 9, pp. 136–211, 1970.

[43] W.C. Swope, H.C. Andersen, P.H. Berens, and K.R. Wilson, "A computer simulation method for the calculation of equilibrium constants for the formation of physical clusters of molecules: Application to small water clusters," *The Journal of Chemical Physics*, vol. 76, pp. 637–649, 1982.

[44] D.W. Brenner, "The art and science of an analytic potential," *Computer Simulation of Materials at Atomic Level*, vol. 217, pp. 23–40, 2000.

[45] J.R. Fried, "Computational Parameters," *Physical Properties of Polymers Handbook*, pp. 59–68, 2006.

[46] J.R. Maple, U. Dinur, and A.T. Hagler, "Derivation of force fields for molecular mechanics and dynamics from ab initio energy surfaces," *Proceedings of the National Academy of Sciences*, vol. 85, no. 15, pp. 5350–5354, 1988.

[47] Accelrys, "http:www.accelrys.com/about/," 2008.

[48] H. Sun, "Ab initio calculations and force field development for computer simulation of polysilanes," *Macromolecules*, vol. 28, no. 3, pp. 701–712, 1995.

[49] M.P. Allen and D.J. Tildesley, *Computer simulation of liquids*, Clarendon Press, New York, 1990.

[50] A. Arnold and C. Holm, "Efficient methods to compute long-range interactions for soft matter systems," *Adv Polym Sci*, vol. 185, pp. 59–109, 2005.

[51] J. Eastwood, R. Hockney, and D. Lawrence, "P3M3DP: The three-dimensional periodic particle-particle/particle-mesh program," *Computer Physics Communications*, vol. 19, pp. 215–261, 1977.

[52] D.C. Rapaport, *The art of molecular dynamics simulation*, Cambridge University Press, Cambridge, 2004.

[53] D. Frenkel and B. Smit, *Understanding molecular simulation: from algorithms to applications*, Academic Press, Orlando, 2002.

[54] P.L. Kapitza, "The study of heat transfer in helium II," *J. Phys.(USSR)*, vol. 4, no. 3, pp. 181–210, 1941.

[55] I.M. Khalatnikov, "Discontinuities and large amplitude sound waves in helium II," *Zh. Eksp. Teor. Fiz*, vol. 23, pp. 253–260, 1952.

[56] R. M. Mazo, "Theoretical studies on low temperature phenomena," Ph.D. dissertation, Yale University, New Haven, 1955.

[57] W.A. Little, "The transport of heat between dissimilar solids at low temperatures," *Canadian Journal of Physics*, vol. 37, no. 3, pp. 334–349, 1959.

[58] D. M. Lee and Henry A. Fairbank, "Heat transport in liquid he^3," *Phys. Rev.*, vol. 116, no. 6, pp. 1359–1364, Dec 1959.

[59] A. C. Anderson, J. I. Connolly, and J. C. Wheatley, "Thermal boundary resistance between solids and helium below 1°k," *Phys. Rev.*, vol. 135, no. 4A, pp. A910–A921, Aug 1964.

[60] L. J. Challis, K. Dransfeld, and J. Wilks, "Heat transfer between solids and liquid helium *II*," *Proceedings of the Royal Society of London. Series A, Mathematical and Physical Sciences*, vol. 260, no. 1300, pp. 31–46, 1961.

[61] D.S. Matsumoto, C.L. Reynolds Jr, and A.C. Anderson, "Thermal boundary resistance at metal-epoxy interfaces," *Physical Review B*, vol. 16, no. 8, pp. 3303–3307, 1977.

[62] N. S. Shiren, "Surface roughness contribution to kapitza conductance," *Phys. Rev. Lett.*, vol. 47, no. 20, pp. 1466–1469, Nov 1981.

[63] E.T. Swartz and R.O. Pohl, "Thermal resistance at interfaces," *Applied Physics Letters*, vol. 51, no. 26, pp. 2200–2202, 2009.

[64] D.A. Young and H.J. Maris, "Lattice-dynamical calculation of the Kapitza resistance between fcc lattices," *Physical Review B*, vol. 40, no. 6, pp. 3685–3693, 1989.

[65] S. Pettersson and G.D. Mahan, "Theory of the thermal boundary resistance between dissimilar lattices," *Physical Review B*, vol. 42, no. 12, pp. 7386–7390, 1990.

[66] R. Kubo, "The fluctuation-dissipation theorem," *Reports on Progress in Physics*, vol. 29, pp. 255–284, 1966.

[67] M.S. Green, "Markoff random processes and the statistical mechanics of time-dependent phenomena. II. Irreversible processes in fluids," *Journal of Chemical Physics*, vol. 22, pp. 398–413, 1954.

[68] M.J. Gillan and M. Dixon, "The calculation of thermal conductivities by perturbed molecular dynamics simulation," *Journal of Physics C: Solid State Physics*, vol. 16, pp. 869–878, 1983.

[69] P. Jund and R. Jullien, "Molecular-dynamics calculation of the thermal conductivity of vitreous silica," *Physical Review B*, vol. 59, no. 21, pp. 13707–13711,

1999.

[70] F. Muller-Plathe, "A simple nonequilibrium molecular dynamics method for calculating the thermal conductivity," *The Journal of Chemical Physics*, vol. 106, pp. 6082–6085, 1997.

[71] A. Cummings, M. Osman, D. Srivastava, and M. Menon, "Thermal conductivity of Y-junction carbon nanotubes," *Physical Review B*, vol. 70, no. 11, pp. 115405, 2004.

[72] A. Maiti, G.D. Mahan, and S.T. Pantelides, "Dynamical simulations of nonequilibrium processes - heat flow and the Kapitza resistance across grain boundaries," *Solid state communications*, vol. 102, no. 7, pp. 517–521, 1997.

[73] A. Tenenbaum, G. Ciccotti, and R. Gallico, "Stationary nonequilibrium states by molecular dynamics. Fourier's law," *Physical Review A*, vol. 25, no. 5, pp. 2778–2787, 1982.

[74] P.K. Schelling, S.R. Phillpot, and P. Keblinski, "Kapitza conductance and phonon scattering at grain boundaries by simulation," *Journal of Applied Physics*, vol. 95, pp. 6082–6091, 2004.

[75] L. Xue, P. Keblinski, S.R. Phillpot, S.U.S. Choi, and J.A. Eastman, "Two regimes of thermal resistance at a liquid–solid interface," *The Journal of Chemical Physics*, vol. 118, pp. 337–339, 2003.

[76] H. Xiang, P.X. Jiang, and Q.X. Liu, "Non-equilibrium molecular dynamics study of nanoscale thermal contact resistance," *Molecular Simulation*, vol. 34, no. 7, pp. 679–687, 2008.

[77] S. Wang and X. Liang, "Thermal conductivity and interfacial thermal resistance in bilayered nanofilms by nonequilibrium molecular dynamics simulations," *International Journal of Thermophysics*, pp. 1–10, 2008.

[78] S. Maruyama, Y. Igarashi, Y. Taniguchi, and Y. Shibuta, "Molecular dynamics simulations of heat transfer issues in carbon nanotubes," in *The 1st International Symposium on Micro & Nano Technology Honolulu, Hawaii*. Citeseer, 2004.

[79] H. Zhong and J.R. Lukes, "Interfacial thermal resistance between carbon nanotubes: Molecular dynamics simulations and analytical thermal modeling," *Physical Review B*, vol. 74, no. 12, pp. 125403, 2006.

[80] P.A. Greaney and J.C. Grossman, "Nanomechanical Energy Transfer and Resonance Effects in Single-Walled Carbon Nanotubes," *Physical review letters*, vol. 98, no. 12, pp. 125503, 2007.

[81] S. Shenogin, L. Xue, R. Ozisik, P. Keblinski, and D.G. Cahill, "Role of thermal boundary resistance on the heat flow in carbon-nanotube composites," *Journal of Applied Physics*, vol. 95, pp. 8136–8144, 2004.

[82] T.C. Clancy and T.S. Gates, "Modeling of interfacial modification effects on thermal conductivity of carbon nanotube composites," *Polymer*, vol. 47, no. 16, pp. 5990–5996, 2006.

[83] V.U. Unnikrishnan, D. Banerjee, and J.N. Reddy, "Atomistic-mesoscale interfacial resistance based thermal analysis of carbon nanotube systems," *International Journal of Thermal Sciences*, vol. 47, no. 12, pp. 1602–1609, 2008.

[84] C. F. Carlborg, J. Shiomi, and S. Maruyama, "Thermal boundary resistance between single-walled carbon nanotubes and surrounding matrices," *Phys. Rev.*

B, vol. 78, no. 20, pp. 205406, Nov 2008.

[85] S. Plimpton, "Fast parallel algorithms for short-range molecular dynamics," *Journal of Computational Physics*, vol. 117, no. 1, pp. 1–19, 1995.

[86] LAMMPS, "http://lammps.sandia.gov/index.html," Jan. 2008.

[87] E. Polak, *Optimization: algorithms and consistent approximations*, Springer Verlag, New York, 1997.

[88] W.G. Hoover, "Canonical dynamics: Equilibrium phase-space distributions," *Physical Review A*, vol. 31, no. 3, pp. 1695–1697, 1985.

[89] W.G. Hoover, "Constant-pressure equations of motion," *Physical Review A*, vol. 34, no. 3, pp. 2499–2500, 1986.

[90] C.J. Yu, A.G. Richter, A. Datta, M.K. Durbin, and P. Dutta, "Molecular layering in a liquid on a solid substrate: an X-ray reflectivity study," *Physica B: Physics of Condensed Matter*, vol. 283, no. 1-3, pp. 27–31, 2000.

[91] G.V. Bykov, "Valence-vibration frequencies and electronic bond charges for CH bonds in hydrocarbons," *Russian Chemical Bulletin*, vol. 7, no. 6, pp. 743–745, 1958.

[92] S. Lifson and P.S. Stern, "Born–Oppenheimer energy surfaces of similar molecules: Interrelations between bond lengths, bond angles, and frequencies of normal vibrations in alkanes," *The Journal of Chemical Physics*, vol. 77, pp. 4542–4550, 1982.

[93] J.H. Lii and N.L. Allinger, "Molecular mechanics. The MM3 force field for hydrocarbons. 2. vibrational frequencies and thermodynamics," *Journal of the American Chemical Society*, vol. 111, no. 23, pp. 8566–8575, 1989.

[94] P. Derreumaux, M. Dauchez, and G. Vergoten, "The structures and vibrational frequencies of a series of alkanes using the SPASIBA force field," *Journal of molecular structure*, vol. 295, pp. 203–221, 1993.

[95] M.S. Dresselhaus and P.C. Eklund, "Phonons in carbon nanotubes," *Advances in Physics*, vol. 49, no. 6, pp. 705–814, 2000.

APPENDIX A

MISCELLANEOUS GRAPHS

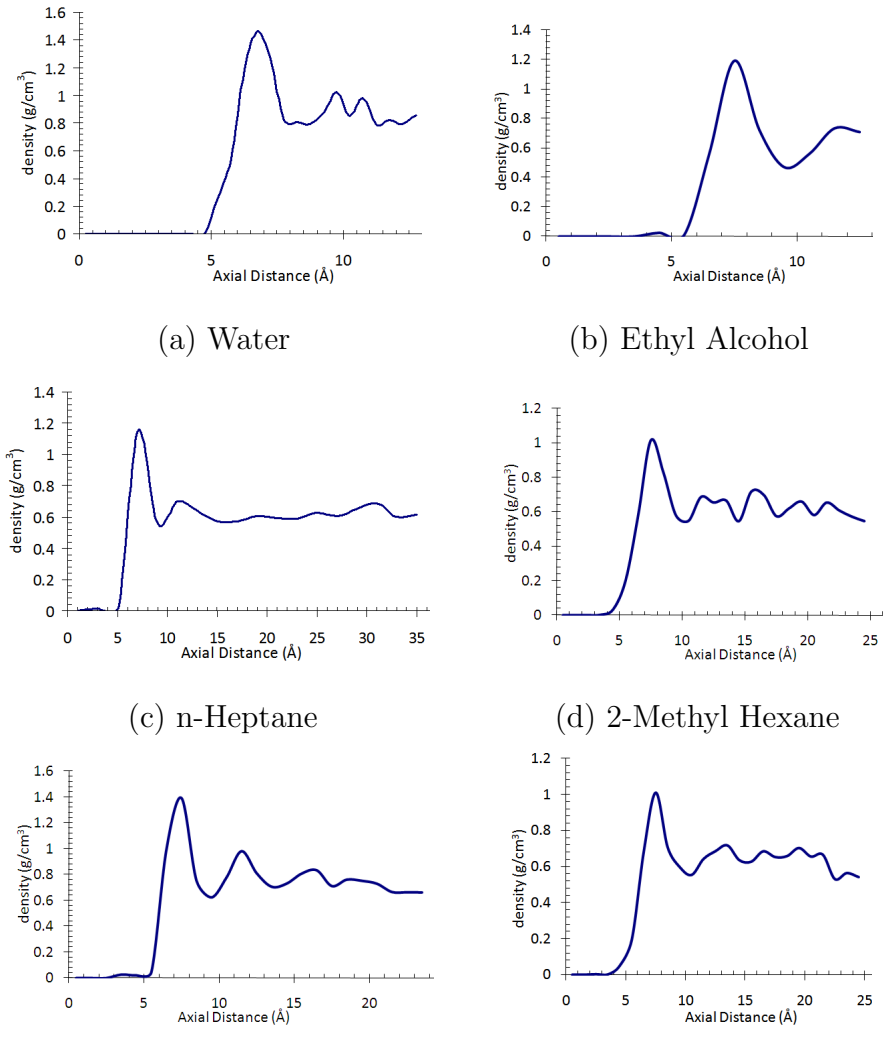

(a) Water

(b) Ethyl Alcohol

(c) n-Heptane

(d) 2-Methyl Hexane

(e) 3-Methyl Hexane

(f) Heptane & its Mixtures

Fig. 29. Radial variation of density of common coolants within simulation domain.

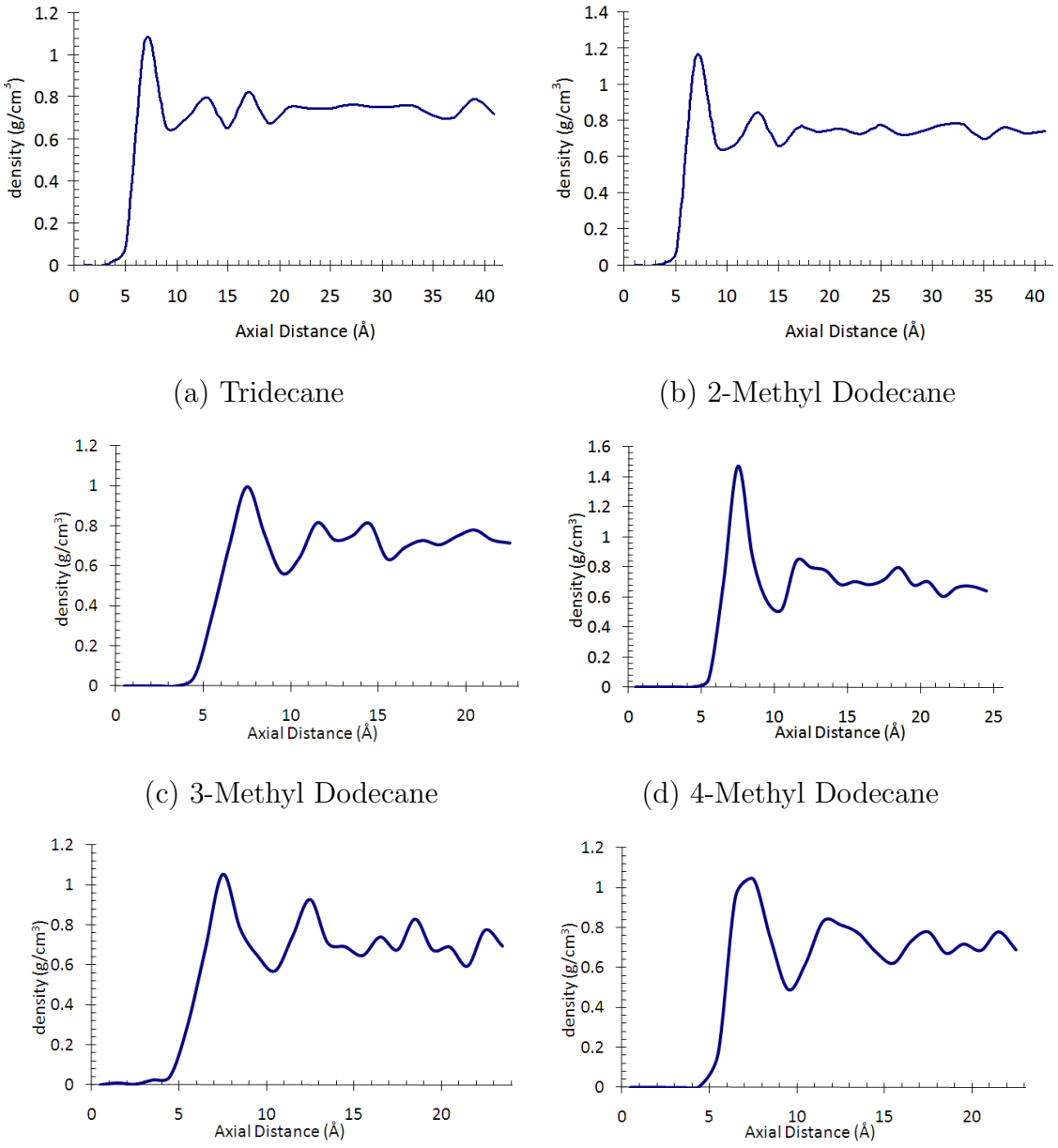

(a) Tridecane

(b) 2-Methyl Dodecane

(c) 3-Methyl Dodecane

(d) 4-Methyl Dodecane

(e) 5-Methyl Dodecane

(f) 6-Methyl Dodecane

Fig. 30. Radial variation of density for n-tridecane and its isomers.

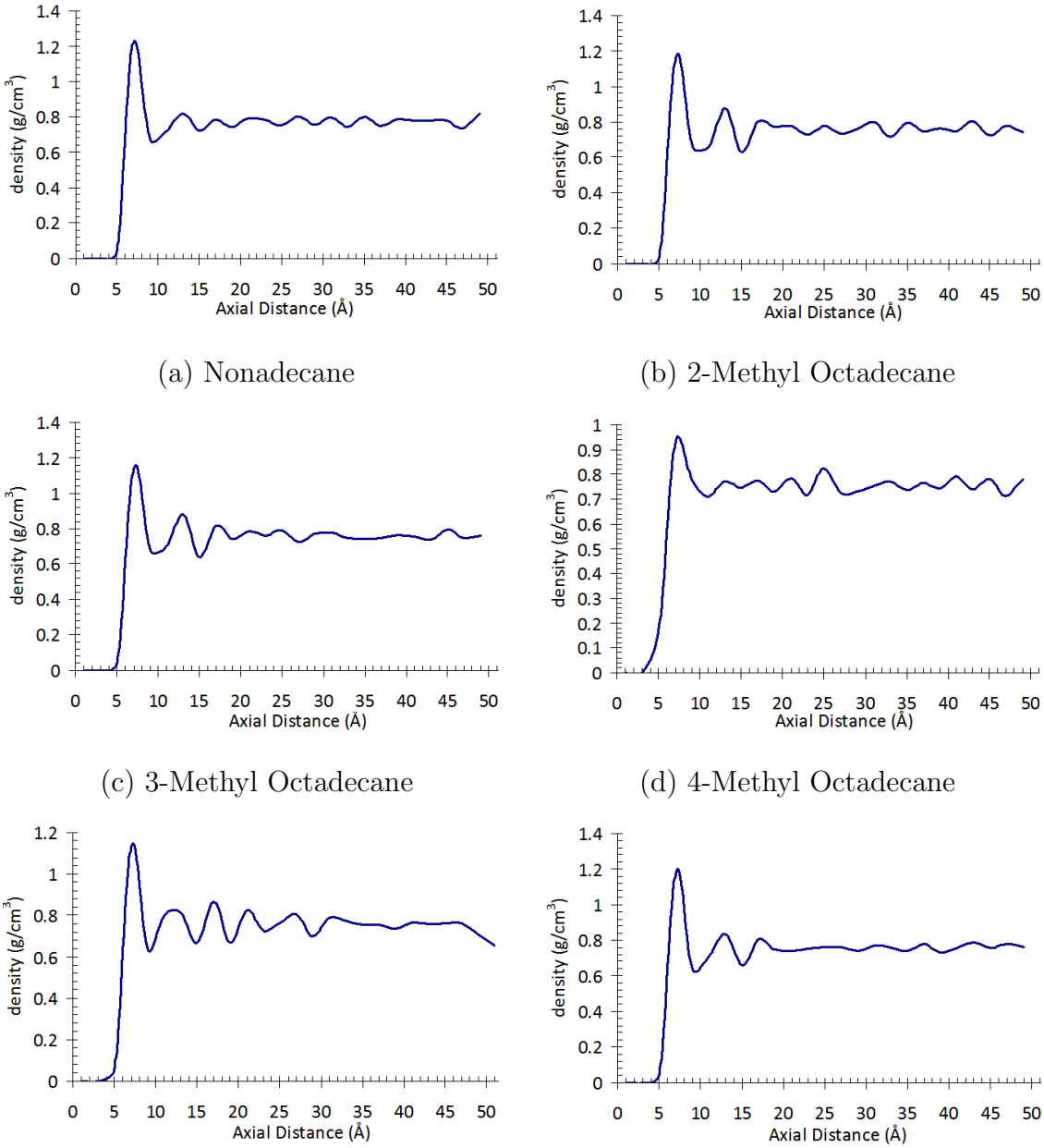

(a) Nonadecane

(b) 2-Methyl Octadecane

(c) 3-Methyl Octadecane

(d) 4-Methyl Octadecane

(e) 5-Methyl Octadecane

(f) 6-Methyl Octadecane

Fig. 31. Radial variation of density of n-nonadecane and its isomers in the simulation domain.

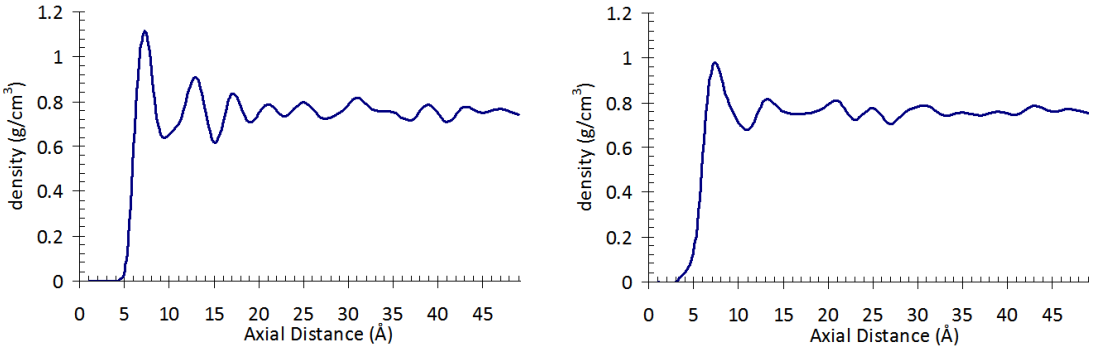

(a) 7-Methyl Octadecane

(b) 8-Methyl Octadecane

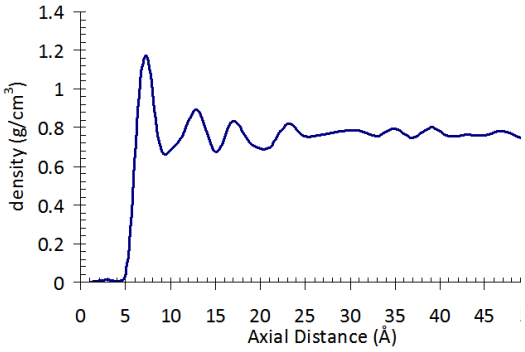

(c) Mixtures of Trimers (22(c))

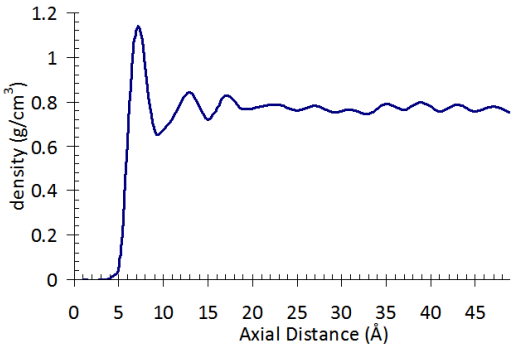

(d) Mixtures of Trimers (22(d))

Fig. 32. Radial density variation for isomers of n-nonadecane and their mixtures.

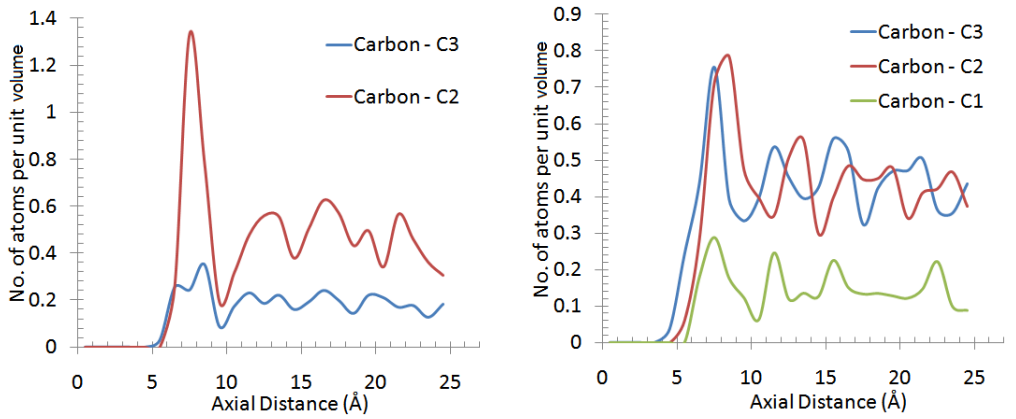

(a) n-Heptane

(b) 2-Methyl Hexane

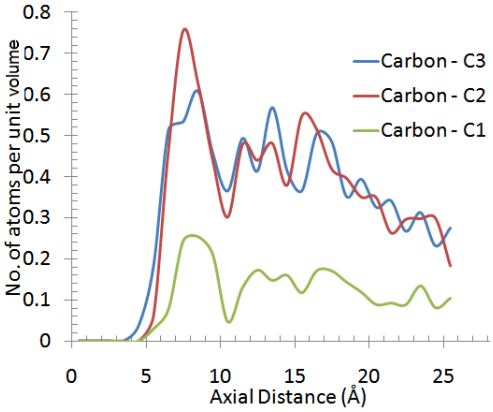

(c) 3-Methyl Hexane

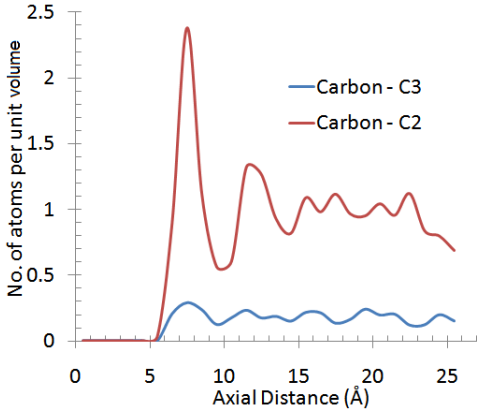

(d) n-Tridecane

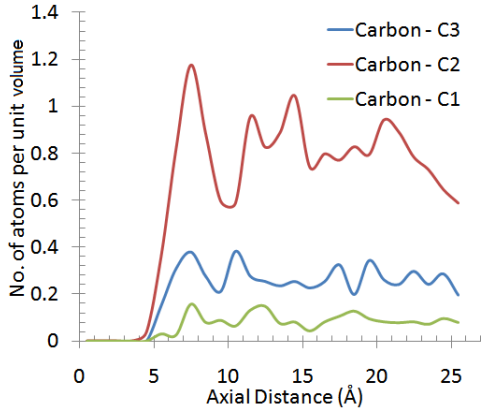

(e) 3-Methyl Dodecane

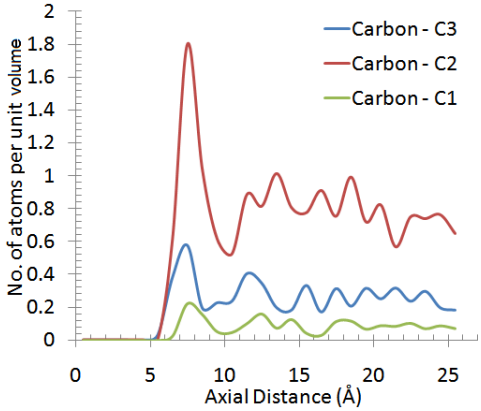

(f) 4-Methyl Dodecane

Fig. 33. Distribution of carbon atoms in radial direction for n-heptane, n-tridecane and their isomers.

C_n stands for carbon with n hydrogen atoms

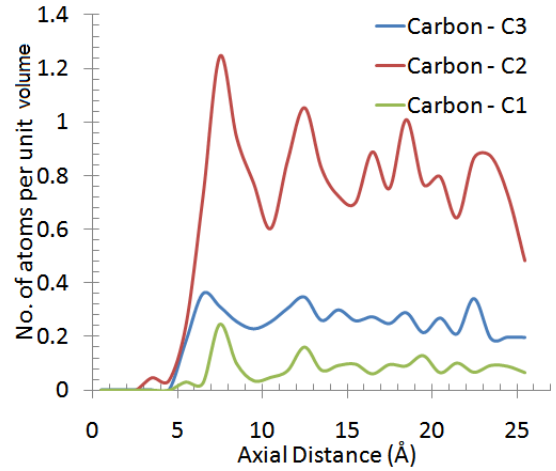

(a) 5-Methyl Dodecane

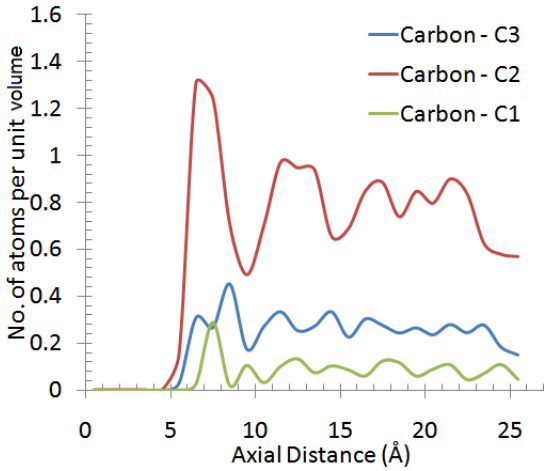

(b) 6-Methyl Dodecane

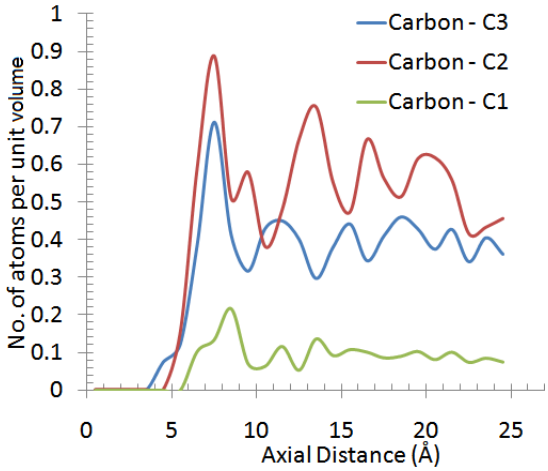

(c) Mixture of Heptane & Isomers

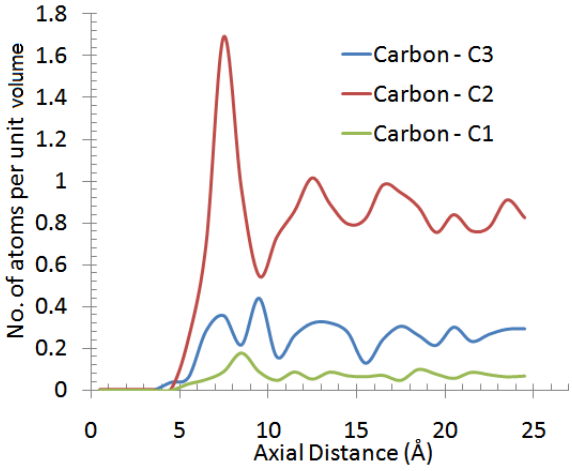

(d) Mixture of Tridecane & Isomers

Fig. 34. Radial distribution of carbon atoms isomer of n-tridecane and their mixtures. C_n stands for carbon with n hydrogen atoms.

VITA

Name: Navdeep Singh

Address: Department of Mechanical Engineering
c/o Dr. Debjyoti Banerjee
Texas A&M University
College Station, TX 77843-3123

Education: Ph.D., Mechanical Engineering,
Texas A&M University, College Station, Dec 2010
M. Tech, Mechanical Engineering,
Thapar University, India, Dec 2003
B. Tech, Mechanical Engineering,
Punjab Technical University, India, June 2001

Publications:

- **N. Singh** and D. Banerjee, "Analysis of Thermal Interfacial Resistance between Nanofins and Various Coolants", *International Journal for Computational Methods in Engineering Science & Mechanics* (*submitted*).

- **N. Singh**, V. Sathyamurthy, W. Peterson, J. Arendt, and D. Banerjee, "Flow Boiling Enhancement on a Horizontal Heater Using Carbon Nanotube Coatings", *International Journal of Heat and Fluid Flow*, vol. 31, pp. 201-207, 2010.

- J. Siegrist, M. Amasia, **N. Singh**, D. Banerjee and M. Madou, "Numerical Modeling and Experimental Validation of Uniform Microchamber Filling in Centrifugal Microfluidics", *Lab on a chip*, vol. 10, pp. 876-886, 2010